Integrated Design and Control Optimization of Hybrid Electric Marine Propulsion Systems based on Battery Performance Degradation Model

by

Li Chen
M.Sc, Tongji University, 2011
B.Eng, Shanghai University of Electric Power, 2008

A Dissertation Submitted in Partial Fulfillment
of the Requirements for the Degree of

DOCTOR OF PHILOSOPHY

in the Department of Mechanical Engineering

Supervisory Committee

Integrated Design and Control Optimization of Hybrid Electric Marine Propulsion Systems based on Battery Performance Degradation Model

by

Li Chen
M.Sc, Tongji University, 2011
B.Eng, Shanghai University of Electric Power, 2009

Supervisory Committee

Dr. Zuomin Dong, Department of Mechanical Engineering
Supervisor

Dr. Curran Crawford, Department of Mechanical Engineering
Departmental Member

Dr. Brad Buckham, Department of Mechanical Engineering
Departmental Member

Dr. Kin Fun Li, Department of Electrical and Computer Engineering
Outside Member

Abstract

This dissertation focuses on the introduction and development of an integrated model-based design and optimization platform to solve the optimal design and optimal control, or hardware and software co-design, problem for hybrid electric propulsion systems. Specifically, the hybrid and plug-in hybrid electric powertrain systems with diesel and natural gas (NG) fueled compression ignition (CI) engines and large Li-ion battery energy storage system (ESS) for propelling a hybrid electric marine vessel are investigated. The combined design and control optimization of the hybrid propulsion system is formulated as a bi-level, nested optimization problem. The lower-level optimization applies dynamic programming (DP) to ensure optimal energy management for each feasible powertrain system design, and the upper-level global optimization aims at identifying the optimal sizes of key powertrain components for the powertrain system with optimized control.

In recent years, Li-ion batteries became a promising ESS technology for electrified transportation applications due to their high energy and power density. However, these costly Li-ion battery ESSs contribute to a large portion of the powertrain electrification and hybridization costs and suffer a much shorter lifetime compared to other key powertrain components, particularly for pure electric and hybrid electric propulsions in large commercial vehicles and marine vessels. The performance degradation of Li-ion battery is pertinent to battery materials, manufacturing processes, operation conditions, and other factors. Three commonly used battery performance modelling methods are reviewed to identify the appropriate degradation prediction approach. Using this approach and a large set of experimental data, the performance degradation and life prediction model of $LiFePO_4$ type battery has been developed and validated. This model serves as the foundation for determining the optimal size of battery ESS and for optimal energy management in powertrain system control to achieve balanced reduction of fuel consumption and the extension of battery lifetime.

In modelling and design of different hybrid electric marine propulsion systems, the life cycle cost (LCC) model of the cleaner, hybrid propulsion systems is introduced, considering the investment, replacement and operational costs of their major contributors, the Li-ion battery ESS and the NG-fueled CI engines. The costs of liquefied NG (LNG), diesel and electricity in the LCC model are collected from various sources, with a focus on

present industrial price in British Columbia, Canada. The greenhouse gas (GHG) and criteria air pollutant (CAP) emissions from traditional diesel and cleaner NG-fueled engines with conventional and optimized hybrid electric powertrains are also evaluated.

To solve the computational expensive nested optimization problem, a surrogate model-based (or metamodel-based) global optimization method is used. This advanced global optimization search algorithm uses the optimized Latin hypercube sampling (OLHS) to form the Kriging model and uses expected improvement (EI) online sampling criterion to refine the model to guide the search of global optimum through a much-reduced number of sample data points from the computationally intensive objective function. Solutions from the combined hybrid propulsion system design and control optimization are presented and discussed.

The new integrated design and control optimization method is applied to the design of hybrid electric propulsion system of a harbour tugboat. Results from the simulations and optimizations have been compared with that from original mechanical propulsion system to validate the newly introduced approach and to demonstrate its superior capability. The resulting hybrid propulsion system with NG engine and Li-ion battery ESS presents a more economical and environmentally friendly propulsion system design of the tugboat.

This research has further improved the methodology of model-based design and optimization of hybrid electric marine propulsion systems to solve complicated co-design problems through more efficient approaches, and demonstrated the feasibility and benefits of the new methods through their applications to tugboat propulsion system design and control developments. Other main contributions include incorporating the battery performance degradation model to the powertrain size optimization and optimal energy management; performing a systematic design and optimization considering LCC of diesel and NG engines in the hybrid electric powertrains; and developing an effective method for the computational intensive powertrain co-design problem.

Table of Contents

List of Tables

List of Figures

List of Abbreviations

AC	alternating current
ACO	ant colony optimization
ADP	adaptive dynamic programming
AES	all-electric ships
A-PMP	approximate PMP
BC	British Columbia
BMS	battery management system
CC-CV	constant current-constant voltage
CFD	computational fluid dynamics
CH_4	methane
CI	compression ignition
C-rate	charge and discharge current rate
DC	direct current
DOD	depth of discharge
DOE	design of experiment
DOF	degree of freedom
DP	dynamic programming
ECA	emission control areas
ECMS	equivalent consumption minimization strategy
ECMS	equivalent consumption minimization strategy
ECU	engine control unit
e-CVT	electric continuously variable transmissions
EEDI	energy efficiency design index
EGR	exhaust gas recirculation
EIA	U.S. Energy Information Administration
EIS	electrochemical impedance spectroscopy
EMS	energy management system
EPA	U.S. Environmental Protection Agency

ESS	energy storage system
EV	electrical vehicle
FDM	finite difference method
GA	genetic algorithm
genset	engine generator set
GHG	greenhouse gases
GNS	graphene nanosheet
GPMM	the generic parametric mathematical model
GSA	gravitational search algorithm
GWO	grey wolf optimizer
GWP	Global Warming Potential
HES	hybrid electric propulsion system
HEV	hybrid electric vehicle
HFO	heavy fuel oil
HIL	hardware-in-the-loop
ICE	internal combustion engine
IMO	international maritime organization
LCC	life cycle cost
LCO	LiCoO2
LFP	LiFePO4
Li	lithium
LiC_6	litigated carbon
Li-ion battery	lithium-ion battery
LMO	LiMn2O4
LNG	liquefied natural gas
LNO	LiNiO2
LOA	the lion optimization algorithm
LTO	lithium titanate
MARPOL	marine pollution
MCU	motor control unit
MDO	marine diesel oil

ME	main engine
MG	motor/generator
MGO	marine gas oil
MOO	multi-objective optimization
MSS	the marine systems simulator
NCA	Lithium Nickel Cobalt Aluminum Oxide
NFL	no free lunch theorem
NG	natural gas
NMC	Lithium Nickel Manganese Cobalt Oxide
NN	neural network
NPV	net present value
OCV	open circuit voltage
OGV	ocean-going vessels
P2D	Pseudo 2-dimensional model
PDE	partial differential equation
PHES	plug-in hybrid electric propulsion system
PM	particulate matters
PMC	model predictive control
PMP	Pontryagin Minimum Principle
PSO	particle swarm optimization
PTI	power take-in
PTO	power take-off
RC	resistor-capacitor
RL	reinforcement learning
RMSE	root-mean-squared error
SA	simulated annealing
SCR	selective catalytic reduction
SEEMP	ship energy efficiency management plan
SEI	solid-electrolyte layer
SOC	state of charge
SOH	state of health

SPM	single particle model
SQP	sequential quadratic programming
TOC	total ownership cost
UC	ultracapacitor
ULSD	ultra-low sulphur diesel
UVic	University of Victoria

Nomenclature

Q_{max}	the maximum capacity of battery
Q_{rated}	the rated capacity of battery
V_{meas}	measured battery voltage
V_{sim}	simulated battery voltage
V_{oc}	battery open circuit voltage
R_i	battery inner resistance
R_1, R_2	resistance in battery RC circuits
C_1, C_2	capacitance in battery RC circuits
V_i, V_1,V_2	the voltage of inner resistance and two RC circuits
V_t	terminal voltage (or output voltage)
I	current
t	time
t_o	the initial time
t_f	the end of time
i	the time step
Z	the impedance
α	coefficient of SOC
j^{Li}	microscopic Li ions flow rate
δ_n, δ_p, δ_{sp}	the thickness of negative, positive electrode and separator
A	the electrode surface area
α_a, α_c	the anodic and cathodic charge transfer coefficient
a_s	the active surface area per electrode unit volume
R	the ideal gas number
F	Faraday’s number
η	overpotential
ϕ_s, ϕ_e	the solid and electrolyte potential
U	the equilibrium open circuit potential
c_s	ion concentration in solid phase particle

$c_{s,max}$	the maximum solid concentration
j_0	the exchange current density at the equilibrium state
k	the reaction rate
c_e, c_{se}	the ion concentration in the electrolyte and SEI
D_s	the solid phase diffusion coefficient
r	the particle radius
c_s^{avg}	the average value of total ions installed in the solid particle
V	the volume of solid particle
SOC	state of charge
θ_n	the percentage of the actual concentration compared to the maximum concentration
$\theta_{100\%}$, $\theta_{0\%}$	theoretical maximum and minimum concentration percentage
D_e^{eff}	the effective electrolyte phase diffusion coefficient
ε_e	the electrolyte phase volume fraction
t^0	the transference number
R_f	the film resistance inside the cell
$\phi_{s,p}, \phi_{s,\mathrm{n}}$	the solid phase potential at the positive electrode (cathode) and the negative electrode (anode)
Q_{loss}	battery capacity losses
E_a	the activation energy
A, B	the coefficients in the battery life prediction model
z	the exponent of time in the battery life prediction model
T	temperature
A_h	battery throughput discharge capacity
N	battery cycling numbers
DOD	battery depth of discharge
C_{rate}	battery current rate
m_{fuel}	mass of engine fuel consumption
$P_{eng,t}$	the engine power output at time t
$BSFC_P$	the brake specific fuel consumption at corresponded power P

E	engine emissions
EF_P	the emission factor at power P
EF_{SO_x}	the emission factor for SO_x
$S\%$	the sulphur content of the marine fuel
LCC	life cycle cost
C_{cap}	capital cost
C_{ope}	operational cost
C_{resd}	residual cost
NPV	net present value
C_t	the net cost in year t
N_t	total lifetime in year
r	the annual discount rate/inflation rate
C_{eng}	engine cost
C_{buk}	bunkering system cost for NG-fueled engines
C_{ess}	battery ESS cost
C_{hyb}	hybridization and electrification cost
C_{chag}	charging facility cost for plug-in hybrid propulsion systems
C_{rin}	reinvestment cost for battery replacement
P_{eng}	engine power
E_{ess}	battery ESS energy
p_{eng}	price of engine
p_{ess}	price of battery ESS
L_{bat}	lifetime of battery
k_t	the battery replacement frequency
C_{energy}	total energy consumption cost
C_{maint}	engine maintenance cost
C_{fuel}	marine fuel cost
p_{fuel}	price of marine fuel
m_{fuel}	total mass of consumed fuel

C_{elec}	electricity cost
p_{elec}	price of electricity
e_{elec}	total charged electricity from grid
p_r	price for the battery's remaining value
Q_r	battery remaining capacity
x	the direction along battery thickness from anode to cathode
x_p	the plant design variable
h, g	upper level equality and inequality constraints
$u(t)$	control variable
$x(t)$	system state variable
Ψ, η	lower level equality and inequality constraints
x_0	the initial state value
$x_{up} \in X_{up}$	upper level decision variable and decision space
$x_l \in X_L$	lower level decision variable and decision space
F_{up}	upper level objective functions
f_{low}	lower level objective functions
$G_k, k = 1, \dots, K$	upper level constraints
$g_j, j = 1, \dots, J$	lower level constraints
$c \in C$	lower-level control variable and control space
$s \in S$	system state variable and state space
c^*	the global optimal control policy
J	the multi-objective cost function
a	the weighted factor for each objective
K	the scaler

Acknowledgments

I would like to express my sincere gratitude to my supervisor, Prof. Zuomin Dong, for his close guidance and unremitting support during my PhD journey. His wise and unique perspectives have inspired me in solving complicated engineering problems on both the automobile and marine clean transportation research.

I also want to thank all of my colleagues in the UVic clean transportation team for their valuable advice and discussions, especially Miss. Yuqi Tong for her assistances in providing and preparing battery experimental data, Dr. Huachao Dong for helping construct surrogate-model based optimization algorithms, and Anthony Truelove for sharing marine knowledge and providing valuable editorial advice. I am extremely thankful to my committee members for their time and effort in reviewing this work.

Finally, I would like to say thank you to my family, without whose support and encouragement this work would have never been done. I love you all for everything you have done for me.

Dedication

This dissertation is dedicated to my husband Keda and our daughter Jean. You have enriched my life.

Chapter 1 Introduction

1.1 Motivation

1.1.1 Background

Today, the marine industry is facing the most challenging emission standards in the world. Maritime transportation has carried more than 80% of the world trade which emitted about 2%-3% global CO_2, 10%-20% NO_x, and various other pollutants [1]. Under the high pressure of keeping the global average temperature rise below 2ºC above pre-industrial levels in this century [2], the International Maritime Organization (IMO) has taken a crucial step and decided to reduce the shipping CO_2 to half of their 2008 levels by 2050 [3]. Specifically, the IMO International Convention for the Prevention of Pollution from Ships (also known as the MARPOL, as an abbreviation of marine pollution) has listed detailed restrictions for marine pollutions. Annex VI of MARPOL was put into effect on 19 May 2005, with the aim of gradually reducing greenhouse gases (GHG) emissions and harmful pollutants from ships in defined emission control areas (ECA) [4].

Emissions from increased shipping activities have caused many problems for both the environment and human health. More stringent regulations have been made by IMO to restrict specific air contaminants emitted by near shore ship operations in the ECAs to avoid harmful impacts for humans. Those specific contaminants include sulphur oxides (SO_x, including mostly SO_2 and some SO), nitrogen oxides (NO_x, include NO_2 and NO,) and particulate matters (PM), all of which can cause potential heart diseases, lung diseases and cancer. The restriction of SO_x emissions is achieved by limiting the sulphur content of the fuel oils used in both main and auxiliary engines onboard. Currently, the sulphur content in marine fuels used in ECAs is limited to 0.1% (i.e. 1000 ppm), which is 35 times lower than that of outside ECAs. The NO_x emission from ship engines larger than 130kW must meet required limits corresponding to its construction date and engine speed. New ships built after 2016 are restricted to emit NO_x between 2 and 3.4 g/kWh accoring to the engine speed, which is about 5 times lower than engines built before 2000. The energy efficiency design index (EEDI) and ship energy efficiency management plan (SEEMP) are adopted to encourage ship operators to improve ship efficiency and reduce emissions by employing new technologies [5].

The west coast region of Canada has very prosperous shipping activities among various islands in British Columbia (BC). As one of the largest passenger ferry companies in the world, BC Ferries owns 47 ports of call and operates more than 500 sailings every day in BC, providing necessary transportation services and feeder services to different island communities. The Port of Vancouver is the largest port in Canada, facilitating 27 major marine cargo terminals which receive over 3,100 ocean-going vessels (OGVs) every year [6]. It has been reported in Canada's Air Pollutant Emission Inventory [7] that ship-emitted SO_x and NO_x are the main contributors in the transportation sector of BC. The activities of shipping near the coastal area of BC are within ECAs and must obey the emission standards issued by IMO.

Under such conditions, this research intends to design a more environmentally friendly solution for the marine industry, based on the collaboration project between the University of Victoria (UVic) and some ship companies in BC, Canada. Recently, various solutions have been proposed to reduce marine emissions, which can be categorized into three main strategies: (i) using low sulphur content fuels; (ii) using after-treatment technologies for exhausted gases; (iii) adopting new technologies such as hybrid and electric propulsions.

First, low-sulphur distillate oils currently used in the ship industry include marine diesel oil (MDO) and marine gas oil (MGO). The convention marine fuel is the heavy fuel oil (HFO, also known as residual fuel oil) and has 3.5% sulphur content. The MGO lowers this value to about 0.1% that can greatly reduce total SO_x emissions. Moreover, vessels operating on the inland waters of Canada and The United States are required to use ultra-low sulphur diesel (ULSD), which has a sulphur content of only 0.0015% (or 15 ppm) [8]. However, the lower the sulphur content, the more expensive the fuel cost. The price of MGO is more than double that of HFO, increasing about $11 CAD per cargo tonne [9]. As such, liquefied natural gas (LNG) has become more and more popular in the marine industry due to its negligible sulphur content and lower price. Many groups have conducted feasibility studies into using LNG-fueled vessels, and have investigated the perspectives and challenges with respect to the legal, economic and technological factors [10, 11]. More and more LNG-fueled vessels are operating worldwide, with reported lower CO_2 emissions and less operational cost [12].

Second, the after-treatment of exhausted gas has been widely adopted to reduce heavy emissions, especially in those conventional vessels using cheap and dirty HFO. Ships can install scrubbers to reduce SO_x and PM, and use selective catalytic reduction (SCR) or exhaust gas recirculation (EGR) for NO_x cleaning. The combination of using scrubbers with SCR or EGR provides an effective solution to fulfil the emission requirements in ECAs. The main advantage of using after-treatment technologies is that it can cooperate with the existing fuel system to meet emission standards and use cheap fuels. However, it also increases the investment cost for installing and maintaining the equipment.

Third, hybridization and electrification technologies have been used in ship propulsion systems to improve efficiency and reduce carbon emissions. These systems involve additional cleaner power sources and provide more flexible configurations. By disconnecting the engines with the propellers, main engines can operate at higher efficiency area when needed, and store surplus energy in rechargeable energy storage system (ESS). Renewable energy technologies, such as rechargeable battery ESS, ultracapacitor (UC), fuel cell, and flywheel, have been deeply examined as potential prime movers [13]. Among them, lithium-ion (Li-ion) battery ESS presents as the most promising technology considering energy density, cost, and reliability. The hybrid configuration of powertrain systems enables more flexible control and higher operational efficiency [14]. Unlike conventional mechanical propulsions that only use internal combustion engines (ICE), hybrid powertrain systems adopt a rechargeable battery ESS and electric motors to partially or fully substitute ICE in certain conditions. Preliminary studies of applying hybrid electric technology to different vessels have shown great emissions reductions and fuel savings compared to the original ones [15-17].

Among the aforementioned possible solutions to solve ship emission problems, taking hybrid electric technology and using low-sulphur content marine fuels appear more attractive. The cost and performance evaluation of using NG-fueled engines versus ULSD-fueled engines is currently a hot topic in the marine industry. Moreover, there have been many successful experiences in the automotive industry with using hybrid technologies to substitute conventional vehicles, which can be adopted to benefit the marine industry as well. However, the flexibility of hybrid powertrain systems raises additional difficulties in system design and optimal energy management. The special characteristics of Li-ion batteries require advanced control logics and induce uncertain performance degradation during usage. It is therefore of great interest to investigate the design and control of hybrid electric marine propulsions with Li-ion battery ESS, and compare the performance of using NG-fueled engines vs. diesel engines.

1.1.2 General Review

Hybridization and electrification are considered effective methods to improve system efficiency and reduce emissions from both land- and water- based transportations [18, 19]. Hybrid electric powertrain systems normally include an ICE, a large battery ESS, electric machines (generators and motors) and power electronics[19]. Commonly used hybrid powertrain configurations can be classified into series, parallel, and series-parallel (or power-split) hybrid systems [20]. Depending on their configurations, various gear sets and gear reductions may also be needed. All electric ships are also achievable if an integrated electric power system is built so that all the energy in hybrid configurations is transferred into electricity. The application of hybrid marine propulsion systems has been reviewed in many studies [19, 21, 22]. In conclusion, the main advantages include

- providing more flexible operation;
- increasing the system redundancy;
- improving engine fuel economy by optimizing its operation conditions;
- reducing fuel consumption and air emissions;
- canceling auxiliary engine generator sets (Genset) by providing electricity via ESS;
- reducing engine operational time and maintenance cost.

In hybrid marine propulsion system design, the main challenges are the component sizing and the energy management of the main power sources–engine and battery ESS. The design of other components, such as electric machines and power electronic converters, are directly related to these two components.

NG-fueled engines create both opportunities and challenges for the marine industry. As discussed, LNG is a clean and non-sulphur fuel. Exhausted emissions such as SO_x and NO_x can be negligible if using LNG engines. Natural gas consists of more than 90% of methane (CH_4). The high hydrogen to carbon ratio of CH_4 implies lower CO_2 emissions and higher water vapor. Changing engine fuel from diesel to natural gas can significantly reduce GHG emissions and air pollutants [23]. When natural gas is cooled to -162ºC, LNG is obtained with only 1/600th volume compared to the original gas. LNG is more favorable in transportation due to its reduced gas volume, which makes it efficient to store and transport. NG-fueled engines normally can be categorized as dual-fueled (with diesel pilot) compression-ignition engines and lean-burn spark-ignition engines. Dual-fueled LNG engines have more flexibility to use either natural gas or diesel fuel. Suppliers such as Wärtsilä and MAN have developed mature dual-fueled LNG engines. Lean-burn ignited LNG engines use a spark plug to ignite the natural gas/air mixture. Their suppliers include Rolls-Royce and Mitsubishi. Currently, there are 76 LNG-fueled vessels in operation worldwide (excluding LNG carriers) [24]. Ship companies in Canada are on the leading edge of transferring their vessels to LNG-fueled ones. BC Ferries has updated two of the 548-foot-long Spirit-class ferries to LNG-fueled vessels. They also adopted three new Salish-class ferries that are capable of running duel-fuel (either LNG or ULSD). Robert Allan Ltd. has developed LNG-fueled (and LNG-diesel dual-fueled) escort tugs with powerful bollard pulls [12]. Several studies have discussed the environmental and economic benefits of using NG-fueled engines in different types of ships [11, 25, 26].

However, these studies are all based on conventional vessels with mechanical propulsion systems. It is of great interest to discover the potential benefits of adopting NG-fueled engines in hybrid marine propulsions.

Li-ion batteries are the most widely applied type of ESS in hybrid powertrain systems with outstanding performance of energy and power density. They are also called “rocking-chair” batteries due to the nature of transferring, instead of consuming, the Li ions between the anode and cathode during charging and discharging processes. Even though the price of Li-ion batteries has considerably decreased in recent years, it is still very expensive compared to engines and other electrical machines[27]. Another critical problem of using Li-ion battery ESS under high power demand is the aging phenomenon caused by irreversible microscopic electrochemical reactions inside each single battery cell [28]. Materials, manufacturing, operating temperatures and other conditions can affect battery deterioration rates [29]. The performance degradation of batteries would induce capacity decay and impedance increment, eventually reducing their lifetime. In general, Li-ion battery ESS tends to have a much lower lifetime than other components (such as engines, electric machines) in hybrid powertrain systems. The requirement of replacing a battery pack would aggravate its total ownership cost. A better understanding of the battery aging process can be critical to avoid its deterioration and prolong its lifetime.

It is an urgent need to develop an accurate battery model that can quantitatively analyze its performance deterioration rate and support hybrid powertrain system design. Battery performance degradation and life heavily depend upon the actual use pattern and operating temperature. The control algorithm of hybrid systems plays an important role in extending battery lifetime by avoiding harsh charging and discharging at high current rate. An accurate Li-ion battery model is crucial in developing optimal energy management system. Three main types of modelling methods are mostly used in the literature [30-32]: the empirical model, the equivalent circuit model, and the electrochemical model (or "Doyle-Fuller-Newman" model [32]). Depending on complexity, accuracy and computational time, these models have been used for different purposes. A more specific review on battery modelling methods will be discussed in Chapter 2.

The integrated design and control of hybrid electric powertrain systems are complicated problems. For power systems with only one type of energy source, such as pure mechanical or pure electric architecture, there is no possibility to develop an advanced energy management strategy. Hybrid propulsion systems, on the other hand, offer more freedom for power control due to the increased additional power source. Therefore, the intelligent control strategy must be decided in the energy management system to take optimal decisions of power distribution between the engine and battery ESS. Heuristic-based and optimization-based control strategies have been deeply investigated in the automotive industry for hybrid electric vehicles. However, the marine industry still lacks sufficient study of optimal control for hybrid propulsions. Most hybrid vessels take a rule-based control strategy [33, 34]. A few investigated the equivalent consumption minimization strategy (ECMS) for optimal hybrid tugboat control [35]. Moreover, previous studies of hybrid marine propulsions[14, 19] [33-35], to the best of the author's knowledge, did not consider the combined system design and control optimization.

The integrated design and control optimization of hybrid marine propulsions must solve the component sizing optimization and energy management strategy optimization simultaneously in its searching algorithm. Most studies on hybrid electric vehicle (HEV) design focused on optimal component sizing with pre-determined control rules [36], then find the global optimal control strategy based on selected (not necessarily optimized) power components [37]. The problem complexity can be greatly increased when encountering two jointed intricate optimization problems. Fathy, et al. [38] discussed the combined plant and controller design optimization problem on coupled conditions, in which the nested and simultaneous optimization strategies are proven to find the global optimum. In recent years, more and more studies take a step forward to solve the combined hybrid powertrain system component design and control in a nested framework, with the top level optimizing component sizes and the bottom level searching for the optimal control rules [39, 40]. It is therefore a great time to examine the possibilities of solving the integrated hybrid propulsion system design and control optimization for marine applications.

It is usually computationally expensive to solve the complex integrated design and control optimization problems. Population- and/or evolutionary-based heuristic optimization algorithms are commonly adopted to solve the design problem, such as particle swarm optimization [41], genetic algorithm [42]. The model-based optimal control strategies for both on-line and off-line implementations in a PHEV are discussed in [20]. It is usually cost a heavy computational burden in searching for global optimal control rules. For those types of work, a surrogate model (or meta-model) can be developed as an approximation of the actual simulation model with reduced computational time. Commonly used metamodeling techniques in building surrogate models, including the experimental design (or sampling methods), different types of surrogate models, and model fitting methods will be discussed in Chapter 4.

Given these circumstances, this study is motivated to develop a methodology to effectively solve the combined design and control optimization for hybrid electric marine propulsions in a bi-level, nested approach, discovering all potential benefits of using NG-fueled engines and Li-ion battery ESS. The model-based design and optimization method is introduced to support the hybrid propulsion design with detailed engine efficiency and emission models, proposed battery performance degradation model and developed hybrid energy management system model.

1.2 Define Research Goals

The main goal of this dissertation is to identify the challenges and solve the problems in optimal hybrid marine propulsion system design and control. Meanwhile, this dissertation fills the gap in modelling Li-ion batteries in the marine industry by adopting advanced mathematical models of electrochemical batteries to demonstrate their performance degradation. Finally, it draws on the experiences of hybrid powertrain system design from the automotive industry and optimization methodologies from the optimization community to solve the design and control problems. This involves hybrid propulsion system design, modelling and sizing of the key components, and the development of optimal hybrid system control strategies. The system design, in this dissertation, refers to the dimensioning of key components in hybrid propulsions. The control strategy of hybrid systems means properly distributing the power demands to different power sources to achieve less fuel consumption and emissions. The most challenging part is that the optimization of hybrid system design is coupled with the optimal control strategy development. Therefore, advanced optimization algorithms must be adopted to solve this problem. The optimized hybrid systems should obtain the best economic and environmental benefits.

In the marine industry, the propulsion system design still heavily rely on the engineering experiences due to the lack of model-based design and optimization tools. The performance degradation of Li-ion battery obviously aggravates this situation, making the sizing of battery ESS even more difficult. Therefore, this research develops an integrated hybrid marine propulsion system design platform with accurate battery performance degradation and life prediction model. It can support optimal design and control by reflecting all the economic impacts, including the initial investment cost (affected by the component design) and operational cost (affected by control decisions), to the ultimate total life cycle cost (LCC). Moreover, advance algorithms from optimization community are introduced and discussed in solving the intricate complex design and control optimization of hybrid propulsion systems. Surrogate model-based optimization methods are adopted to improve computational efficiency.

To summarize, the research goals in this dissertation include:

- build an accurate Li-ion battery performance degradation and life prediction model to support optimal energy management in hybrid powertrain systems;
- develop an integrated ship modelling platform that can support the design and control of hybrid marine propulsion systems;
- build the life cycle cost (LCC) model of hybrid ship propulsions to reflect the economic variations of powertrain hybridization and electrification;
- formulate the combined hybrid plant design and control problems as an integrated optimization problem;
- find an efficient global optimization algorithm to solve the complex optimization problem;

- implement proposed methodology on a real marine vessel to find the optimal hybrid propulsion system design.

1.3 Dissertation Organization

The arrangement of this dissertation is organized as follows. Chapter 2 develops a Li-ion battery performance degradation and life prediction model based on acquired experimental data. Chapter 3 discusses the detailed component models and control strategies of hybrid marine propulsion systems based on the integrated ship simulation platform. A LCC model of hybrid propulsions is also developed in this chapter based on collected price information for ships operating in BC, Canada. Chapter 4 proposes a surrogate model-based global optimization framework to solve the nested co-design optimization problem for hybrid propulsion system design and control. The proposed method is implemented for a harbour tugboat design case study. Chapter 5 draws conclusions and outlooks of this research.

Chapter 2 Li-ion Battery Performance Degradation Modelling

Li-ion batteries have been widely used in hybrid powertrain systems because of their extraordinary performances, massive production capability, and matured manufacturing technology. However, challenges remain in the battery cost and its performance degradation phenomena. The inevitable aging process of battery during usage will not only reduce its designed capacity, but also increase cost for maintenance and replacement. This problem will be severer in hybrid marine systems since it has much higher capacity of battery ESS than other applications (e.g., HEVs). The appropriate sizing of the battery ESS and the energy management/power control strategies depend upon the accurate prediction of battery degradation under the specific use pattern – the foundation of powertrain system design and control optimization. In this chapter, a systematical review is presented to conclude the main degradation mechanisms and relevant affecting factors. A battery performance degradation and life prediction model is developed and verified using acquired experimental data.

2.1. Review on Battery Degradation Mechanisms

The characteristics of metallic Li enable high energy and power density of Li-ion batteries [43]. The performance and degradation mechanisms of different types of Li-ion battery are highly related to the materials used in the cathode, anode, and electrolyte. Therefore a good understanding on available commercial materials and their characteristics is important for further modelling works.

2.1.1 Li-ion Battery Materials

Anode Materials

The most commonly used anode material in commercial Li-ion batteries is litigated carbon (LiC_6). Carbon material has abundant natural reserve volume therefore can offer very low price for the market. This layered crystal compound is very stable during ion's intercalating processes, providing great cycling performance. Moreover, the overpotential of LiC_6 is about 0.5V vs. Li/Li^+, which can help construct a high battery overall voltage (usually between 3 and 4.5V, depending on the cathode material). However, it has only 372 mAh/g theoretical energy density, much less than metal Li (3860 mAh/g). Therefore, LiC_6 is not very competitive in providing high energy density battery.

Lithium titanate (LTO) is another type of anode material developed in recent years. It can provide longer cycling lifetime and has higher tolerance of large current rate compared to LiC_6. With negligible volume change during Li ions' intercalation, LTO has excellent cycling performance [44]. The overpotential of LTO anode is about 1.55V against Li/Li+, which is about 3 times higher than LiC_6. This high equilibrium potential has both pros and cons, it can help avoid the formation and growth of anode solid-electrolyte layer (SEI) and reduce capacity losses, but also lower the overall battery voltage (to about 2.4V, depending on the cathode material). The theoretical capacity of LTO is only half of graphite anode (about 170 mAh/g) thus also hard to achieve high energy density.

There are many other advanced anode materials under development and not yet commercialized, such as metallic Li anode, graphene nanosheet anode, Si-based alloy anode, etc.

Metal Li could be an ideal choice as the anode material , because (i) it is the lightest metal element and offers the lowest density (0.534 g/cm^3), which are favorable for high energy density; (ii) it has the lowest reduction voltage (-3.04V vs. standard hydrogen electrode), allowing the battery to achieve a high potential. However, the charging/discharging processes can cause severe dendrite growth on the metallic Li. This poses risks in inducing battery inner short-circuit and other safety issues. It also has poor cycle performance and low Columbic efficiency. Although there has been some improvements on the stable cycling performance of lithium mental anode [45], it is hard to see its commercialization in the near future.

Graphene has been known as the thinnest and lightest compound, which are favorable for achieving high energy density. It also has the strongest mechanic structure and great electric conductivity. Graphene nanosheet (GNS) can provide large reaction surface areas and a stable structure as the anode material of Li-ion battery. GNS can improve the battery capacity and energy density through merging nanomaterials into the graphene [46, 47], but the cyclic performances and safety issues are still unsolved problems.

Silicon (Si) based anode has drawn the most attention in recent years because of its abundance, performance, and non-toxicity characteristics. It has 10 times more specific capacity than carbon-based anodes, which can provide extremely high volumetric and gravimetric capacity. However, it also has poor cyclability due to the large volume change of Si during the Li ions intercalations [48]. The nanostructured Si anode can potentially avoid the severe volume expansion. Different nanostructure design, such as nanowires, hollow nanostructures, and clamped hollow structures, have been showed in [49].

The ideal anode material should have high capacity, low potential against Li/Li^+, long lifetime, and low cost. Considering these factors, the most commonly used materials and most promising materials in the future have been compared in Table 1.

Table 1: Comparison of Anode Materials

	C	**LTO**	**Li**	**Si**
Specific Capacity (theoretical) (mAh/g) [50]	372	175	3862	4200
Potential vs. Li (V) [50]	0.05	1.55	0	0.4
Volume Change (%)	12%	1%	100%	420%
Density (g/cm^3)	2.25	3.5	0.53	2.3
Advantages	• low cost; • good cycle performance;	• long lifetime; • high cycle rate;	• high energy density; • high voltage;	• high energy density;
Disadvantages	• low energy density	• high cost; • low voltage; • low energy density;	• dendrite growth;	• high volume expansion;

Cathode Materials

The cathode materials used in Li-ion batteries include a variety of lithium metal oxide compounds, such as the Lithium Ion Phosphate (LFP), Lithium Cobalt Oxide (LCO), Lithium Nickel Manganese Cobalt Oxide (NMC), Lithium Nickel Cobalt Aluminum Oxide (NCA), and so on. The application of these different materials highly depends on their energy density, voltage, safety, cost and many other factors [43, 48, 51].

$LiCoO_2$ (or LCO) is one of the earliest commercialized cathode materials. It has very high theoretical specific capacity and can provide high voltage [43, 52-54]. The major issue of LCO is its low thermal stability due to the layered structure. Thermal runaway can be observed at about 200ºC, where exothermic reaction happens between released oxygen from LCO and other organic materials in the battery. The high cost of Co is also a concern for the large-scale application. Structure distortion and deterioration of LCO can be observed under high cycle currents.

$LiNiO_2$ (or LNO) has similar characteristics of LCO, which also has layered structure and high specific energy capacity (about 275mAh/g in theory and 150mAh/g in practice). The synthesis process of LNO usually gains over-stoichiometric phases of extra Ni ions, hence, introduces unstable factors and causes low stability, poor cycling performance and rapid capacity fading.

$LiMnO_2$ (or LMO) battery, compared to the layered structure of LNO and LCO, is well known for its three-dimensional spinel structure that is easily for ions' insertion and extraction. The excellent reversibility inside spinel LMO makes its practical specific capacity almost the same as LNO and LCO, even though its theoretical capacity is only half of them. The advantages also include lower internal resistance, safer thermal stability, cheap cost and non-toxicity for environment. Drawbacks include low specific energy density, materials dissolution upon cycling, and poor cycle life.

$LiFePO_4$ (or LFP) has an olivine structure, which is very stable and can provide superior cycling performance. The strong bonding of oxygen in phosphate group makes it stable to resist thermal runaway, thus, have a safe performance at high temperature. However, the theoretical specific capacity is not very high. It also has a flat potential platform of 3.4V vs. Li/Li^+. LFP has been largely used in electrical vehicles (EVs) and HEVs in the automotive industry.

To gain all the strengths from LNO, LMO and LCO, a combination of these three has been invented. Ni-based materials have higher energy density, low cost, and longer lifetime than Co-based ones. Mn-based systems benefit from the spinel structure and can achieve a low internal resistance and high voltage. Doping small amount of Co, Mn or Al into Ni-based materials can greatly improve the overall performances and gain all the advantages. The combinations of these metals are able to provide high energy and power density with the stable thermal behavior. $LiNiMnCoO_2$ (or NMC) and $LiNiCoAlO_2$ (or NCA) are two recently commercialized and widely used cathode materials in Li-ion batteries. They have been gradually substituting conventional LFP or LCO in the hybrid powertrain systems in transportation area. The property of NMC-type battery is determined by the proportion of Ni, Mn and Co in its mixture. Usually the common proportions are NMC(1:1:1), NMC(5:3:2), NMC(6:2:2) , or NMC(8:1:1) [50]. The trend is to reduce the usage of expensive material Co and increase the proportion of Ni to have a lower price.

NMC and NCA are both Ni-based material with high specific energy, low internal resistance, and long lifetime. They have similar characteristics. Normally the proportion of Al in NCA is very small, such as the $LiNi_{0.8}Co_{0.15}Al_{0.05}O_2$. NCA is reported to have higher specific capacity (about 300Wh/kg), however, it can have unstable thermal behavior at elevated temperatures. Battery manufacturers are producing NMC and NCA based on their own considerations. For example, LG Chemicals has cooperated with General Motors to provide batteries for their EVs with NMC811, NMC622, and NMC712 types of Li-ion batteries. Panasonic, on the other hand, produces NCA type of batteries for Tesla EVs. Battery manufacturers who produce NMC batteries include (but not limited to) LG Chemicals, Samsung SDI, SK Innovation, CATL, etc. Generally, NMC811 cathode is reported to have greater cycle life and lower cost than NCA.

Conversion cathode materials, such as fluorine and chlorine compounds, sulfur and lithium sulfide, or selenium, usually have high theoretical specific and volumetric capacities. However, they normally suffer from poor cycling performance, large volume expansion and unwanted side reactions [48]. These type of materials have not yet been commercialized; therefore, will not be considered in the application of hybrid powertrain system design.

The comparisons of these commercialized cathode materials have been showed in Table 2. Recent studies on advanced battery materials showed that the NMC-based cathode and silicon alloy-based anode will be the most promising type of Li-ion batteries with higher energy density and decreased cost [50]. However, the LFP cathode with carbon-based anode battery is still one of the most popular types of battery at present, mainly because of its superior safety performance. LFP battery has been widely applied in many HEVs and EVs, therefore, it was tested and measured to help construct battery performance degradation model in this study.

Table 2: Comparison of Commercialized Cathode Materials

	$LiMn_2O_4$ (LMO)	**$LiFePO_4$ (LFP)**	**$LiCoO_2$ (LCO)**	**NMC**	**NCA**
Theoretical Specific Capacity (mAh/g)[48]	148	170	274	280	279
Average Voltage (V) [48]	4.1	3.4	3.8	3.7	3.7
Structure	Spinel	Olivine	Layered	Layered	Layered
Lifetime	*	***	**	***	**
Cost [50]	*	**	**	***	***
Advantages	• high thermal stability;	• high safety;	• high capacity;	• high energy/power density; • long lifetime; • low internal resistance; • low cost;	
Disadvantages	• low capacity; • low lifetime;	• low energy density;	• poor stability; • high cost;	• low thermal stability at high temperature; • NMC811 has higher cycle life and lower cost than NCA;	

Electrolytes in Li-ion batteries play an important factor to build stable electrochemical windows for battery reductions and oxidations. Commercial electrolytes normally include organic solvents, Li salts and some additives. Experiments have showed that the stable voltage range of the liquid electrolyte is from 0.8V to 4.5V vs. Li/Li^+. Apparently, the most widely used carbon-based anodes (0.5V vs. Li/Li^+) are outside this range. Hence, electrochemical reactions will happen between carbon-based anodes and organic solvents spontaneously and form a solid-electrolyte interface (SEI) along the active anode surface. After the SEI is built up, it acts as a barrier to stop further corrosions from electrolytes. The SEI formation and growth can greatly affect battery performance degradation. On the one hand, the SEI can protect the active anode material and facilitate more stable cycling performance. On the other hand, it also consumes cyclable ions and increases the impedance, which deteriorates the cell performance. This characteristic of SEI is the unique feature of using carbon-based anode material.

2.1.2 Battery Performance Degradation Mechanisms

The performance deterioration of Li-ion batteries is an inevitable process due to the irreversible electrochemical side reactions. Temperature, current, and battery state of charge (SOC) are all relevant to the degradation rate. Depending on if the battery is in a working or storage situation, the degradation mechanisms perform differently on the anode and cathode materials.

Cyclic capacity decay starts right after the first charge/discharge process. As discussed, the formation of SEI on the anode surface not only consumes available ions but also increases battery inner resistance. A sharp capacity decay can be observed at the negative electrode at the beginning of battery life [55]. To solve this problem, usually more than adequate Li ions and carbon materials are provided to improve overall cycling efficiency. However, extra anode material on the negative electrode makes battery performance limited by the positive electrode. Bourlot, et al. [56] compared fresh batteries with 1.5 years-aged ones and showed that the SEI layer on negative electrode stayed relatively stable while binder dissolutions and active metal Li were found on positive electrodes, which implies positive electrode limited cycling performance. Furthermore, constantly periodic cycling may aggravate this situation, causing SEI layer becoming harder and thicker. Ramadass, et al. [31] showed the battery film resistance increases with the cycling numbers. The losses of available lithium ions are the main reason for cyclic capacity decay. The study in [57] showed that battery cyclic capacity fading has a direct link with the thickness of SEI layer. Moreover, microscopic side reactions happen all the time and cause compound structure deformation, active materials wearing and many other damages to battery materials [56].

Many factors can affect battery cyclic performance deterioration. Temperature is the most important one. When battery is cycled at the elevated temperature (e.g., higher than 40 ºC), it can cause structure exfoliations of cathode materials [58]. If a battery is charged at low temperature (e.g., less than -20ºC), it can cause metal Li plating along the anode materials. The formation of dendritic Li not only decreases battery capacity but also induces potential risks of inner short circuit [59]. The charge and discharge current rate (C-rate) is another important factor. A 1C discharge rate means all the energy inside a battery can be completely released in 1 hour. If battery is discharged at higher current rates, large amounts of Li ions will accumulate on the anode surface in a short time. If the diffusion process of ion is restricted (or limited by the characteristics of battery materials), dendrite

Li might be generated. Low C-rate, on the other hand, is more favorable for a safer performance and longer life. The battery SOC indicates the percentage of remaining energy that battery can release compared to the rated capacity. The variation of SOC in a cycle, sometime referred as the depth of discharge (DOD), can also affect battery cyclic performance. The higher the DOD, the more throughput capacity the battery has to provide. In another word, higher DOD means harsher usage of the battery therefore can accelerate the degradation [60].

When battery is in storage or on the rest, chemical reactions still happen due to the thermodynamic instability of battery materials. Side reactions, mainly on negative electrode due to spontaneous reactions between the LiC_6 and electrolyte, are believed to be the main reason of calendar life fading [6]. The reaction rate and intensity are highly related to material properties, storage temperature, and battery open circuit voltage (OCV). The OCV is determined by the distribution of ions on the cathode and anode; therefore, it has a direct connection with battery SOC. If the battery is stored at a higher temperature, it will facilitate secondary reactions and speed up the corrosions [61]. Mild or low temperatures, on the other hand, can depress the reaction. In general, the storage temperature is more critical than storage voltage (or SOC) level for calendar life degradation [61].

In conclusion, the main consequences of battery performance degradation include the capacity decay and impedance increment. The capacity decay is mostly due to the SEI formation on the anode and side reactions on the cathode, while the battery impedance can be affected by the material disordering and decomposition as well as the formation of SEI. Specifically, main reasons for carbon-based anode deterioration are SEI formation and growth, corrosion of active carbons, lithium metal plating at low temperatures or high rate currents, etc. As for lithium metal oxide cathodes, wearing of active materials, compound structure changings, and electrolyte dissolving are relevant to the performance decay. Generally, cyclic aging is much severer than storage aging. To reflect all the influences by the former discussed factors, battery capacity losses (Q_{loss}) can be expressed as a function of current rate (C_{rate}), DOD, temperature (T) and total operational time (t).

$$Q_{loss} = f(C_{rate}, DOD, , T, t) \tag{1}$$

2.2. Battery Performance Degradation and Life Prediction Model

Based on the previous discussions, a battery performance degradation and life prediction model is proposed in this section to capture the battery dynamic behaviors and reflect the deterioration rate. In which, the performance model calculates battery voltage, SOC, and other characteristics in each charge/discharge cycle. The life prediction model estimates the accumulated performance deterioration based on historical usages and gives a prediction of remaining lifetime under given load profiles.

Different modelling methods are discussed in this section, including previously mentioned equivalent circuit model, the electrochemical impedance spectroscopy model, single particle model, and empirical model. The battery performance degradation model is developed and validated by the 18Ah $LiFePO_4$ battery cycle-life tests. As discussed in previous section, $LiFePO_4$ has superior safe performance especially at elevated temperatures, therefore, has been widely used in many hybrid powertrain systems. And it can certainly be used in the marine industry due to its lower price and good cycling performance.

2.2.1 Li-ion Battery Cycle-life Experiment Data

The specifications of tested $LiFePO_4$ battery are listed in Table 3. This commercialized battery was purchased and tested in the State-assigned Electric Vehicle Power Battery Testing Center in Beijing, China.

Table 3: $LiFePO_4$ Battery Specification

Rated Voltage	3.2V
Capacity	18 Ah
Weight Energy Density	120 Wh/kg
Charge/Discharge Cut-off Voltage	3.6V/2.5V
Standard/Fast Charge Current Rate	1C/2C
Continuous/Max. Discharge Currant Rate	3C/15C

The open circuit voltages (V_{oc}) of this battery under charge and discharge conditions are plotted in Figure 1.

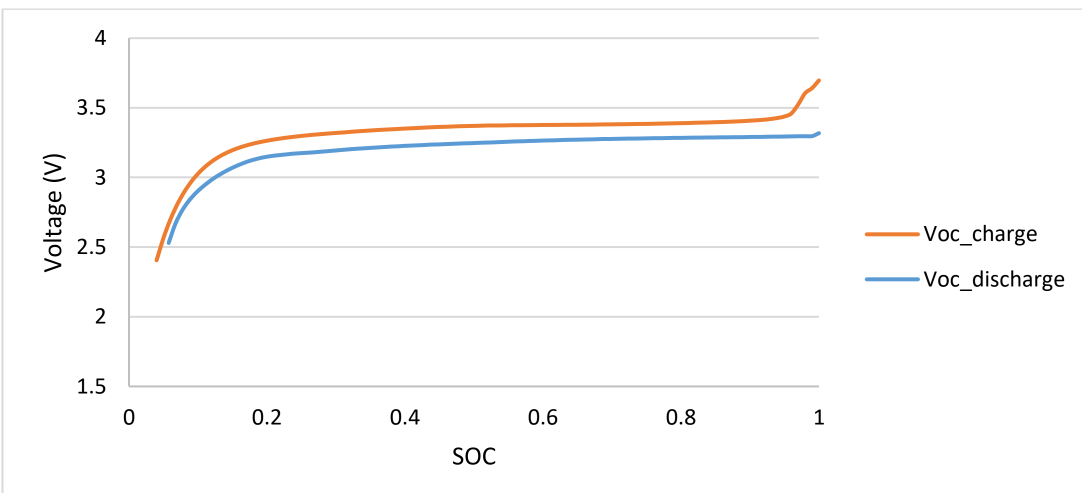

Figure 1: Battery Charge and Discharge Open Circuit Voltage

The main purpose of battery cycle-life tests is to measure battery performance degradation characteristics through constant periodically cycling. Specifically, the battery is charged and discharged under pre-defined current profiles repeatedly and its voltage, total charging energy and discharged energy are measured. When its capacity reduces to the 80% of normal capacity, it is recognized as a dead battery and is not suitable for further usage in transportation application. The cycle-life experiments can be divided into two groups:

- cycling tests: battery is charged at 1C and discharged at 2C
- capacity tests: battery is charge and discharged at 1/3C

Cycling tests and capacity tests serve different purposes, thus, having distinct cycling profiles. Cycling tests are usually under higher C-rate to save experimental time. To fully measure the available battery capacity, capacity tests were performed after every 25 cycles under slow charge/discharge process. The cycle-life test profile is showed in Figure 2.

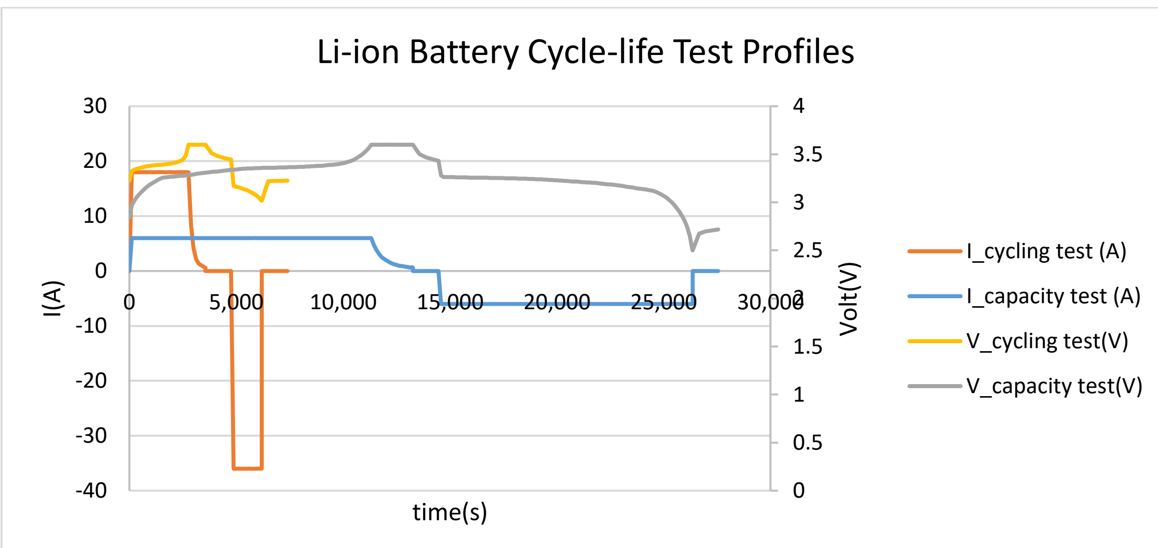

Figure 2: Li-ion Battery Cycle-life Test Profile

The charging protocol is the standard constant current-constant voltage method (CC-CV). For the capacity test, the battery is charged at 1/3C current rate until it reaches the maximum voltage (which is 3.6V in this case). Then it will change to the constant voltage charge at the maximum voltage until the charging current reaches to 0A. The discharging protocol is much simpler. The battery is discharged constantly at designed current rate until its voltage reaches to the cut-off voltage (in this case 2.5V). To ensure a safety testing environment, the battery was placed in an environmental chamber at 20ºC.

It is quite time consuming to perform thousands of such cycling tests. So far, it has been cycled about 2000 times and some of the representative curves are plotted in Figure 3.

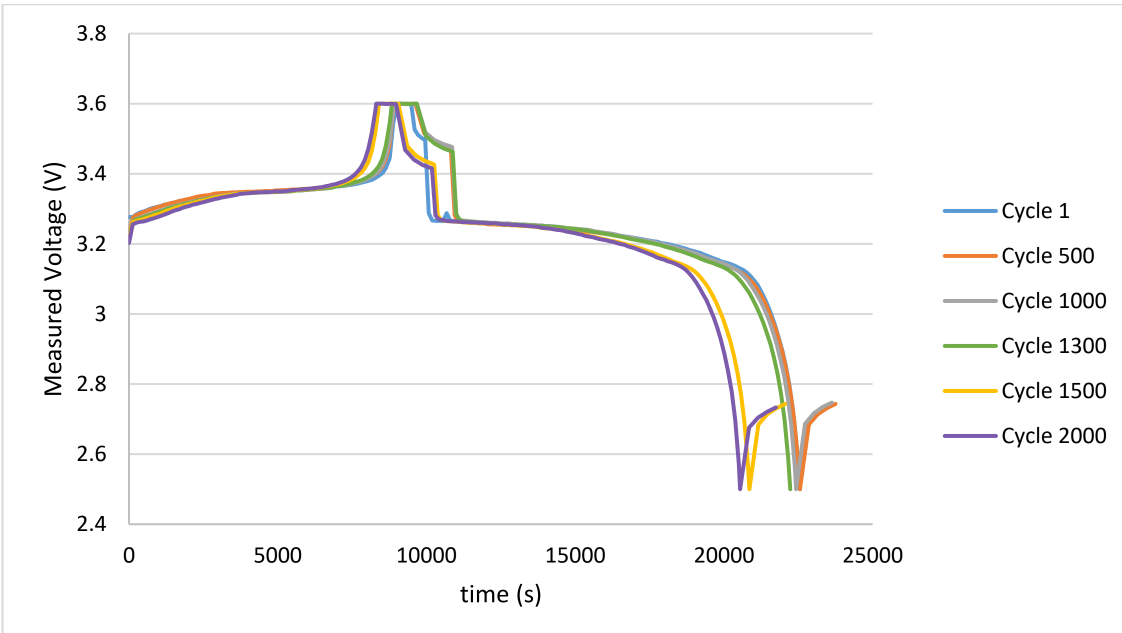

Figure 3: Battery Cycling Curves

Two significant features can be observed from the curves showed in Figure 3. First is the reduced experimental time when the cycling number increases. This indicates that the maximum capacity (Q_{max}) is decreased thus less energy can be put into the battery. The second feature is the variation of measured battery voltage in different cycles. Under the same charge/discharge protocol, the voltage can only be influenced by the battery inner resistance and/or capacitance. The measurement data have clearly led the conclusions that have been discussed in the previous section: the performance degradation can cause capacity decay and resistance increment.

The measured battery capacity also verifies the deterioration when the cycling number increases, as showed in Figure 4.

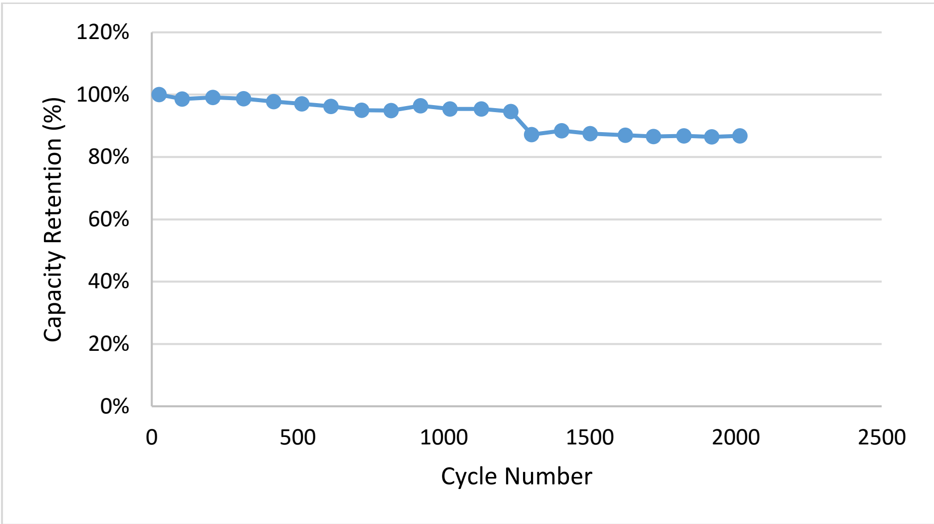

Figure 4: Measured Battery Capacity in Different Cycles

These acquired battery data will be used to build the battery performance degradation model. 80% of the measured voltages under charge/discharge current profile are used to build battery performance model and obtain model parameters' value, while the rests are used for validation. Different battery modelling methods have been compared in this study. The simulated battery voltage from developed battery models has to be validated to find the most appropriate model for the hybrid system design and modelling. The flowchart of battery modelling and validation process is presented in Figure 5.

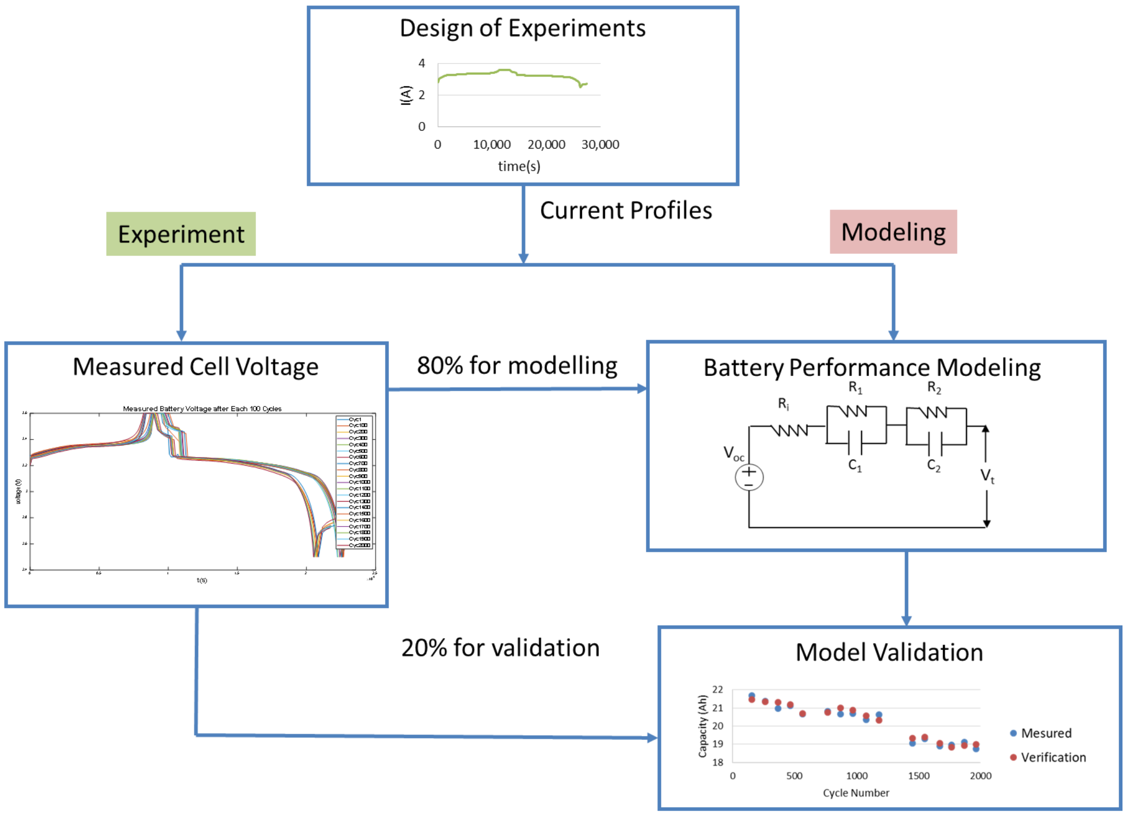

Figure 5: Flowchart of Building the Battery Performance Model

2.2.2 Battery Modelling Methods

The battery performance decay, as denoted in the measurement data, can be mathematically modelled in different approaches, either model-based or data-driven machine learning-based approach [62-66]. This section will discuss both the advantages and disadvantages of three model-based battery modelling methods, and use acquired battery experimental data to get the modelling results and compare their accuracies.

<u>(1) Equivalent Circuit Model</u>

Equivalent circuit model adopts resistor-capacitor (RC) circuits to simulate the concentration polarization and electrochemical polarization during the battery charge/discharge process (also known as dual-polarization model). The physical battery is simplified as a circuit with a voltage source and several passive elements. A typical equivalent circuit model has a DC voltage source V_{oc}, an internal resistor R_i, and two RC circuits with R_1, C_1 and R_2, C_2 (as illustrated in Figure 6).

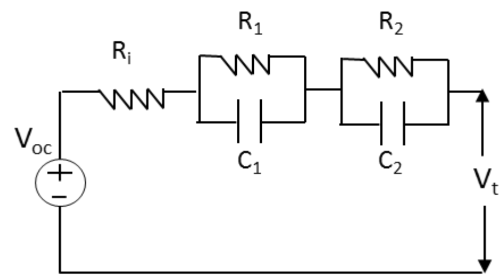

Figure 6: Equivalent Circuit Model of Li-ion Battery

The battery SOC denotes the available capacity a battery stored at this moment compared the maximum available capacity Q_{max} . It is usually calculated based on the Coulomb counting method. Assuming the discharge current is positive and charge current is negative, the SOC can be calculated as:

$$S\dot{O}C = -\frac{I}{Q_{max}} \tag{2}$$

where t_o to t_f are the initial and end of time; I is the current (A); Q_{max} is the maximum battery capacity (Ah).

The charge and discharge open circuit voltages (V_{oc}) of tested battery have been showed in Figure 1. The discharging V_{oc} can be expressed as a polynomial function of SOC and the coefficients of this function can be fitted from the data in the curves.

$$V_{OC}(SOC) = a_0 + a_1(\mathrm{SOC}) + a_2(\mathrm{SOC})^2 + \cdots, a_i \in \mathbb{R} \tag{3}$$

The charging V_{oc} curve can also be fitted using the same method. Both charging and discharging V_{oc} will be treated as polynomial functions with different coefficients when calculating the final output voltage.

The voltage drop caused by the inner resistance and two RC circuits are expressed as:

$$V_i = IR_i \tag{4}$$

$$\dot{V}_1 = -\frac{V_1}{R_1C_1} + \frac{I}{C_1} \tag{5}$$

$$\dot{V}_2 = -\frac{V_2}{R_2C_2} + \frac{I}{C_2} \tag{6}$$

where V_i, V_1, and V_2 are voltage drops caused by R_i, R_1, and R_2. C_1 and C_2 are capacitors.

The battery terminal voltage is determined by Kirchhoff laws:

$$V_t = V_{oc} - V_i - V_1 - V_2 \tag{7}$$

The level of battery performance degradation is indicated as the battery state of health (SOH). SOH compares actual maximum capacity (Q_{max}) a battery can provide at time *t* to the rated capacity (Q_{rated}).

$$SOH = \frac{Q_{max}}{Q_{rated}} \times 100\% \tag{8}$$

For a fresh battery, Q_{max} is equal to the rated capacity Q_{rated}. However, Q_{max} will be gradually decreased along the battery lifespan due to the aging phenomena. When $Q_{max} = 80\%Q_{rated}$, i.e., SOH decreases to 80%, the battery has to be replaced.

The parameters in the equivalent circuit model must be identified to simulate battery performance. In total, there are six parameter ($Q_{max}, R_i, R_1, R_2, C_1, C_2$). They can be obtained through optimization algorithms. With acquired battery test data, these parameters can be fitted by minimizing the root-mean-squared error (RMSE) between the measured voltage and model output voltage. The main objective of this optimization problem is to:

$$\min_{x} \sqrt{\frac{1}{n}\sum_{i=1}^{n}(V_{meas,i}(x) - V_{sim,i}(x))^2} \tag{9}$$

subject to: $g(x) \leq 0$

where V_{meas} is the measured output voltage, V_{sim} is the model similated output voltage. $x = [Q_{max}, R_i, R_1, R_2, C_1, C_2\ ]'$ is the set of unknown parameters. i is the time step from 1 to n. $g(x)$ is the constraint of x.

For this nonlinear objective function, gradient-based conventional optimization methods such as steepest descent method or Newton's method are not appropriate to use. Heuristic global optimization algorithms, such as genetic algorithm (GA), simulated annealing (SA) and particle swarm optimization (PSO), are often used in the literature to solve such problems [67]. Among them, GA has been used to solve this problem due to its widely application in identifying battery parameters [64, 65]. After 500 generations of searching, it converges to a global optimal result. The variations of battery maximum capacity Q_{max} and resistance R_i are plotted in Figure 7.

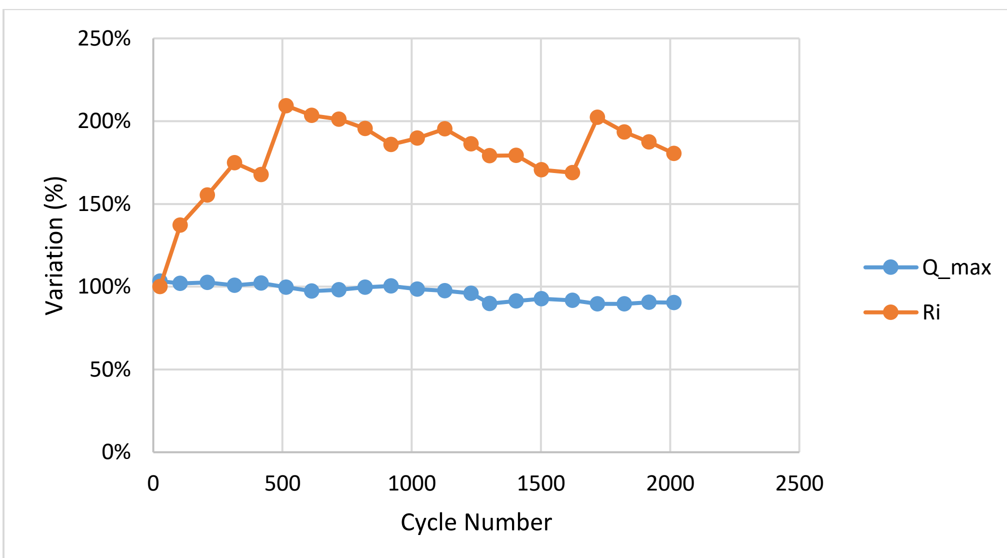

Figure 7: Variation of Battery Capacity and Resistance in Different Cycles

Based on developed battery performance degradation model, the output voltage, SOC, capacity and many other characteristics can be simulated for any given profiles. 80% of cycling data are used in model development, while the rest 20% of measurement data are used to validate the model accuracy. The simulated performance degradation results showed average 0.88% error. The validation results and errors of battery capacity variation (Q_{max}) are plotted in Figure 8.

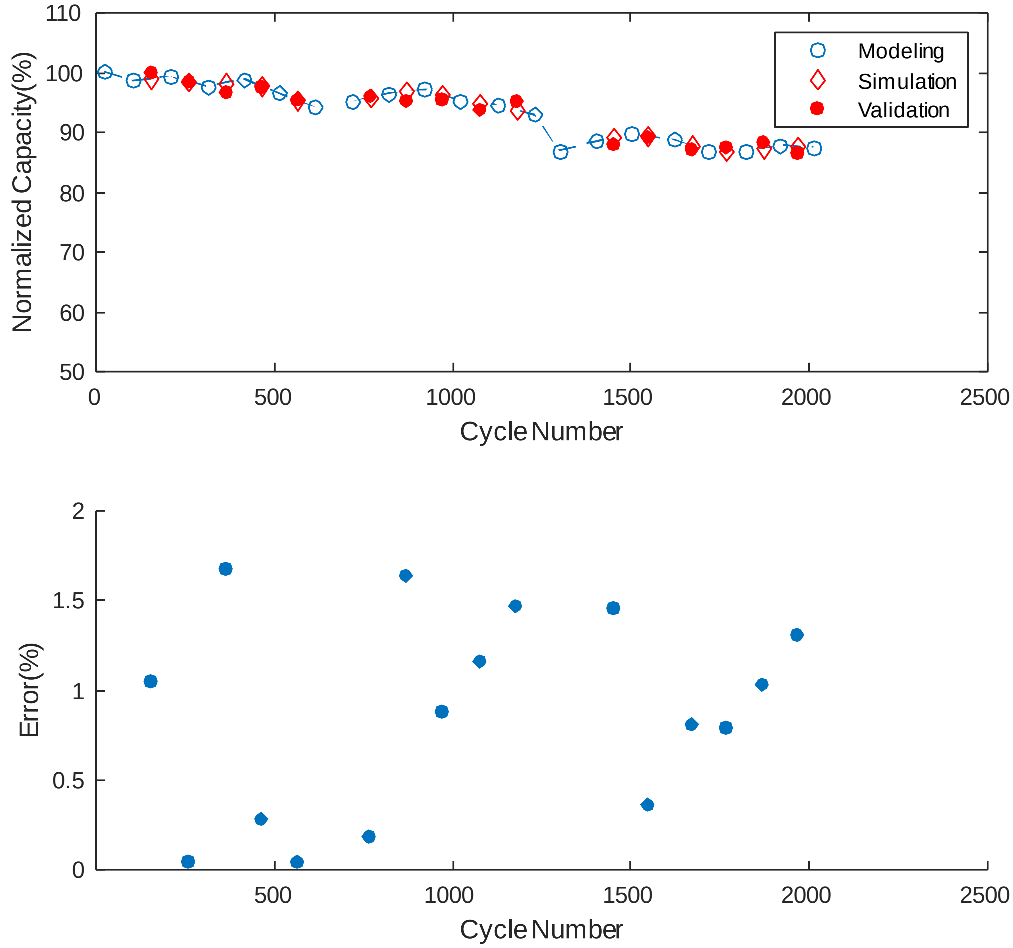

Figure 8: Validation of Battery Performance Degradation Model

The equivalent circuit built for battery simulation can also be interpreted using electrochemical impedance spectroscopy (EIS) method (or ac impedance method) [68]. EIS is a powerful tool for the analysis of complex processes of electrochemical reactions. It has been widely used to capture key characteristics of Li-ion batteries, such as revealing the influence of operating conditions and SOC on the Li-ion battery impedance [68], or studying the changes of electrode material lattice during the insertion/extraction of lithium ions [69].

EIS experiments record battery responses by applying a sinusoidal alternating current (AC) signal with wide spectrums (e.g. from 0.1 mHz to 10 kHz). At above 1000Hz, the load behaves more like a DC signal for Li-ion battery due to the large time constant of RC circuit. The battery impedance is the frequency response to the sinusoidal current.

$$V_{t(jw)} = Z_{(jw)} I_{(jw)} \tag{10}$$

where I is the input current signal, Z is the impedance, V_t is the measured voltage.

In order to get the transfer function, the Laplace transformation is applied to the former developed electrical equivalent circuit model:

$$\begin{aligned} SOC_{(s)} &= -\frac{1}{Qs} I_{(s)} \\ V_{i(s)} &= R_i I_{(s)} \\ V_{1(s)} &= \frac{R_1}{R_1 C_1 s + 1} I_{(s)} \\ V_{2(s)} &= \frac{R_2}{R_2 C_2 s + 1} I_{(s)} \end{aligned} \tag{11}$$

The linearized open circuit voltage V_{oc} can be showed as:

$$V_{oc(s)} = \alpha SOC_{(s)} \tag{12}$$

where α is the coefficient.

The expression of output voltage V_t in Eq. (7) is re-formulated as:

$$V_{t(s)} = -\frac{\alpha}{Qs} I_{(s)} - R_i I_{(s)} - \frac{R_1}{R_1 C_1 s + 1} I_{(s)} - \frac{R_2}{R_2 C_2 s + 1} I_{(s)} \tag{13}$$

Therefore, the transfer function can be obtained by combining Eq.(10) and Eq. (13).

$$Z_{(j\omega)} = -\frac{\alpha}{Qj\omega} - R_i - \frac{R_1}{R_1 C_1 j\omega + 1} - \frac{R_2}{R_2 C_2 j\omega + 1} \tag{14}$$

Based on the identified parameters in the previous equivalent circuit model, a Nyquist plot of the fresh battery can be obtained by plotting the real part of *Z* on the X axis and the imaginary part on the Y axis (as showed in Figure 9).

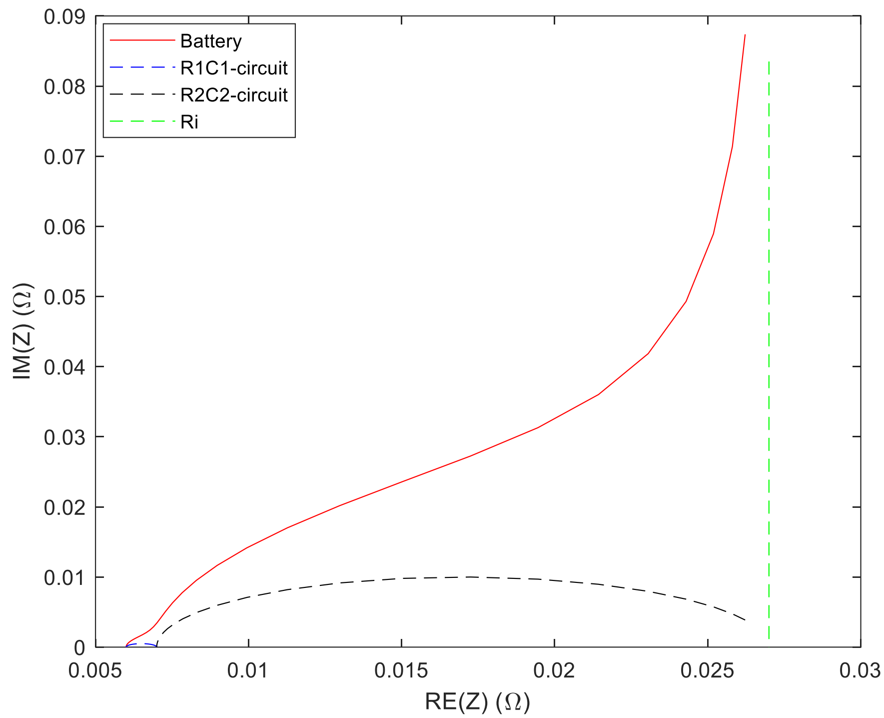

Figure 9: Nyquist Plot for the EIS Model

Due to the lack of EIS measurement data, the accuracy of the EIS model built in this section has not been validated. If more data is available, this model can be used to reveal the degradation characteristics of battery.

<u>(2) Electrochemical Model (or "Doyle-Fuller-Newman" model)</u>

Electrochemical models are built based on first principles of electro-chemical reactions during battery charge/discharge processes [70-72]. The first electrochemical model was proposed by Doyle, et al. [32] in 1993, known as "Doyle-Fuller-Newman" model in the literature. It adopts a large set of partial differential equations (PDEs) to capture ions' diffusion dynamics inside the solid materials and soluble electrolyte. These PDEs are highly nonlinear and difficult to solve. Some hypotheses are made in order to improve its computational ability [73, 74]. If a uniform current density is assumed along both negative and positive electrodes, the full-order 'Doyle-Fuller-Newman' model can be simplified to a so-called "Pseudo 2-dimensional model" (or P2D). P2D model calculates the ions' concentration variation along 2 dimensions: one is the radius of solid compound particles and the other is the thickness of battery [16]. If the electrolyte concentration is assumed uniformly inside battery, it is called the "single particle model" (or SPM). SPM only captures the ions' movement in one particle of each compound materials on the anode and cathode. The order of partial differential equations in the original model can be greatly reduced and hence calculations are much easier.

A demonstration of ion's movement inside battery during the discharge process is showed in Figure 10. The external applied current I is transformed into microscopic ions flow rate j^{Li}. δ_n, δ_p, δ_{sp} are the thickness of negative, positive electrode and separator. x indicates the direction of battery thickness. As stated before, that discharging current is positive and charging current is negative.

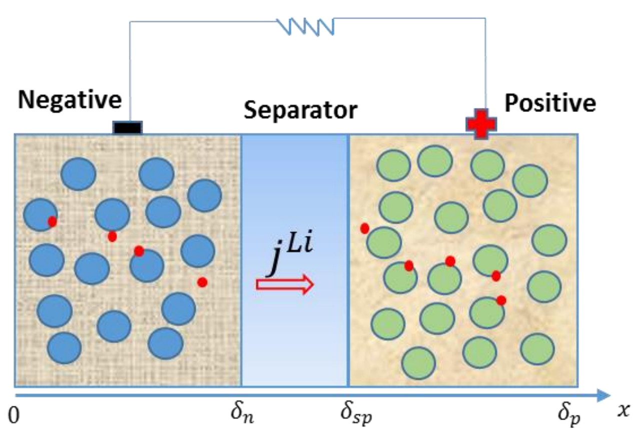

Figure 10: Demonstration of Ions' Movement during Discharge

(i) Modelling the Electrochemical Reaction

Based on the assumption of uniform current density along electrodes, the ion flow rate of Li in the battery j^{Li} is determined by the applied current. The relationship between the macroscopic current I and microscopic ion flux density is expressed as:

$$\frac{I}{A} = \int_0^{\delta_n} j^{Li}(x)dx \tag{15}$$

where j^{Li} is the ions flux density; δ_n is the thickness of negative electrode; A is the electrode surface area, I is the discharge current.

Moreover, the Butler-Volmer kinetic equation builds the connections between the battery overpotential and microscopic current density:

$$j^{Li} = a_s j_0 \left[\exp\left(\frac{\alpha_a F}{RT}\eta\right) - \exp(-\frac{\alpha_c F}{RT}\eta)\right] \tag{16}$$

where, α_a, α_c are the anodic and cathodic charge transfer coefficient; a_s is the active surface area per electrode unit volume; R is the ideal gas number; F is the Faraday's number. η is the overpotential:

$$\eta = \phi_s - \phi_e - U(c_s) \tag{17}$$

where ϕ_s and ϕ_e are the solid and electrolyte potential, U is the equilibrium open circuit potential, which is a function of solid phase ion concentration (c_s).

j_0 is the exchange current density at the equilibrium state,

$$j_0 = k(c_e)^{\alpha_a}\left(c_{s,max} - c_{se}\right)^{\alpha_a}(c_{se})^{\alpha_c} \tag{18}$$

where k is the reaction rate, c_e and c_{se} are the electrolyte concentration and SEI concentration, respectively.

(ii) Modelling of Solid Phase Diffusions

The concentration variation inside solid spherical particles is governed by ions' diffusion process during the intercalation process. Fick's law is adopted to calculate concentration change along the radius of solid particle [63].

$$\frac{\partial c_s}{\partial t} = \nabla_r (D_s \nabla_r c_s) \tag{19}$$

where c_s is the ion concentration in the solid particle; D_s is the solid phase diffusion coefficient; r is the particle radius, and t is the time.

The average concentration c_s^{avg} is the mean value of total ions installed in the solid particle:

$$c_s^{avg} = \frac{1}{V}\int_0^V c_s(r,t)dV \tag{20}$$

where V is the particle volume.

The SOC indicates the proportion of currently stored ions to the maximum available ions.

$$SOC = \frac{\theta_n - \theta_{0\%}}{\theta_{100\%} - \theta_{0\%}} \tag{21}$$

where $\theta_n = \frac{c_s^{avg}}{c_{s,max}}$ is the percentage between the actual and maximum concentration. $\theta_{100\%}$ and $\theta_{0\%}$ are parameters depending on the materials.

(iii) Modelling of Solution Phase Diffusions

The movements of ions in the electrolyte are determined by the total current density and the diffusion rate in the solution. The variation of electrolyte concentration c_e can be expressed as:

$$\frac{\partial \varepsilon_e c_e}{\partial t} = \nabla_x \left(D_e^{eff} \nabla_x c_e\right) + \frac{1 - t^0}{F} j^{Li} \tag{22}$$

where x is the direction along battery thickness from anode to cathode; D_e^{eff} is the effective electrolyte phase diffusion coefficient; ε_e is the electrolyte phase volume fraction; t^0 is the transference number.

Based on the uniform electrolyte concentration assumption, $c_e(x,t) = c_e(t)$, the solution phase concentration variation is simplified as:

$$\frac{\partial \varepsilon_e c_e}{\partial t} = \frac{1 - t^0}{F} j^{Li} \tag{23}$$

(iv) The Overall Output Voltage Calculation

The output voltage of Li-ion battery is the overall electrode potential differences minus the inner resistance voltage drops.

$$V_t = \phi_{s,p} - \phi_{s,n} - R_f I \tag{24}$$

where R_f is the film resistance inside the cell; $\phi_{s,p}$, $\phi_{s,\mathrm{n}}$ are the solid phase potential at the positive electrode (cathode) and the negative electrode (anode).

Numerical solutions are usually adopted to solve these high nonlinear, complex PDEs in the electrochemical model [71, 73]. This research takes the finite difference method (FDM). The discretization process of SPM has been put in Appendix A. In total, there are 20 physical and chemical parameters that need to be fit to run this model, which are also showed in Appendix A. Similarly, GA was adopted to identify these parameters. The RSME of output voltage calculated from SPM is 8.83%, about ten times higher than the equivalent circuit model (as showed in Figure 11).

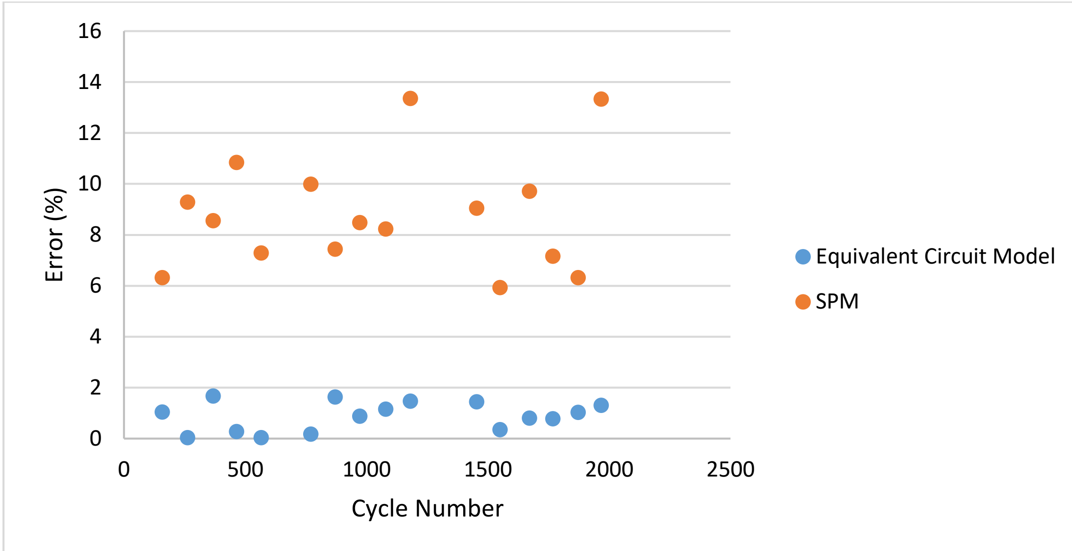

Figure 11: Errors of Different Modelling Methods

2.2.3 Battery Life Prediction Model – Equivalent Circuit Model with Degradation Amendment Term

The battery life prediction model is very important in the hybrid powertrain system design to support the estimation the total investment cost of battery ESS. More importantly, it can support the optimal hybrid energy management and achieve a longer battery lifetime, while maintaining the low operational cost. To fulfill these purposes, the battery performance and life prediction model is developed in this section. As showed in Figure 12, the battery performance degradation model evaluates the capacity deterioration in each cycle, and the accumulated performance decay will be used for more accurate lifetime estimation. As discussed in the previous section, the equivalent circuit model can provide more accurate result and is easier to implement in the control algorithm. Therefore, the life prediction model will be incorporated into the equivalent circuit model as the degradation amendment term.

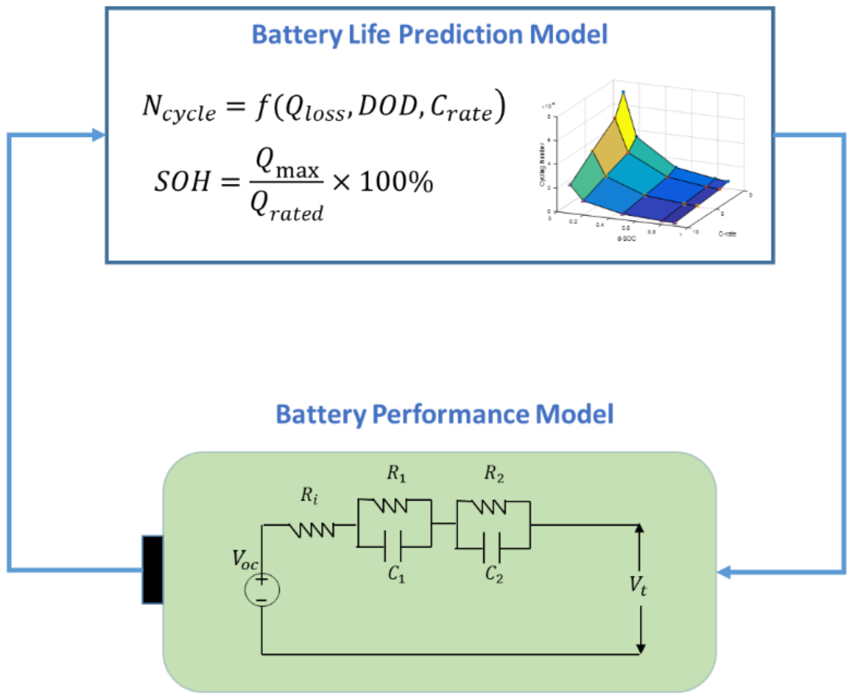

Figure 12: Battery Performance Degradation and Life Prediction Model

An accurate battery life prediction model should consider all the influence from different factors: temperature, DOD, and C-rate. It is, therefore, must rely on adequate testing data. Most researches focus on modelling the battery capacity fading at different operation temperature [61] [75], or different SOC[76], or the combined temperature and SOC thereof [77]. The rain-flow cycle counting model [78] and machine learning approaches [66]are also investigated in battery life prediction models to explore the extreme non-linear aging process under different usage conditions with moderate cycling experiment data.

Most battery life prediction model developed in the literature [29, 79, 80], combining both dynamic C-rate and DOD effects, are all built empirically based on pre-acquired experimental data. However, it usually takes years of time to complete total required tests. Due to the lack of adequate data in this research, a semi-empirical battery life model is developed based on the previous work done by many research groups, such as Tsinghua

University and The University of Michigan [80], HRL Laboratories and GM Corp. [79], etc.

This study creatively combines battery SOC (in each mission cycle) and SOH (over battery lifespan) to accurately estimate battery performance degradation rate and remaining cycling numbers. The calendar life of battery has minor influence on performance degradation compared to cycling life [56, 81], therefore, is not considered in our model. It has been assumed that temperature can be controlled in appropriate ranges by advanced thermal management system.

The battery capacity losses (Q_{loss}) follows Arrhenius kinetics as a function of temperature, DOD, C-rate and operation time [79]:

$$Q_{loss} = A \cdot e^{\left(\frac{-E_a + B \cdot C_{rate}}{RT}\right)} (A_h)^z \tag{25}$$

where, A is the pre-exponential factor, E_a is the activation energy, B is the coefficient of C-rate; R is the ideal gas constant, T is the temperature, z is the exponent of time and usually is 0.5. A_h is the total throughput capacity as a function of maximum available capacity (Q_{max}), cycling numbers (N) and DOD.

$$A_h = N \cdot DOD \cdot Q_{max} \tag{26}$$

After combing Eq. (25) and (26) , battery cycle numbers can be derived as:

$$N = \left(\frac{Q_{loss}}{A \cdot e^{\left(\frac{-E_a + B \cdot C_{rate}}{RT}\right)}} \right)^{\frac{1}{z}} \frac{1}{Q_{max} \cdot DOD} \tag{27}$$

The unknown parameters in Eq.(27) are A, B, z, and E_a. They have been identified in the aforementioned literature, and also validated in this study through the $LiFePO_4$ cycle-life experiment data. The battery life prediction model was implemented in

MATLAB/Simulink. The final results of total cycle numbers for this type of $LiFePO_4$ as a function of C_{rate} and DOD have been plotted in Figure 13.

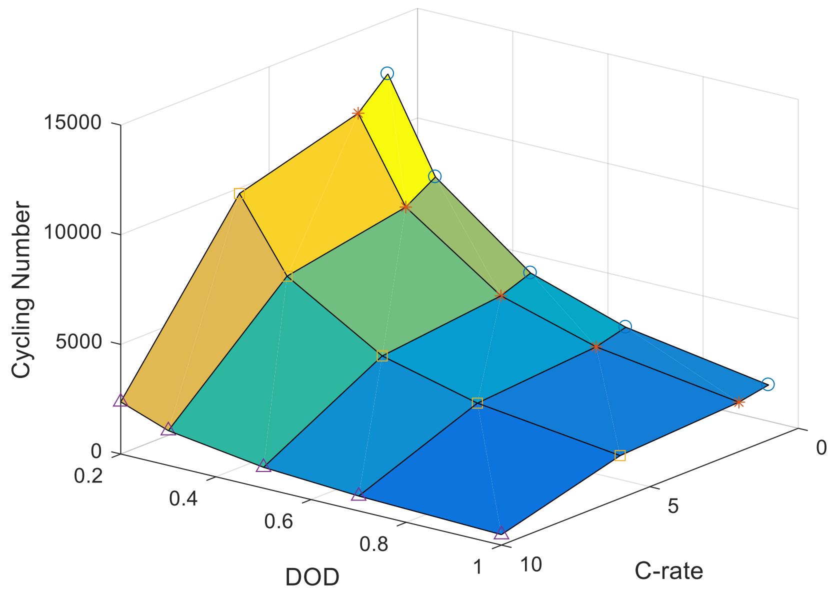

Figure 13: Battery Cycling Number Prediction under Different C-rate and DOD

The developed battery performance degradation and life prediction model builds a solid foundation for the hybrid electric marine propulsion design. It brings possibilities for optimal energy management to prolong battery lifetime through adjusting the battery discharge C-rate and working DOD.

2.2.4 Summary on Model Fitting and Validation

During this research, 2,000 sets of performance degradation data of a commercialized lithium iron phosphate (LiFePO4 or LFP) batteries have been acquired from the State-assigned Laboratory for Electric Vehicle Power Battery Testing in Beijing, China. Large portions of these data (about 80% of capacity test data) have been used in this work to form the three types of battery performance degradation models, and the rest 20% data have been used to validate the accuracy of the models.

As discussed in the previous subsections, the first battery performance degradation model of using equivalent circuit model has 6 model parameters, the model fitting using least-square fitting method produced a model with relatively accurate simulation result with RSME of 0.88% after validation. The second battery performance degradation model used EIS method. Although it lacks EIS data to validate this model, it presented a potential way in explaining battery degradation mechanisms when the data is available. The third battery performance degradation model of SPM has 20 model parameters, the model fitting using least-square fitting method produced a model with relatively higher accuracy of 8.83%.

All three models can be used to support the optimal sizing of the battery ESS and the optimal energy management of the hybrid electric propulsion system. The EIS model and SPM model have offered deep insight into the fundamental battery electrochemical reactions. However, due to the lack of EIS data and the specific battery material characteristics, the accuracies cannot be guaranteed. Equivalent circuit model, on the other hand, is more suitable for realistic application in the hybrid propulsion system design.

The Q_{max} used in the battery performance degradation model means maximum capacity that a battery can store and release, which is also a key parameter that reveals its degradation degree during lifetime. In general, when Q_{max} has lost 20%, i.e., the $Q_{loss} = 20\%$, the output voltage, power and total energy from the battery will be decreased to a certain level that can significantly affect total system performance in the hybrid propulsion systems. Therefore, the battery will be considered as a dead battery and must be replaced. The variation of Q_{max} has been identified from previous section using equivalent circuit model. It was stored as a lookup table in the model that can assist model simulation, and provide more accurate available capacity in different cycling numbers. The reduced capacity, resulted from previous cycles, will be counted in the degradation amendment term. The remaining cycles before Q_{loss} reaches 20% therefore can be predicted from the semi-empirical life prediction model.

Chapter 3 Hybrid Marine Propulsion System Design, Modelling and Life Cycle Cost Calculation

The benefits of using hybrid powertrain configurations for land-based and sea-based transportation have been deeply discussed in the literatures [18, 82]. One of the unique features of marine vessels that is different from conventional passenger vehicles is its case-dependent driving/load cycles, as well as hull drag and propeller thrust. This chapter will introduce the integrated hybrid electric ship-modelling tool based on modularized key component models. In the developed modelling tool, different hybrid marine propulsion configurations will be discussed and modelled. Their life cycle cost (LCC) will be calculated for the economic and environmental comparison.

3.1. Design of Hybrid Marine Propulsion Systems

The design of hybrid marine propulsion system is subjected to the ship application and the overall hull, propeller performance. In order to focus our research on the marine propulsion system design, an integrated hybrid electric ship modelling platform is developed with separated and modularized component models. This ship modelling tool is implemented in the MATLAB/Simulink environment. However, in order to perform an accurate simulation, the performance equations/characteristics/maps/coefficients of each ship component must be acquired from other resources, by either simulation or experiment. The input/output interfaces between each modular have been clearly defined, so that different modelling methods can be testified for each component without interfering in other sub-systems.

A similar system simulator of a marine vessel and its power plant was developed by researchers in NTNU [83], which is also capable of simulating the mechanical system with diesel engines, the electrical system with generators, and the plant level controller with dynamic positioning, thrust control and power management system. The marine systems simulator (MSS) has been developed by Fossen and Perez [84] as a MATLAB/Simulink library for parametric identification of radiation-force models and fluid memory effects of marine crafts. Moreover, Fossen also generated a 6 degree of freedom (DOF) unified dynamic positioning and maneuvering model [85] to simulate ship hydrodynamic forces and moments. A mathematical model of diesel-electric propulsion systems for marine vessels has been studied [86], with special attentions on the interconnection of several synchronous generators to match the power generating part and power consumption part. These modelling tools focus on ship hydrodynamic calculation and synchronizing the distribution power grid in hybrid propulsion systems. This dissertation, on the other hand, will focus on system level hybrid power plant design and energy management for various marine applications.

3.1.1 The Integrated Hybrid Electric Ship Modelling Tool

This research adopts a modularized modelling method to reduce the complexity of ship simulation and provide more versatile solutions for ship propulsions. The main ship components are categorized into several functional modules, while each module can be built and validated separately before integrated together. The intention of using modularized modelling method for ship simulation in MATLAB/Simulink environment is to partition a complicated ship model into several sub-systems. By categorizing all the components into different modules, it would be much easier to integrate all together systematically after building and verifying simulation models for each module. The complicity and computational time can also be reduced through defining the input and output signals between each module instead of tangling all the components together.

As complicated as a bulk ship can be, the ship simulation model can be separated into four main modules: (1) ship control module; (2) integrated powertrain module; (3) propeller module; (4) ship maneuvering module. An example of developed simulation platform for a ferry ship has been showed in Figure 14. The input/output interfaces of these modules have been clearly defined and presented in Table 4.

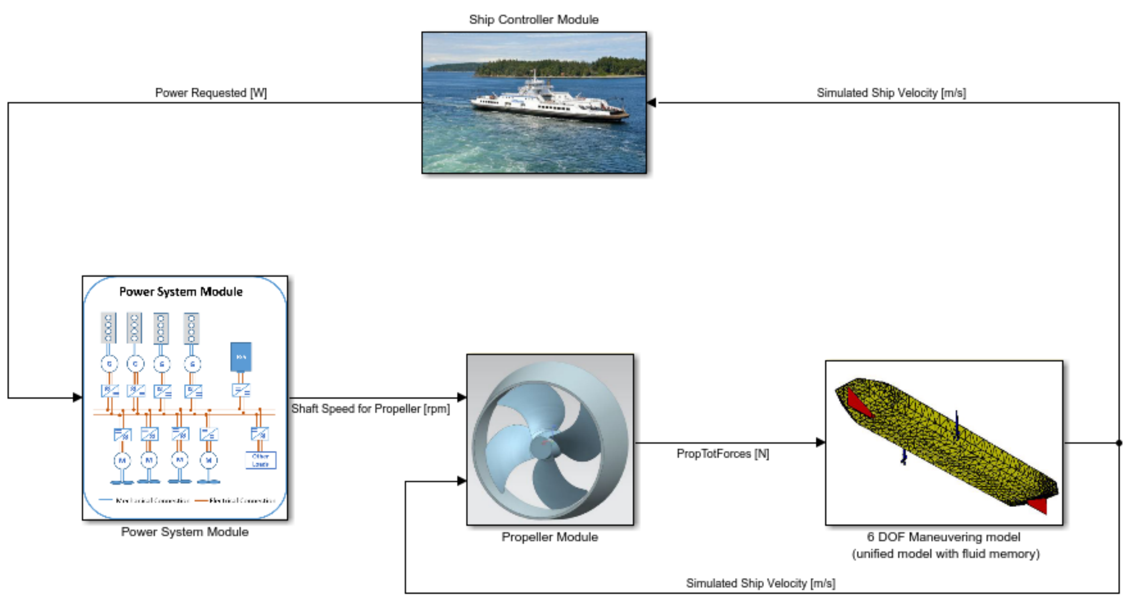

Figure 14: Modularized Hybrid Electric Ship Simulation Platform

The integrated powertrain module is the power supply system that consists of all the prime movers aboard. Depending on the configuration, it could be pure mechanical, pure electric, or hybrid propulsions. Detailed powertrain design and modelling will be discussed in the following section. Inside this module, a supervisory controller exists to generate a high-level control strategy for power distributions between engines and battery ESS. Intelligent energy management can be developed for this controller.

Table 4: Input/output Signals in the Integrated Ship Modelling Platform

Module		Input Signal(s)	Output Signal(s)
1	Ship Control Module	1.Measured ship course data; 2.Simulated ship velocity (m/s)	1. Power requirement (kW)
2	Integrated Powertrain Module	1. Power requirement (kW)	1. Propeller speed (rpm)
3	Propeller Module	1. Propeller speed (rpm) 2. Propeller inflow velocity (m/s) 3. Azimuth angle (if needed)	1. Force (N) 2. Torque requirement (Nm)
4	Ship Maneuvering Module	1. Propeller force (N) 2. Wind, wave, current signal	1. Ship velocity (m/s) 2. Propeller inflow velocity (m/s)

The propeller module takes signals from the powertrain and ship hull-maneuvering model to determine working conditions for each propeller. The characteristics of propeller can be stored in pre-generated look-up tables, containing the propeller thrust and torque coefficient acquired from the full-scaled computational fluid dynamics (CFD) calculation. The control of propeller can be developed to reduce ship noise and cavitation issues.

The ship maneuvering module accepts thrust forces from propellers and resistances caused by ship maneuvering and ocean conditions (such as wave, wind, and current) to calculate the ship hydrodynamic performance. The ship hull resistance and propeller performance can be modelled through full-scaled CFD simulations, experimental sea trial and tow tank data, reduced-order or dedicated low-order hydrodynamic model, or generic mathematical model[87]. The sea experiment and full-scale CFD simulation can provide more accurate results, however also require expensive time. The dedicated low-order hydrodynamic model is built through stability book of specific ship hull, or simplified CFD simulation. The generic parametric mathematical model (GPMM) was developed and validated by Truelove [87] in the UVic clean transportation team. It can generate representative propeller and steering gear states (torque, speed, power) for any arbitrary monohull surface vessels, which is very suitable for the ship design and analysis if lacking of sufficient experimental data.

Ship control model or guidance system compares the simulated ship speed with measured speed to give instructions to the integrated powertrain module. Both backward-facing and forward-facing modelling method can be used to develop the integrated modelling tool. Backward-facing modelling assumes the required power (or torque, speed) can be satisfied by the power plant at any situation, therefore, the consistency of simulation results regarding to the desired ones is guaranteed. It is a quasi-steady model thus not suitable for on-line simulation. Forward-facing control, on the other hand, builds a driver/captain model to reflect a real-world driving test. It can be implemented in the hardware-in-the-loop (HIL) system to validate control logics and to get insight into the limits and design margins of powertrain components.

After finishing the modular simulation and validation, the integrated hybrid electric modelling tool can be achieved by connecting all the modules together. The systematic simulation error can be reduced since all the sub-systems have been tested to be accurate and robust for simulation. Depending on the modelling complexity and accuracy, each module can have several different approaches, such as power loss model or detailed plant model. Lookup tables are needed for power loss model. Different ship propulsion architectures can be built in the powertrain module for the ship design. Detailed information can be found in Figure 15.

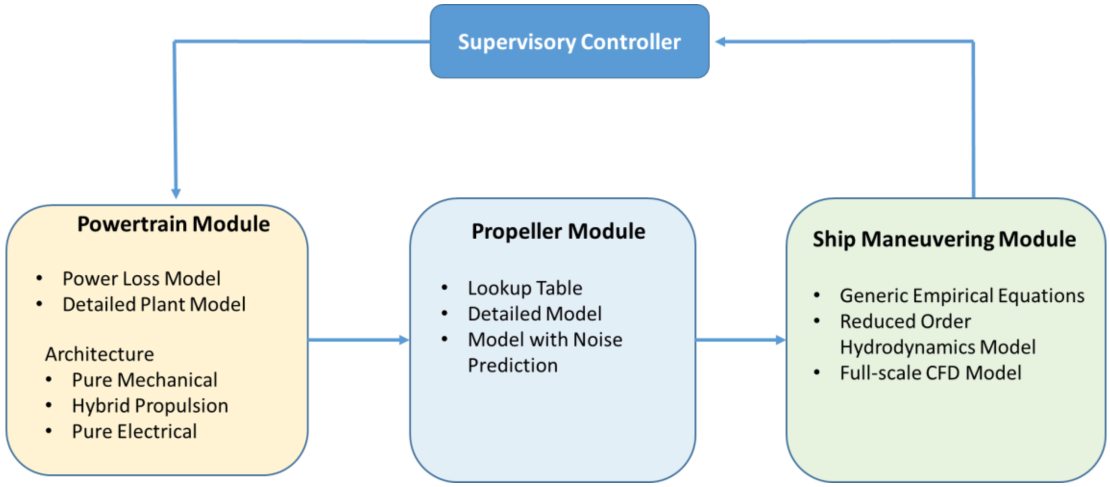

Figure 15: Integrated Hybrid Electric Ship Model

Through the modularized ship modelling platform, this research will focus on the designing, modelling and optimization of hybrid marine propulsion systems in the integrated powertrain modular.

3.1.2 Design of Hybrid Electric Propulsions

The concept of using electric ship propulsions has been proposed more than100 years ago [19, 22, 88]. However, there are still not clear definitions on different types of hybrid electric marine propulsion configurations, regarding the type of energy sources, the path of power transmission, etc. This section will present a review of conventional marine propulsions, and propose different hybrid propulsion architectures based on some concepts from the hybrid electric vehicles.

Hybrid powertrain systems, as discussed in the first chapter, consist two different power sources: the engine and the Li-ion battery ESS. In automotive industry, the hybrid powertrain architecture is defined by the way that power is transferred in the driveline. In general, there are three types of hybrid configurations [89]. The series hybrid powertrain transforms all mechanical energy from the engine into electrical energy and provides pure electrical drive. The parallel configuration has two energy flow paths, the mechanical driving from the engine to the wheels via gear sets, or electrical driving from the battery ESS via electric motor(s). The power split or series/parallel configuration offers more flexible operation by adopting power split devices (usually a planetary gear set), so that the energy flow in the drivetrain can be merged electrically and/or mechanically. The power split hybrid mode combines both advantages from the series and parallel configuration.

Conventional Marine Propulsions

Currently, the majority of ship propulsions are mechanical. The rotational power from engines (or gas-turbines) is transferred to the propeller through shafts, gearboxes, and associated couplings[90]. Pure mechanical propulsion is the most convenient structure in modern ships. One or a few separate engine-generator set(s) (or Genset) must be installed to provide auxiliary electrical power. A demonstration of mechanical propulsion with two mine engines (ME) and two Gensets are showed in Figure 16. The blue line indicates mechanical drive. The red arrowed line shows the electricity flow direction. Main engines are connected to propellers through clutches and gear reductions.

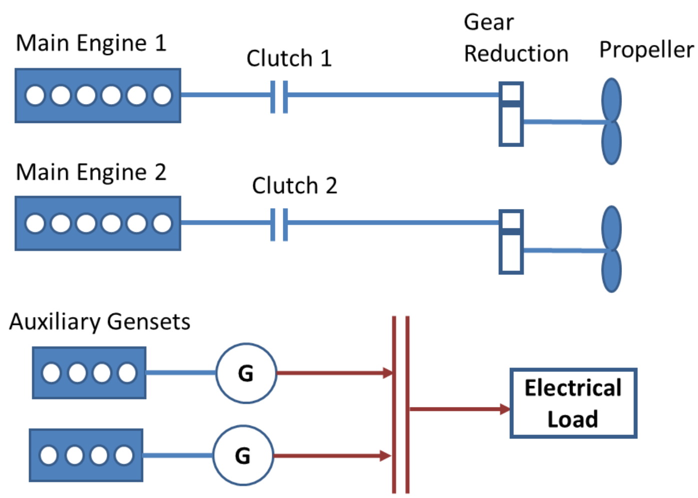

Figure 16: Mechanical Propulsion Configuration

The power take-in (PTI) /power take-off (PTO) configuration are invented to better facilitate the cooperation between main engines and Gensets [91]. A powerful electrical motor/generator (MG) is needed. In PTI mode, energy from Gensets can be taken to support main engines through electrical motors. In PTO mode, extra energy from main engines will be taken-off to support the auxiliary load through electrical generator. It can improve the efficiency of main engine and reduce the cost. As showed in Figure 17, the red line with arrows indicates the electrical energy flow direction. PTO and PIT mode rely on properly designed power coupling devices, as well as the added electrical machines (generator/motor).

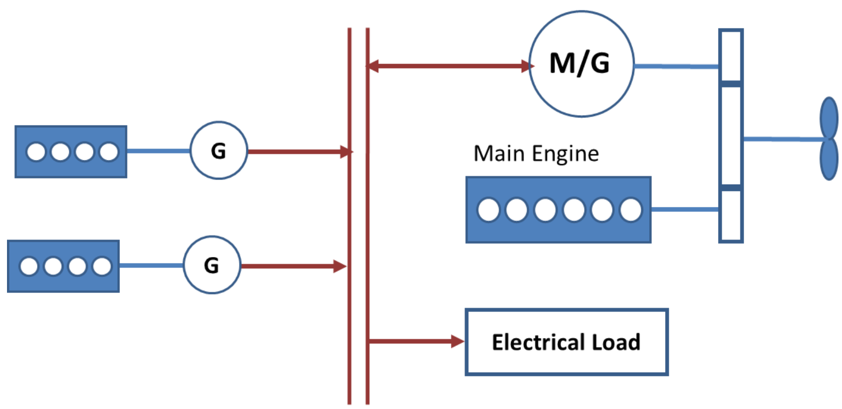

Figure 17: PTI/PTO Configuration

The electrical propulsion of ships are getting more popular for those exposed to large power demand variations, such as offshore supply vessels, cruise ships, icebreakers, war ships, etc. With the rapid development of power electronics and MGs, fully electrified vessels or so-called all-electric ships (AES) [14] are becoming available in the marine industry. Through using the integrated power systems (IPS), a common electrical platform can be built for ship propulsions and service loads through AC or DC power buses [88], which enables more flexible operations and higher system redundancy and reliability [92].

The engines can be cooperated together to fulfill load demand and work in the optimum energy efficiency point in the meantime.

The attraction of using DC distribution architectures onboard has overwhelmed traditional AC system, especially in the ships that have heavy electrical loads, such as navy vessels. The DC system uses power electronic converters to connect all power sources and load subsystems to a centralized DC distribution bus (Figure 18). The propulsion unit in the AES can be shaft propeller, azimuth thruster or podded propulsion unit [93]. The shaft propeller is normally driven by a variable-speed electric motor through a gear reduction. Azimuth thruster can rotate and produce thrust in any direction, with a vertically mounted motor and L-shaped gear transmission. The podded propulsion unit also can rotate and produce trust just like azimuth thruster, but with a compact design that integrated the electrical motor directly to the propeller shaft inside a sealed pod unit under the vessel hull. A demonstration of IPS with DC power bus is showed in Figure 18.

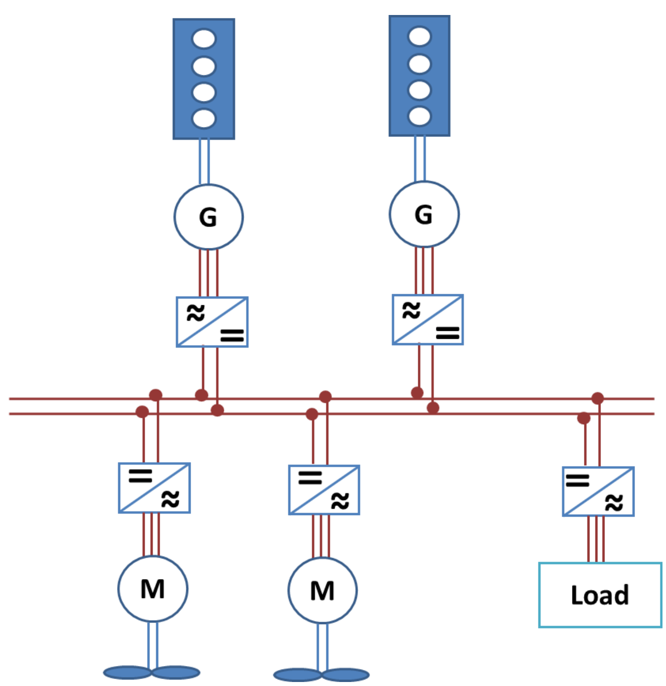

Figure 18: Diesel-electric Propulsion with DC Bus

Hybrid Marine Propulsions

The hybrid electric propulsion system differs from conventional systems by adding a large battery ESS to allow the supply of propulsion power from at least two paths. The ESS disengages the engine speed and the propeller speed, so that the engine can operate at its most efficient area and the ESS can provide and store energy to support the whole propulsion system. The main advantages of using hybrid marine propulsions include:

- providing more flexible operation;
- increasing system redundancy;
- improving engine operational efficiency;
- reducing fuel consumption and emissions;
- reducing engine operational time and maintenance cost;
- abolishing the usage of auxiliary Gensets;

The hybrid propulsion systems offer high operating flexibility as well as more environmental friendly solution. With the fast-developed power electronics and mechanical transmissions, different hybrid modes can be achieved. Similarly, to the hybrid automotive configurations, three different hybrid marine propulsions are proposed here for different using scenarios: series, parallel and series-parallel hybrid systems.

The series hybrid marine propulsion is formed by adding a battery ESS to the integrated diesel-electrical propulsion. It works as a fully electrified system since all the power from engines will be transformed into electric energy (Figure 19). The rechargeable ESS acts as a buffer to store and supply energy. Through optimized powertrain system control, it can be expected to have lower fuel consumption and emissions compared to the conventional counterpart. The main advantage of series hybrid mode is that the engine can work in its most efficient area by de-coupling the mechanical connection between the engine and propeller. If the ESS is sufficiently large, it can provide all required energy and work as pure electric propulsion.

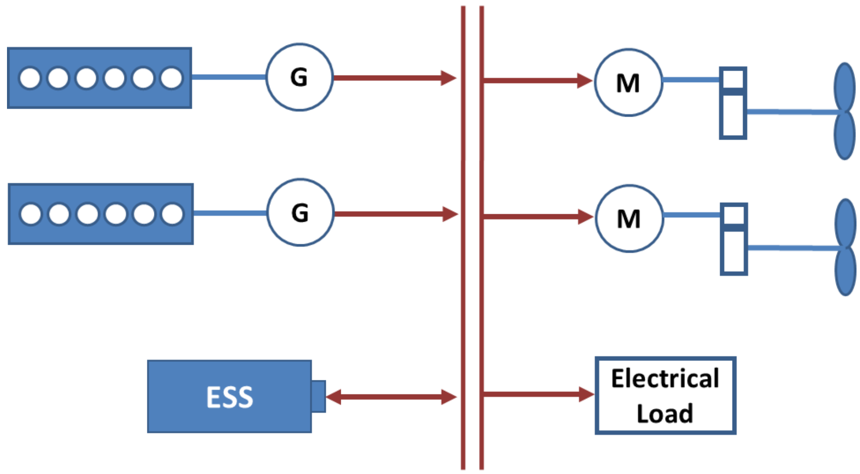

Figure 19: Series Hybrid Electric Propulsion

Parallel hybrid marine propulsion is very similar to the conventional PTI/PTO configuration, except to the added battery ESS. Auxiliary Gensets can be retained or removed, depending on the specific application. Battery ESS can support the requested electrical energy for auxiliary loads and propulsion loads (Figure 20). The engine and electrical drives are coupled in a gearbox to propel the thruster. Parallel configuration can take advantage of mechanical drive from the engine to the propeller directly without sacrificing energy conversions. Thus, a higher system energy efficiency can be achieved at the high load demand.

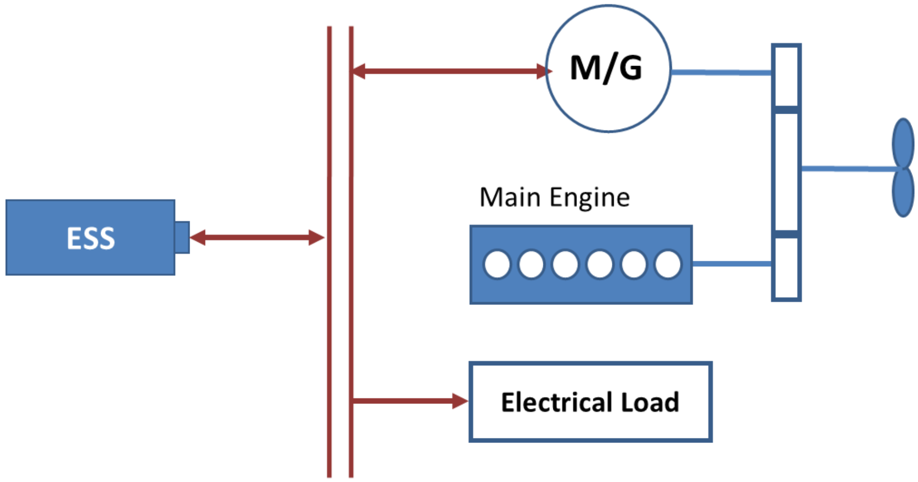

Figure 20: Parallel Hybrid Marine Propulsion

The series-parallel hybrid architecture has the most complicated structure and requires advanced gear sets to transmit the power both mechanically and/or electrically. Planetary gear sets are largely used in ground hybrid vehicles to work as the electric continuously variable transmissions (e-CVT) [94]. The limitations and possibilities of applying e-CVT in power-split marine propulsions are also studied [95], however, it is not a common feature for marine vessel applications. In this research, a series-parallel hybrid configuration is realized through four clutches (C1, C2, C3 and C4) and several gear reduction devices, as showed in Figure 21. The two electrical motor/generators (MG1 and MG2) can work as generator when charging the ESS, or as motor when using electrical energy to boost the engines.

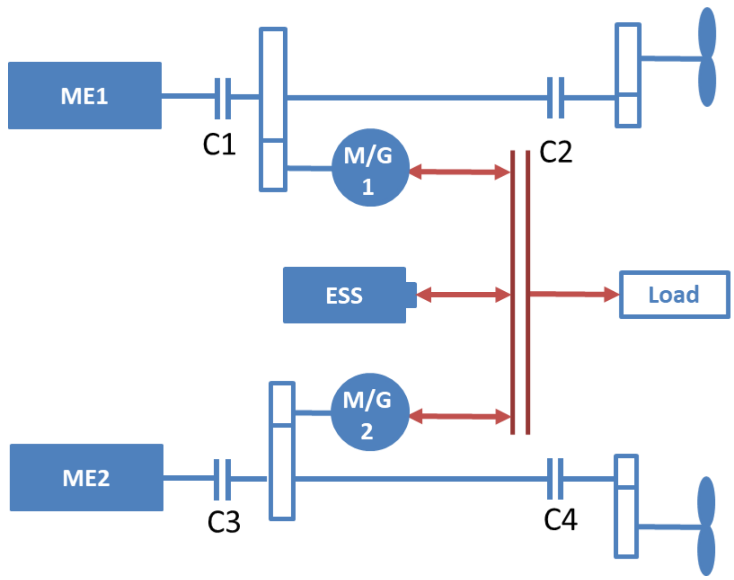

Figure 21: Series-parallel Hybrid Marine Propulsion

The combination of using both series and parallel hybrid mode provides more flexible operations and can help achieve higher system efficiency. Although the complexity of system design is increased, it offers more degree of freedoms to optimize the control algorithm for a better system performance. Specifically, it can work as in five different modes:

(1) the pure electric (or series) mode can work under the low or medium power demands to reduce pollutions, where the power is supplied by the ESS and all engines are shut down (or operated in high efficiency area to charge the battery);

(2) the engine start mode uses the electrical energy from battery ESS to start main engines, so that no auxiliary Gensets are needed;

(3) the pure engine mode is more suitable under the high load demand situation, where the main engines can drive propellers through gear reductions directly with the lest energy conversion losses;

(4) the parallel model allows the ESS and engine work together to create higher torque/power for the propeller;

(5) the series-parallel mode can be achieved if one of the main engines is operated to mechanically propel one propeller and electrically drive the motors for another propeller.

The different operation modes are demonstrated in Table 5. By using two electrical M/G machines, engines can provide mechanical energy to propeller or split a port of extra energy to charge the battery. Both MGs can absorb energy from the battery to drive propeller. The mechanical propulsion path is indicated as green lines and electric propulsion path is indicated as red lines in different operation modes.

The complexity consideration of implementing series-parallel configuration in marine vessels is different from automotive industry. Hybrid electric vehicles have different choices to achieve series-parallel hybrid transformation, either by using planetary gear sets or a few gear reductions with clutches. A typical example would be the Hybrid Synergy Drive (HSD), which is a refinement term of Toyota Hybrid System (THS), used in the Toyota hybrid electric vehicles. The HSD consists of a planetary gear set to provide continuously variable transmission, therefore, it is also called power-split hybrid configuration. Although the study of using power-split propulsion system in ships showed promising feasibility [95], the gear reductions with clutches to change power transmission paths are more applicable regarding to the cost, reliability, complexity, etc.

Table 5: Series-Parallel Hybrid Operation Modes

1. Pure Electric Mode

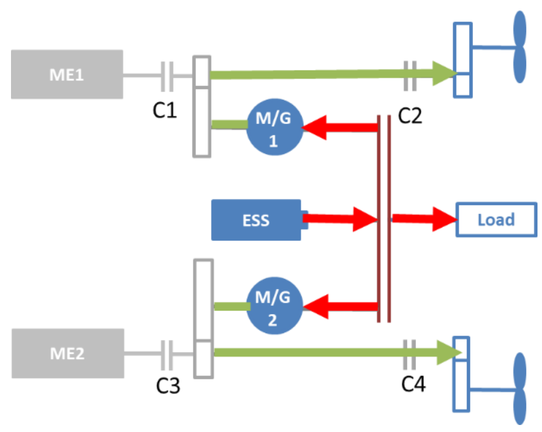

2.Engine Start Mode

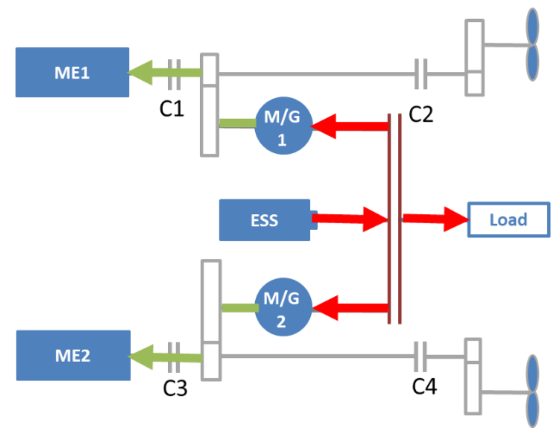

3. Pure Mechanic Mode

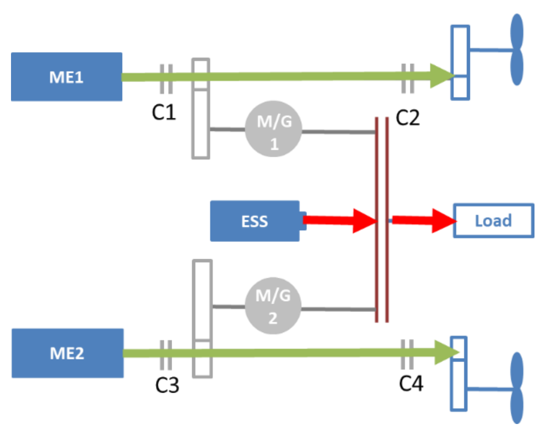

4. Parallel Mode

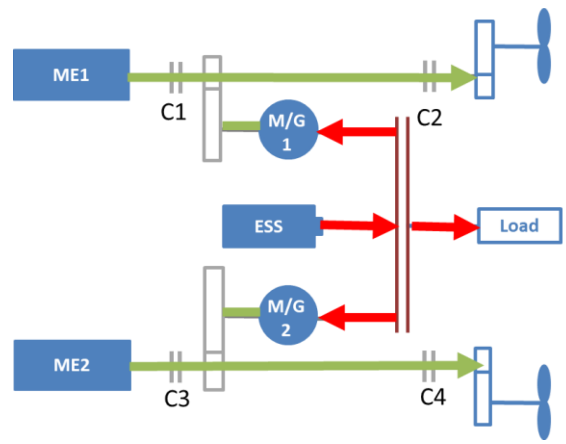

5. Series-Parallel Mode

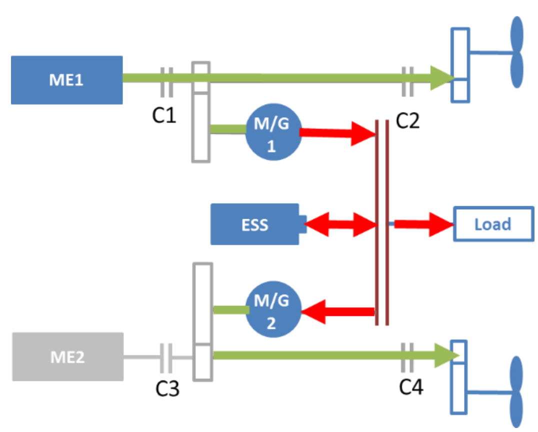

States of Main Components

Mode	ME 1	C1	C2	MG 1	ME 2	C3	C4	MG 2	ESS
1	0	0	1	M	0	0	1	M	1
2	0	1	0	M	0	1	0	M	1
3	1	1	1	0	1	1	1	0	1
4	1	1	1	M	1	1	1	M	1
5	1	1	1	G	0	0	1	M	0,1
	0	0	1	M	1	1	1	G	

0: turn off the devices

1: turn on the devices

Pure Electric Propulsion

Pure electric propulsion, in this paper, means that the main power sources are purely electrical components and no engines are adopted. The power sources can be battery, ultracapacitor, fuel cell, or any of these combinations. It provides only electrical energy to the motors to drive the propellers. A demonstration of pure electric propulsion with battery powered ESS is showed in Figure 22.

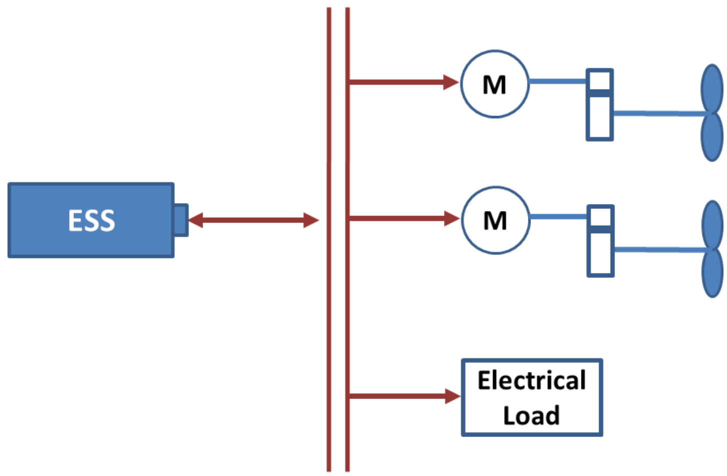

Figure 22: Pure Electric Marine Propulsion

One thing that must be clarified is that pure electric propulsions require additional facilities to charge the battery ESS through plugging into the power grid. Similarly, other hybrid propulsion systems (HES) also can be designed as plug-in hybrid system (PHES) if charging facility exists.

3.2. Modelling of Hybrid Electric Marine Propulsions

The modelling of hybrid marine propulsion systems is important to facilitate a better system design. It involves two key aspects: building an accurate detailed model for key components and developing optimal control strategies for the hybrid energy management.

3.2.1. Modelling of Key Components

Key components in former developed hybrid propulsion systems are obviously the engine and Li-ion battery ESS. The battery performance degradation analysis and modelling methods are deeply investigated in Chapter 2. Therefore, this section will focus on the modelling of engine performance and emissions. Other components such as electrical generator/motors and power electronics are developed using power loss models with specific efficiency maps.

Both diesel engines and NG-fueled engines are investigated in this research. The fuel consumption and emissions from marine engines are calculated based on the engine efficiency and emission maps. The specific fuel consumption maps of different engines are plotted in Figure 23.

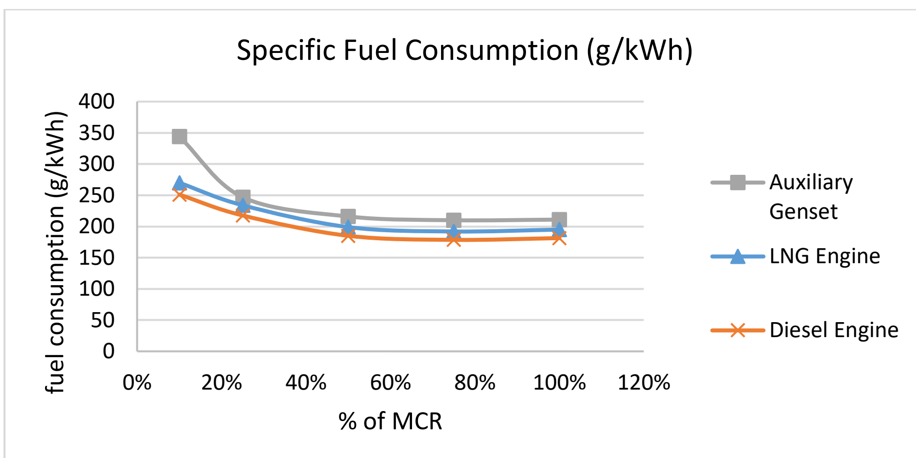

Figure 23: Specific Fuel Consumption Map for Different Engines

The mass of engine fuel consumption (m_{fuel}) is calculated using the engine specific fuel consumption map.

$$m_{fuel} = \int_{t_0}^{t_f} \left(P_{eng,t} \times BSFC_P\right) dt \tag{28}$$

where t is the time step from t_0 to t_f; $P_{eng,t}$(kW) is the power output at time t; $BSFC_P$(g/kWh) is the brake specific fuel consumption at corresponded power P.

Various substances and air pollutants are generated during the engine operation. These emissions are categorized as GHG emissions and criteria air pollutants (CAPs), where each of them is calculated separately. GHGs normally refer to gases that can trap heat in the atmosphere and aggravate global warming. According to U.S. Environmental Protection Agency (EPA), CO_2, N_2O, and CH_4 are the main GHGs emitted from transportation area [8]. CAPs include a set of common air pollutants that can seriously harm human health and damage environment [96], such as NO_x, SO_x, volatile organic compound (VOC), PM, carbon monoxide (CO), ammonia (NH_3), etc. NO_x and SO_x can cause smog and contribute to respiratory problems. PM that are 10 micrometers in diameter or smaller can enter into human bodies, affecting heart and lungs.

In this study, GHG, include CO_2, N_2O, and CH_4 are calculated. CAPs, include SO_x, NO_x and PM, are calculated. For each mission call, engine emissions (E) are determined by the corresponded emission factors [97].

$$E = \int_{t_0}^{t_f} \left(P_{eng,t} \times EF_P\right) dt \tag{29}$$

where EF_P(g/kWh) is the emission factor at power P.

Among all the exhausted emissions, CO_2 and SO_2 are mainly determined by the content level of carbon and sulphur in different fuel type. The 2018 Canada's National Greenhouse Gas Inventory Report compares GHG emissions from various types of fossil fuel [98]. In which, it presented specific emission factors of CO_2, CH_4 and N_2O from refined petroleum products and natural gas. More specifically, it listed emission factors from marine fuels (showed in Table 6).

Table 6: Emission Factor of Different Marine Fuels [98]

	Emission Factors from Marine Fuel (g/L fuel)		
	CO_2	CH_4	N_2O
MGO	2307	0.22	0.063
MDO	2681	0.25	0.072
HFO	3156	0.29	0.082
Natural Gas (Marketable[1])	1.926	0.000037	0.000033

Considering the CH_4 leakage for LNG-fueled marine engines, the CH_4 emission factor is adjusted according to the study from Bengtsson, et al. [23]. They have showed a more reasonable CH_4 emission factor from Wärtsilä LNG dual-fuel engines (including CH_4 slip) at 0.3g/MJ.

To compare the reduced emission by using electricity from the power grid in hybrid propulsions, emission factors of BC Hydro's electricity are also acquired. Since BC has 92% electricity from hydro power, the carbon emissions is about 11tonne per GigaWh [99]. The emission of CH_4 and N_2O can be neglected in the electricity production.

In conclusion, the GHG emission factors from using diesel, LNG, and electricity in BC, Canada are listed in Table 7.

Table 7: GHG Emission Factor from Different Energy Sources

GHG Emission Factors [98]			
	CO_2 (kg/kg fuel)	CH_4 (kg/kg fuel)	N_2O (kg/kg fuel)
Diesel	3.060502	0.285388	0.082192
LNG	2.4075	0.0135 [23]	0.00004125
	CO_2 (g/kWh)	CH_4 (g/kWh)	N_2O (g/kWh)
Electricity	11	---	---

[1] The term "marketable" means it only applies to fuel consumed by the Electric Utilities, Manufacturing Industries, Residential/Commercial and Transport subsectors, which does not include the raw gas consumption. [98]

The concept of total equivalent CO_2 (CO_2e) is adopted to weight the global warming impacts of different types of GHG with respect to the effects of CO_2. The 100-year Global Warming Potential (GWP) is acquired from the website of U.S. Environmental Protection Agency (EPA). Specifically, the GWP for CH_4 and N_2O are 25 and 298, respectively. CO_2e can be calculated by multiplying GWP values to each GHG.

The SO_x emission is a function of sulfur content in the fuel. If assuming all the sulphur content in the fuel are converted to SO_2, a mass-balanced approach can be used to calculate SOx emission factor [100].

$$EF_{SO_x} = S\% \times \frac{molecular\ mass\ of\ SO_2}{atomic\ mass\ of\ S} \times BSFC \tag{30}$$

where, EF_{SO_x} is the emission factor for SO_x (g/kWh); $S\%$ is the sulphur content of the marine fuel; $BSFC$ is the Brake Specific Fuel Consumption of the engine (g/kWh).

Specifically, sulphur content $S\% = 0$ for LNG engine (assume all sulphur were removed from natural gas during the liquefaction process). $S\% = 0.000015$ for ULSD diesel fuel.

NO_x is a harmful emission from marine industry that can form smog and contribute to respiratory problems. It is caused by the nitrogen present in the atmosphere reacted with oxygen under the high temperatures and pressures in combustion engines. Many studies show relatively high emission factor for NO_x due to the outdated engine technology [97, 101]. A new designed medium speed diesel engine must meet about 2g/kWh NO_x emission standard to comply with the tier III NO_x emission standards in the ECAs. The LNG dual-fuel engine from Wärtsilä shows that NO_x emission factor is 1.3 g/kWh., according to [23].

PM is a result of incomplete fuel combustion, including carbon particles, sulphates and nitrate aerosols. Fuels with higher sulphur content usually generate more PM. PM emission factors from LNG and ULSD are 0.04 and 0.25 g/kWh, respectively [102].

The efficiencies of other electrical components and power converters in the hybrid marine propulsion systems are showed in Table 8. These values are based on the averaged efficiencies of different power electronics and electrical machines [35, 103, 104].

Table 8: Efficiency of Electrical Components

Component	Efficiency
Generator and Controller	0.94
Battery ESS and Battery Control Unit	0.99
Motor and Motor Controller	0.94
Battery Charging Facility	0.93

The battery charging facility efficiency highly depends on the charging power. The number we used here is according to the charging efficiency data acquired from charging Tesla electric vehicles.

3.2.2. Hybrid Energy Management (Control Algorithm Development)

Control algorithms in the hybrid energy management system (EMS) can make a huge impact on the overall system performance. The existing of battery ESS enables more flexible operation, also increases the complexity of control hierarchy. EMS takes different control laws to decide the power distribution among different energy sources under certain load profiles. The hybrid EMS usually consists some parallel lower level controllers for each component, such as the engine control unit (ECU), battery management system (BMS), and motor control unit (MCU). Above them, a supervisory controller is built in higher level. The supervisory controller can collect information, make decisions and give instructions to the specific lower level controller (as shown in Figure 24). In general, the energy management problem is to find the optimal control law for a given system under defined load profile over a finite time horizon. The objective of the energy management control in hybrid powertrain systems is to achieve the minimum fuel consumption, reduce emissions and prolong battery lifetime [89].

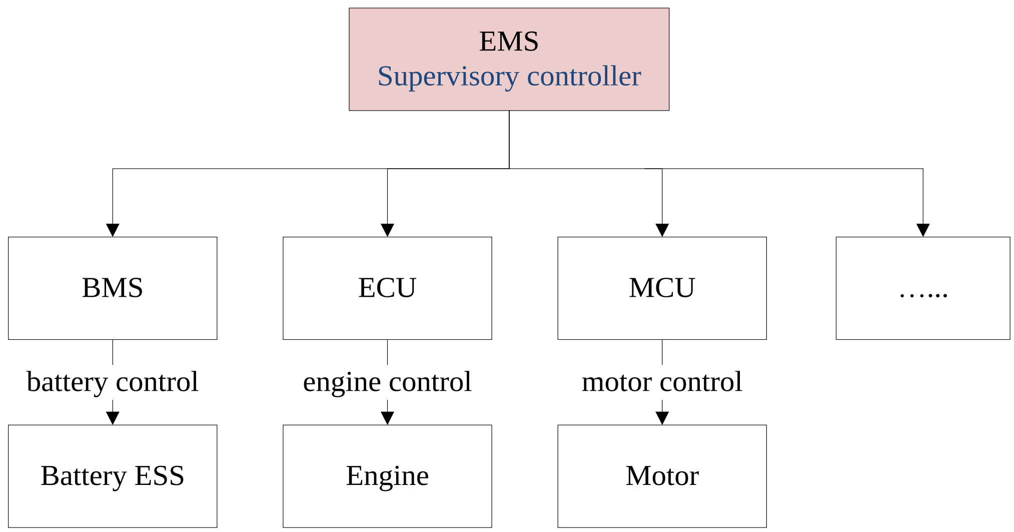

Figure 24: Control Topology in Hybrid Marine Propulsion Systems

The general methods that used in hybrid energy management system can be separated into two categories: the rule-based and model-based optimization methods [89]. Rule-based control logic is a heuristic approach and very effective in real-time implementation. Rules normally acquired based on intuition, experiences, or results from other global optimization methods, therefore, they are not guaranteed to be optimal control rules. Due to its simplicity and easy implementations, it has been widely applied in the optimal design of electric vehicle [36].

Model-based optimization strategies can find a global optimal solution for the system by minimizing a cost function over a fixed load profile. To this end, the model-based optimization control logic must have a known load profile in advance and perform intensive computation to acquire the optimal solution. Both online and offline optimal control strategies have been investigated in the literature [20]. The optimization methods can be numerical or analytical, depending on the formulated problem. The most important thing in model-based optimizations is to find the optimal control laws through optimal control theory.

Optimal control theory deals with the problem of finding a control law for a dynamic system such that a certain optimality criterion is achieved. A control problem includes a cost function that is a function of state and control variables. Early work of optimal control dates back to 1950s with the fundamental researches done by Richard Bellman (1920-1984) and Lev Pontryagin (1908-1988) [105]. Dynamic programming (DP), introduced by Bellman, is still the state-of-the-art method used to solve optimal control problems [37]. The development of minimum principle by Pontryagin (also known as Pontryagin Minimum Principle, or PMP) provides necessary conditions to find the optimal controls [106]. Later in 1980s, reinforcement learning (RL) was developed to deal with more complex control problems that have difficulties to obtain system model. Intelligent control algorithms such as neural networks (NNs) [107], model predictive control (PMC) methods [108], fuzzy logic control [109], etc. provide new ideas to solve the nonlinear control problem.

DP and PMP are the most widely applied methods that can find the theoretical optimal control solution for the hybrid systems in a known load profile. They can only applicable offline and require a priori knowledge about the entire optimization horizon to give the optimal trajectory. DP is a numerical algorithm that can be used to solve a continuous control problem by discretizing the state variables, while PMP can form an analytical formulation for the problem and find a closed-form solution so that the ideal results can be found. Equivalent Consumption Minimization Strategy (ECMS) defines an instantaneous cost function at each time step during the total time horizon, which can lead to the global optimal control strategy if the instantaneous minimization problem is solved appropriately. ECMS approach uses models to convert electricity consumption to an equivalent amount of fuel, and then makes real-time power split decisions to minimize the net fuel consumption. Therefore, ECMS can be used as online optimal control approach. The comparisons of three typical control strategies are showed in Table 9.

Table 9: Comparison of Different Control Strategies

	Rule-based	ECMS	Dynamic Programming
Type	Heuristic	Model-based optimization	Model-based optimization
Application	on-/off-line	online	offline
Optimality	Not optimal	Instantaneous-optimal	Horizon-optimal
Driving cycle pre-request	No	Yes	Yes
Computational Intensive	Low	Low	High

To achieve the real-time optimal control for hybrid electric powertrain systems, the approximate PMP (A-PMP) [110] or adaptive dynamic programming (ADP) [111] algorithm is developed. Their aim are to develop the optimal control that is not relying on the priori knowledge of the future driving conditions, thus, can be implemented in real-time online system.

3.3. Life Cycle Cost Model of Hybrid Marine Propulsions

The life-cycle cost (LCC) model is built in this section to reflect economic influences of hybrid marine propulsions to the whole ship life time operation. It includes capital and operational cost from main powertrain components (i.e. power sources, electric machines and power converters). The costs of other ship elements such as hull and propellers have been excluded; however, they can be easily added into the results to find the total ownership costs (TOC). All the cost and/or price in this study are given in Canadian dollars.

Traditional LCC calculation methods in the marine industry, such as the LCC from NORSOK standards[112], are not suitable for the evaluation of hybrid marine propulsion systems. Due to the cost-intensive Li-ion battery ESS and its relatively short lifetime, it is important to evaluate the battery replacement cost and residual cost during the total ship life.

In this study, a new LCC model for hybrid marine propulsions is proposed. The main elements in the LCC model include the capital cost (C_{cap}), operational cost (C_{ope}), and residual cost (C_{resd}).

$$LCC = C_{cap} + C_{ope} + C_{resd} \tag{31}$$

The net present value (NPV) analysis is used in the LCC model to calculate the present value of cash flows over the entire lifetime. After setting the base year cost, the future cost is discounted back to the base year so that present value of the cost flow can be represented.

$$NPV = \sum_{t=0}^{N_t} \frac{C_t}{(1+r)^t} \tag{32}$$

where C_t is the net cost in year t, which can be assumed equally for every year; N_t is the total lifetime in year; r is the annual discount rate/inflation rate.

3.3.1 Capital Cost

The capital cost (C_{cap}) includes all the purchase cost for main propulsion components. The reinvestment cost of Li-ion battery ESS must be considered due to its short lifespan compared to engines and other components. Moreover, for NG-fueled engines and hybrid propulsions, additional cost may occur.

$$C_{cap} = C_{eng} + C_{buk} + C_{hyb} + C_{ess} + C_{chag} + C_{rin} \tag{33}$$

where, C_{eng} is the engine cost;

C_{buk} is the bunkering system and gas storage cost for NG-fueled engines;

C_{ess} is the battery ESS cost;

C_{hyb} is the cost for hybridization and electrification, including purchasing the electric motors/generators and power converters;

C_{chag} is the charging facility cost for plug-in hybrid propulsion systems;

C_{rin} is the reinvestment cost due to the replacing of battery ESS;

Engine and ESS cost (C_{eng} and C_{ess}) are related to component sizes and prices.

$$C_{eng} = p_{eng} P_{eng} \tag{34}$$

$$C_{ess} = p_{ess} E_{ess} \tag{35}$$

where P_{eng} and E_{ess} are the engine power (kW) and battery ESS energy (kWh), and p_{eng} and p_{ess} are the prices for engine (\$/kW) and ESS (\$/kWh).

C_{rin} is the reinvestment cost, counting for the replacement cost of battery ESS due to the lower lifetime. The operation life of battery ESS (L_{bat}) is calculated based on developed battery life prediction model in Chapter 2.

$$C_{rin} = \sum_{t=0}^{N_t} \frac{C_{ess}}{(1+r)^t} k_t \tag{36}$$

where k_t is the replacement frequency, which is a function of the battery lifetime (L_{bat}). r is the annual inflation rate. L_{bat} is the key parameter that determines the reinvestment capital costs. The optimal result of L_{bat} must be determined at the system level considering both engine and ESS operation conditions.

$$k_t = f(L_{bat}) = \begin{cases} 1, & m = n \cdot L_{bat}, m \leq N_t \\ 0, & otherwise \end{cases} \quad (37)$$

where m is the year time when replacement occurs in the whole lifespan N_t, i.e., the when the battery life is ended. n is integer numbers, $n = 1,2,3$ ... When the battery needs to be replaced in year m, then k_t=1, otherwise, k_t is 0.

3.3.2 Operational cost

Operational cost is generated during the lifetime operation, including the energy consumption and engine maintenance cost. Other costs related to the ship insurance, registration, etc. are excluded.

$$C_{ope} = \sum_{i=0}^{N_t} \frac{C_{energy} + C_{maint}}{(1+r)^i} \quad (38)$$

where C_{energy}, C_{maint} are cost for energy consumption and engine maintenance. r is the annual inflation rate. i is the year from 0 to N_t.

Three different types of energy occurred in proposed hybrid propulsion systems: the LNG, diesel (specifically ULSD), and electricity. The energy cost is dependent on total energy consumption and the price.

$$C_{energy} = C_{fuel} + C_{elec} \quad (39)$$

where C_{fuel}, C_{elec} are costs for marine fuel and electricity respectively.

$$C_{fuel} = p_{fuel} \cdot m_{fuel} \quad (40)$$

where p_{fuel} is the price of marine fuel ($/kg); m_{fuel} is the total mass of consumed fuel (kg).

$$C_{elec} = p_{elec} \cdot e_{elec} \tag{41}$$

where p_{elec} is the price of electricity ($/kWh); e_{elec} is the total charged electricity from grid (kWh).

The energy prices are varied with different types of fuel as well as the end-user groups. And they are the key factors for the total operation cost evaluation. To be clear, prices in this study are intended for industrial consumers in BC, Canada.

(1) <u>Marine Fuel Price in BC</u>

Canada has a large reservation volume of natural gas and is ranked as the fourth largest producer of natural gas in the world. The variation of natural gas price can be found from AECO hub, which is Canada's largest natural gas trading hub [113]. As the marine fuel, the LNG price consists of the cost from the natural gas, the liquefaction, the storage and distribution. Analysis shows that liquefaction cost can be as high as the gas price itself, which is a significant part of the total LNG cost.

A report from the Canadian Natural Gas Vehicle Alliance [102] has estimated all the costs for natural gas liquefaction, delivery and storage, based on the existing facilities utilization in BC. More information have been collected from U.S. Energy Information Administration (EIA) [114], The Alberta Market Price of natural gas [115], BC Ferries fuel strategies report [116], Canadian Natural Gas Vehicle Alliance [102], etc. In conclusion, the price of marine fuels are assumed as $10/GJ for LNG and $24/GJ for ULSD in BC, Canada.

(2) <u>Electricity Price in B.C.</u>

Electricity price differs across the whole country due to a number of factors, such as the main type of power generation and the market structure. British Columbia offers one of the lowest electricity prices in Canada. Benefitting from its 92% hydroelectricity, BC hydro provides low-cost and less GHG emission for all the customers [117].

A report from Hydro Quebec has compared the annual rate of industrial electricity prices for different jurisdictions in North America [118]. According to a report from the Association of Major Power Customer of BC ("AMPC"), BC Hydro's industrial rates have risen faster than other Canadian jurisdiction since fiscal 2011 [119]. The industrial electricity price in Vancouver, BC with provincial sales tax (PST) is 5.87¢/kWh in fiscal 2017.

In conclusion, the prices of energy used in proposed propulsion system are presented in Table 10.

Table 10: Comparison of Energy Prices

Energy Type	USLD	LNG	Electricity
Price (Cad$)	1.04($/kg)	0.45($/kg)	0.0587($/kWh)

Engine maintenance and repair occur periodically during its lifetime. Engines need regular inspection and maintenance to keep it operating properly. The maintaining cost is highly relevant to its maintaining schedule, which is a function of total operation time. Estimating maintenance cost has been difficult as it varies with yearly operational time, manufacturers, and specific maintaining contents. Since engine maintenance cost is closely related to its working time and the initial capital cost (largely associated with engine size). It is assumed that the maintenance will cost half of the engine's initial purchase cost each 10,000 hours, including all the required lubrication oil change, parts replacement and labor fee.

Maintenance cost for LNG engines are considered lower than diesel engines according to the engine vendor [25]. Since natural gas fuel is cleaner, equipment tends to have lower inspection frequency due to reduced deterioration of the fuel supply system. LNG engines are estimated to have 9% lower maintenance cost over the whole life time compared to conventional diesel engines [120].

3.3.3 Residual Cost

The residual cost (or salvage cost) of replaced Li-ion batteries is nontrivial for this expensive component. As stated before, it is usually considered to replace the battery ESS from hybrid propulsion system in transportation application when the battery capacity reduces to 80%. Retired batteries from hybrid transportation vehicles can be reused for residential energy storage and load leveling in the smart grid application. Research has showed that the second use of a Li-ion battery can be provided at a relatively low price based on the techno-economic analysis [121].

In this study, residual cost is the remaining value in the replaced battery ESS, which is also determined by the replacement times and residual price.

$$C_{resd} = \sum_{i=0}^{N_t} \frac{p_r Q_r}{(1+r)^i} k_i \tag{42}$$

where p_r is the price for the remaining value ($/kWh), Q_r is the remaining capacity (kWh), and r is the annual inflation rate.

Chapter 4 Combined System Design and Control Optimization of Hybrid Electric Marine Propulsions – Application on a Harbour Tugboat

This chapter aims at finding the optimal hybrid electric marine propulsion system according to the specific requirement from different vessels. To reach the optimal result, both the plant design and system control must be addressed jointly in a combined optimization problem. Global optimization algorithms are reviewed in order to solve this problem. Surrogate model-based approach is adopted to improve the computational efficiency and ensure the global optimum.

The application of combined hybrid system design and control optimization in the marine industry, to the best of the author's knowledge, has not been studied before. Therefore, a case study on the optimal design of hybrid electric propulsion system of harbour tugboats is shown in this chapter.

4.1 Literature and Motivation

Modern challenging hybrid powertrain system design involves two critical aspects, determining the power specification of main components (sizing) and distributing the energy requirements among different power sources (controlling). Existing studies of optimal hybrid powertrain system design mostly focus on the component sizing to reach the minimum fuel consumption, emission, or their combinations [36, 122]. Control algorithms for hybrid energy management are usually obtained/optimized based on the selected (not necessarily optimized) power components [37, 123]. The commonly used optimal control algorithms in hybrid electric vehicles include DP, PMP and ECMS, which have been discussed in Chapter 3. These online and offline optimal control algorithms have been widely investigated for HEVs [124] and PHEVs [20]. However, the isolated optimization processes for powertrain dimensioning and control system development do not guarantee a global optimal solution for the system design. Recently, more and more researchers realized the coupled condition of these two design problems and developed combined design and control optimization framework.

The combined hybrid system optimal component sizing and optimal control are complex and computationally intensive. Usually, a bi-level optimization framework is adopted to solve the combined design and control problem [125] [40, 126], in which the inner loop deals with the optimal control problem and the outer loop using different algorithms to find the optimized component size. Patil [39] utilized a coupling term to capture the dependence of the optimal control solution on the battery size to reduce the computational time for the optimal design and control of a PHEV. A comparison of different bi-level optimization methods, with the inner loop using the DP and the outer loop using the GA, sequential quadratic programming (SQP), PSO and pattern search are discussed [126]. However, the Li-ion battery performance degradation is seldom considered in aforementioned studied due to the lack of accurate life prediction model. In general, the combined design and control optimization problem is highly nonlinear, non-convex, and expensive to compute. There is an urgent need to find an effective method to solve this type of problem.

Metamodelling-based optimization method can effectively reduce computational time through building explicit approximation (or surrogate model) of the original expensive simulation model, therefore, it can afford much quicker computation. Some gaps remain in using surrogate models to solve hybrid powertrain system design, especially in marine industry. To address this problem, this study initiatively adopts metamodelling approach to solve the complex integrated design and control optimization problem for hybrid electric marine propulsion system. To conclude, some creative ideas in this chapter include:

- adopting a detailed Li-ion battery performance degradation and life prediction model to support battery lifetime estimation;
- using the LCC model as the main objective function of the hybrid marine propulsion design, which can reflect the influences from both the component sizing and control algorithm;
- formulating the integrated optimal design and control problem in a bi-level, nested optimization framework;
- building a surrogate model to solve the nested optimization problem with improved computational efficiency;

In the following part of section 4.1, global optimization methods that are commonly used in solving engineering problems are reviewed. Some background knowledge of solving nested optimization problem through surrogate modelling method is also introduced. In the next few sections from 4.2 to 4.4, the proposed approach is applied for the design of harbour tugboats' hybrid propulsion system. The optimized design solution, acquired through nested optimization for combined system design and control, provides the best result as a benchmark for other design solutions.

4.1.1 Global Optimization Algorithms

Optimization algorithms are essential in finding the best solution of complex real-life engineering design problems. The general optimization approaches can be separated in to analytical methods, graphical methods, experimental methods, and numerical methods [127]. Classic optimization techniques are analytical methods based on the differential calculus which can guarantee to find the global optimal within finite time. Graphical and experimental techniques are of limited usefulness in practical applications due to the complicity of objective functions and constraints. Numerical methods are the most widely applied approaches in solving highly nonlinear complex optimization problems. It is also referred as *mathematical programming* in optimization community, in which iterative numerical evaluations are executed to generate progressively improved solutions. Commonly used mathematical programming includes linear programming, quadratic programming, nonlinear programming, dynamic programming, etc. [127].

Gradient-based classic optimization methods (such as Newton algorithm) require mathematically described objective functions that limit their applications in solving some engineering problems. Heuristic algorithms, on the contrary, are often gradient-free rules that can solve problems when classic methods fail to. Heuristics can find a "good enough" solution in limited time; however, it is hard to measure how close the solution is to the global optima. The trade-offs between the accuracy and computational time have to be clearly considered. Meta-heuristics are higher-level heuristic algorithms that can provide more accurate solutions by generating a set of heuristics iteratively. Most of meta-heuristics are derivation-free, which means they optimize problem stochastically and iteratively. The optimization process starts with random initial values and there is no need to calculate the derivative of search spaces to find the optimum. The stochastic nature of meta-heuristics allows them to easily avoid local optima and search the entire design space extensively. They normally use more sophisticated methods to search globally in the feasible domain and to accept a temporary deterioration of the solution to escape from the local optima. Most of searching algorithms in meta-heuristics are inspired by nature phenomena. Meta-heuristic methods are very popular in solving complex optimization problems due to the simplicity, flexibility, derivation-free mechanism, and local optima avoidance [128].

Nature-inspired meta-heuristic algorithms have been developed over past few decades to solve complex optimization problems with increased problem sizes. Depending on their inspired nature phenomena, the meta-heuristics can be classified as: (1) evolutionary-based algorithms, such as genetic algorithm (GA) [129]; (2) physics-based algorithms which mimic physical rules in universe, such as Gravitational Search Algorithm (GSA) [130]; (3) population-based, or swarm intelligence-based algorithms, such as Particle Swarm Optimization (PSO) [131] and Ant Colony Optimization (ACO) [132]. Population-based meta-heuristic algorithms take advantages from multiple candidate solutions and can better avoid local optima compared to single-solution-based algorithms. The recent popular population-based searching algorithms include the grey wolf optimizer (GWO) [128], the lion optimization algorithm (LOA) [133], and the whale optimization algorithm.

It is usually computationally demanding when apply the meta-heuristics in solving complex optimization problems. It also has to be clarify that no meta-heuristic optimization algorithm that is best suitable for solving all optimization problems, as proved by No Free Lunch (NFL) theorem [134]. In other words, the selections of using which optimization algorithm in specific complex engineering problem rely heavily on engineering experiences. The searching process of population-based meta-heuristic algorithms can be divided into two phases: exploration and exploitation. Exploration determines the way to search for new peaks in unexplored area, while exploitation makes the best decision at given current information. A robust optimization algorithm must balance between the exploration and exploitation to achieve the best performance in searching for the global optimal result.

It is considered as a multi-objective optimization (MOO) problem if a set of different objective functions are optimized simultaneously [135]. The primary goal of MOO is to model the preferences of a decision-maker, where the relative importance of objectives has to be indicated. Different methods can be implemented in solving this type of problems. Depending on how the preferences are articulated, the solutions can be categorized as priori articulation, posteriori articulation, or progressive articulation of preferences, where the decision-maker indicates the relative importance of goals before running the optimization algorithm, after acquiring a set of potential solutions, or adapting inputs during the running of algorithm.

4.1.2 Combined Plant and Controller Optimization

The combined plant design and control optimization has been a difficult task for various applications, mainly due to the increased complexity caused by coupled conditions between the plant and its controller. It is sometimes referred as the *co-design* problem. Reyer [136] and Fathy [38] has deeply discussed various solution strategies for those combined design and control problems, considering the optimality conditions and whether those strategies can find the true system optimum. These strategies can be classified as:

- sequential strategy: optimizing the plant first and then the control. This is naturally followed the system design sequence and often leads to a non-optimal solution;
- iterative strategy: operating the optimization algorithm iteratively, first optimize the plant without sacrificing controller performance, then optimize the control algorithm without compromising plant design;

- simultaneous strategy: formulating the system optimization problem as a function of the two sub-systems (including the objectives and constraints), however the solution can be mathematically and computationally challenging [137];
- bi-level, nested strategy: combining separated design and control optimization problems into two optimization loops in a nested way, the outer (or upper) loop optimizes the plant design, while the inner (or lower) loop generate the optimal control algorithm for each plant selected by the outer loop;
- partitioned strategy: formulating a master problem to govern the interactions between the design problem and control problem, which is a common approach for multidisciplinary optimization problems.

The last three methods is extremely suitable for plant and controller optimization on the coupled conditions, whereas if they are solved sequentially or iteratively, the results are not guaranteed to be the optimum for the combined situation [38]. The definition and quantification of coupling are discussed by Peters [138]. A graphical illustration of different approaches are presented in Figure 25.

The intricate design and control problem of hybrid powertrain systems can be formulated as a nested optimization with multi-objectives. Patil [39] in his dissertation, specifically focused on combined PHEV system design and control optimization to minimize CO_2 emissions and costs and maximize its synergistic interaction with the electric grid. It tackled two optimal control problems for a series PHEV: the on-road power management and the charging strategy. A review of optimization strategies used in the nested problem shows that DP is the most widely accepted benchmark in developing optimal control algorithm (in the inner loop), where GA and PSO are the most commonly used algorithms for component sizing (in the outer loop) [139].

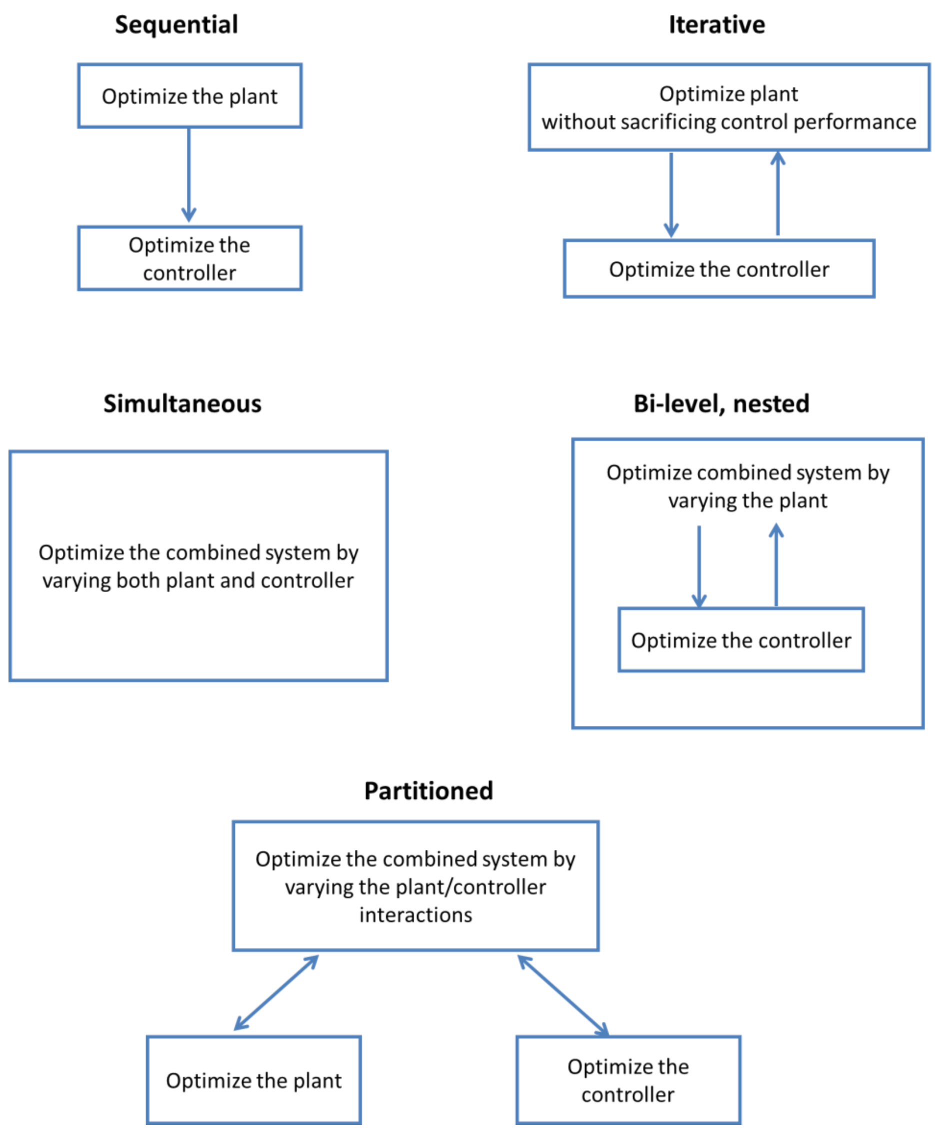

Figure 25: Solutions for Coupled Design and Control Problems (followed [38, 138])

In the bi-level, nested optimization problem, the upper level is usually referred to plant design and typically expressed as a static optimization problem of the following form [38]:

$$\min_{x_p} f_p$$
$$\text{subject to: } h(x_p) = 0 \tag{43}$$
$$g(x_p) \leq 0$$

where x_p is the plant design variable, h and g are the upper level equality and inequality constraints.

The lower level optimization problem is commonly formulated as a dynamic optimization problem as showed below:

$$\min_{u(t),x(t),t_0,T} \left\{ \Phi(x(T),T) + \int_{t_0}^{T} L(x(t),u(t),t)dt \right\}$$

subject to:

$$\dot{x(t)} = f(x(t),u(t),t) \tag{44}$$
$$\Psi(x(T),T) = 0$$
$$\eta(u(t),t) \leq 0$$
$$x(t_0) = x_0$$

where $u(t)$ is the control variable, $x(t)$ is the system state variable, t_0 and T are the initial and end of time, Ψ and η are the lower level equality and inequality constraints, x_0 is the initial state value. Φ and L are cost functions at the final state and during the controlling in the driving profile.

The combined plant/controller design must satisfy all the constraints on the individual problems and also the influence of the plant design on the lower level controller optimization. The two objectives can be weighted together in the combined nested optimization problem through w_p and w_c . Hence, the combined plant/controller optimization problem becomes:

$$\min_{x_p,u(t),x(t),t_0,T}\left\{w_p f_p + w_c\left\{\Phi(x(T),T) + \int_{t_0}^{T} L(x(t),u(t),t)dt\right\}\right\}$$

$$\begin{aligned} \text{subject to:}\quad & h(x_p) = 0 \\ & g(x_p) \leq 0 \\ & \dot{x(t)} = f(x(t),u(t),t,x_p) \\ & \eta(u(t),t,x_p) \leq 0 \\ & \Psi(x(T),T) = 0 \\ & x(t_0) = x_0 \end{aligned} \tag{45}$$

The combined optimization problem has an objective function reflecting both upper- and lower- level cost functions, as well as all the constraints including coupled conditions.

The integrated optimization problem of hybrid powertrain system is non-linear, time-variant system, and with special constraints for different components. The upper level problem relies on a system simulation model involving battery performance degradation model, engine efficiency and emission model, electrical machine efficiency model, and other relevant components model. To solve this problem, the lower level optimization problem (usually very time-consuming) must be solved corresponding to each and every upper level member. This is an effective method, however, also computationally expensive. To address this problem, metamodel-based (or surrogate model-based) optimization algorithm is developed to improve the computational speed with less function evaluations.

4.1.3 Surrogate Model based Optimization

Surrogate models, also known as *Metamodels*, have been widely used in solving engineering design problems due to the expensive computational cost of using high-fidelity simulation models. The numerical simulation model is usually time-consuming, especially when facing the challenge of solving nested optimization problem. The surrogate model (sometimes referred as approximation or response surface) is a model of the simulation model which itself is a model of the real system. Based on a small sample from the actual model, a surrogate model can be built and trained to model the quality characteristics as explicit functions of the design parameters and used subsequently for optimization [140]. The meta-model is well known for its much less simulation time than the original computer model to acquire the system optimum. The most applicable meta-model types are polynomials and Kriging models [141].

Sampling methods can greatly affect the accuracy of the approximation in constructing the surrogate model. Since it is costly to get output Y from a computer simulation model, the selection of input variables x must be appropriately designed and optimized. The design of computer experiments, distinguished from traditional design of physical experiments, can be carried out by determinist simulation model. The efficient design of computer experiments is crucial for the accuracy of approximation.

A good design of computer experiments (DOE) should spread out the sample points over the entire design space as evenly as possible to capture the design behavior. This is usually formulated as an optimization problem to find the globally optimal design and identify locations of multiple samples. Classical DOEs focus on planning computer experiments similar to the physical experiments, and tend to spread the sample points around boundaries rather than evenly fill the design space [142]. Therefore, they are not very efficient for deterministic computer model analyses. The optimized Latin hypercube sampling (OLHS) is a competitive method for constructing optimal design of experiments [143]. The computational cost for building OLHS depends heavily on the algorithms used for the OLHS optimization and the adopted optimality criterion. Through the enhanced stochastic evolutionary algorithm (ESEA), the computational time of OLHS is significantly reduced while maintaining an effective global search [144]. Some basic approximation concepts used in constructing surrogate model are reviewed in [145]. Through the OLHS, the selected data can be executed in original simulation model and prepared for future usage.

The surrogate model is fitted from the input/output data produced by the experiment with the simulation model. Most surrogate models adopt low-order polynomial functions to explain and predict the characteristics of the original simulation model. The Kriging method, also known as spatial statistics, is a very popular interpolation method that can be used to fit the previously generated data and build the approximation [146]. It has been used to solve many engineering problems. Both Schonlau [147] and Sasena [148] state explicitly the efficient global optimization strategy through the Kriging model.

The metamodel validation is an important and challenging process before using it as the surrogate model of the original computation-expensive model. The cross-validation method is commonly adopted in the literature [142]. Generally, it splits original acquired dataset from sampling, uses most of them for training, and leaves out one of the subsets for validation. This leave-one-out cross validation method may not be sufficient enough to estimate the prediction error for different types of surrogate model. Additional points may be required to assess the accuracy of developed surrogate model.

The surrogate model-based optimization can be developed sequentially or adaptively [142]. Traditional approaches in building metamodel-based global optimization take a sequential strategy: first sample the design space, second build a metamodel, third validate the metamodel, and finally do the optimization based on developed metamodel. The adaptive strategy involves optimized results in the sequential loop to update the samples and the metamodel, which can improve the accuracy of approximations. The adaptive surrogate model-based optimization strategy is demonstrated in Figure 26. The hybrid and adaptive metamodelling (HAM) approach is proposed to extend the single metamodel-based optimization to three different types of metamodelling methods to balance the performance and complexity, include the Kriging, the response surface method (RSM) of second-order polynomial, and the radial basis function (RBF) [149]. The HAM method presents a better capability to cover different types of global optimization problems by switching to the most appropriate metamodelling method(s) after the initial search.

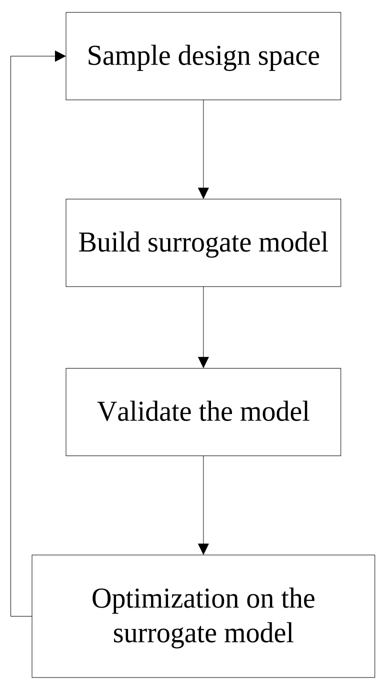

Figure 26: The Adaptive Metamodelling Strategy

4.2 Tugboat Load Profile and Propulsion System Design

This section focus on demonstrating the hybrid marine propulsion design for tugboats, using proposed integrated system design and control optimization via nested approach.

Tugboats are specially designed vessels to assist large ships in confined and restricted water area. They have been noticed as one of the main marine emission resources in BC, Canada [7]. According to the type of work they perform, tugboats can be categorized into several major groups:

a) harbour tugs are employed to assist large ships onto and off their berths by pushing and pulling;
b) escort tugs are designed to provide ship control forces (such as steering and braking) to tankers in confined coastal areas;
c) ocean-going tugs, including offshore support tug, coastal towage tug, offshore rescue or salvage tug, deep sea towage, are generally larger and more sea-capable to work in any rough sea weathers.

There are two reasons why tugboats are suitable for applying hybrid propulsion technology:

a) tugboats are often operated within the ECAs and required to comply with the strict emission standards issued by IMO, which means they are facing more pressure to reduce engine emissions;
b) the collected data of load profile from eight different tugboats, from literature and tug companies as showed in Figure 27, reveals that tugs operate at lower than 20% of main engine power for more than 80% of time, which means the engines mostly work at off-design area.

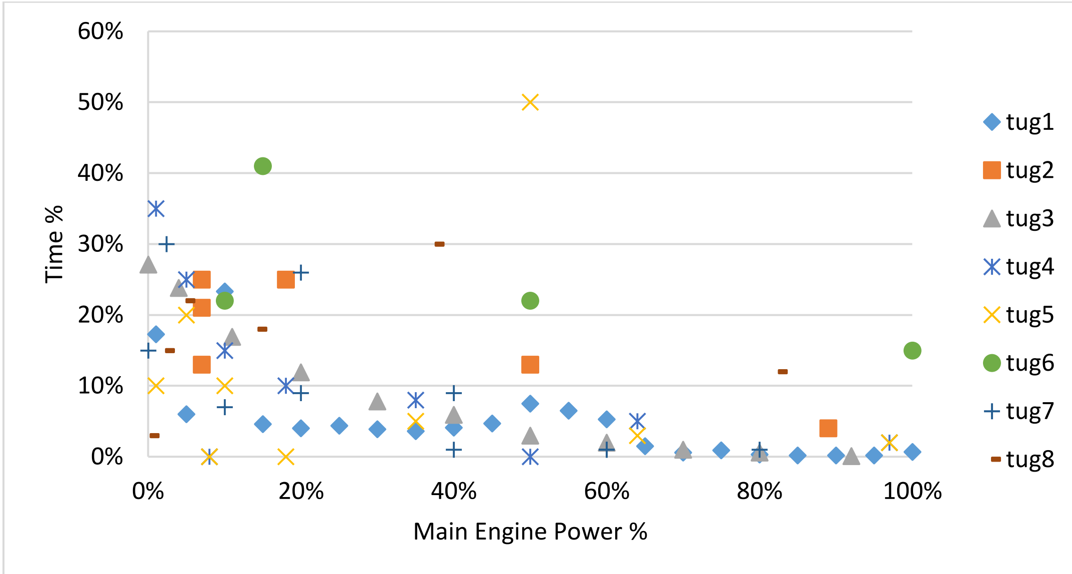

Figure 27: Load and Time Percentages of Different Tugboats

Hybrid electric propulsion can provide more environmentally friendly solution for tugboats. As one of the world leading Canadian tugboat designer, Robert Allan Ltd (RAL) has developed the world's first hybrid-powered tug - the *Carolyn Dorothy*, as well as many tugs with LNG or diesel-LNG dual-fuel systems. The hybrid tug *Carolyn Dorothy* was built in 2009 with two smaller main diesel engines, enlarged diesel-generator sets, and a battery package. It showed great benefits in reducing emissions: about 73% for PM, 51% for NO_x and 27% for fuel related pollutants [15]. Europe also developed hybrid ship handling tug E-KOTUG and hybrid offshore platform supporting vessel, which both were reported to have large amount emission reductions [16] [150].

The interests of adopting hybrid propulsion technologies for tugboats have been increased in recent years. Lindstad and Sandaas [150] provided hybrid propulsion design for offshore support vessels with totally 1000 kWh Li-ion battery ESS.

They compared equivalent CO_2 emissions with traditional diesel generator sets propulsion. Völker [104] presented hybrid propulsion designs for two cases: a harbor tugboat and a motor ferry. The control strategy in hybrid tugboats is also investigated through optimal power management to split the power supply from engines and battery in response to the load demand in [151]. The ECMS control method was adopted in a hybrid all-electric tugboat for power management, and showed 17.6% of fuel saving compare to original rule-based control strategy in [35]. The special needs of control and energy management when hybrid tug is not in service (i.e. in low load demand) was developed by Kifune and Nishio [152].

4.2.1 Modelling of Tugboat Dynamic Load Profile

For conventional tugboats, the component sizing of main engine mainly depends on the maximum bollard pull required by the operation conditions. Therefore, the available tugboat operation data only shows generic power and time percentage, as showed in Figure 27. The design philosophy of hybrid tugboat is very different. Hybrid propulsions create more control variables to achieve better efficiency for engines. Batteries can kick in when the power requests are low, and the engine can be either shut off or operated at a higher load in a more efficient area to charge the battery. The decision to turn on or off the engine must rely on the power requirement profile. Therefore, a dynamic load profile with timescale must be prepared first.

One of the tugboat data from collected information in Figure 27 is chosen as a case to investigate possible fuel savings and emission reductions through optimized hybrid electric propulsion. This tugboat originally has pure mechanical propulsion with two marine diesel engines, each has a maximum 2300kW power. The designed maximum bollard pull of is 75tonne. Two additional diesel generator sets are needed for auxiliary and machinery loads. The generic load data has been shown in Figure 28, with about 2500 hours yearly operation time. Most of its time spends on sailing back and forth from the harbour to ocean or waiting in the sea, which only require 7% of maximum continuous rating power (MCR) of engine. The low, medium and high load demand when assisting ships take about 18%, 50% and 89% of MCR. Main engines only have 4% of chances to work in efficiency area (when performing high load assisting jobs). Obviously, it can result in high fuel consumption and air pollutants when the engine works in the off-design area.

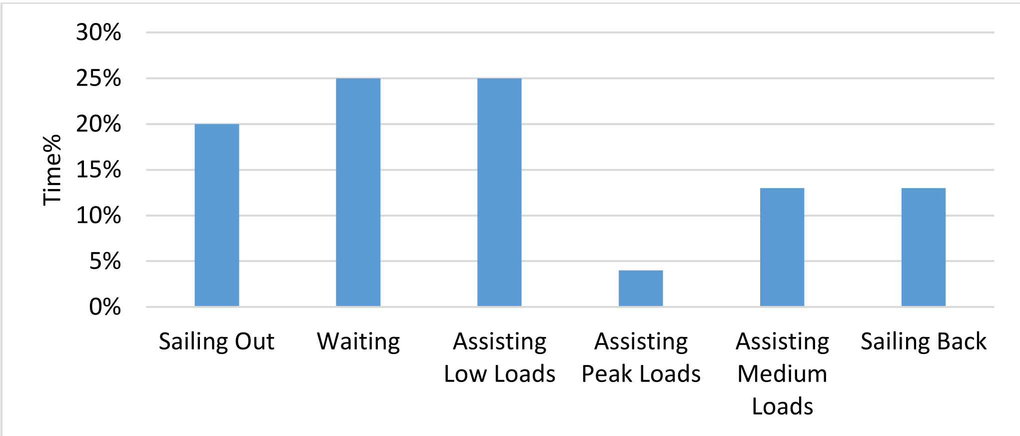

Figure 28: Generic Tugboat Operation Profile

The dynamic tugboat operational profile is developed based on the previous generic data (as shown in Figure 29). When modeling the ship operation in one mission cycle, it follows a general work sequence by sailing out and waiting for orders, then giving pushes and pulls, finally finishing the job and returning in 2.5 hours. The total time percentage for each engine operation condition is statistically coincident with previous generic data. With created power requirement profile, it is possible for future hybrid propulsion system design and optimal power management.

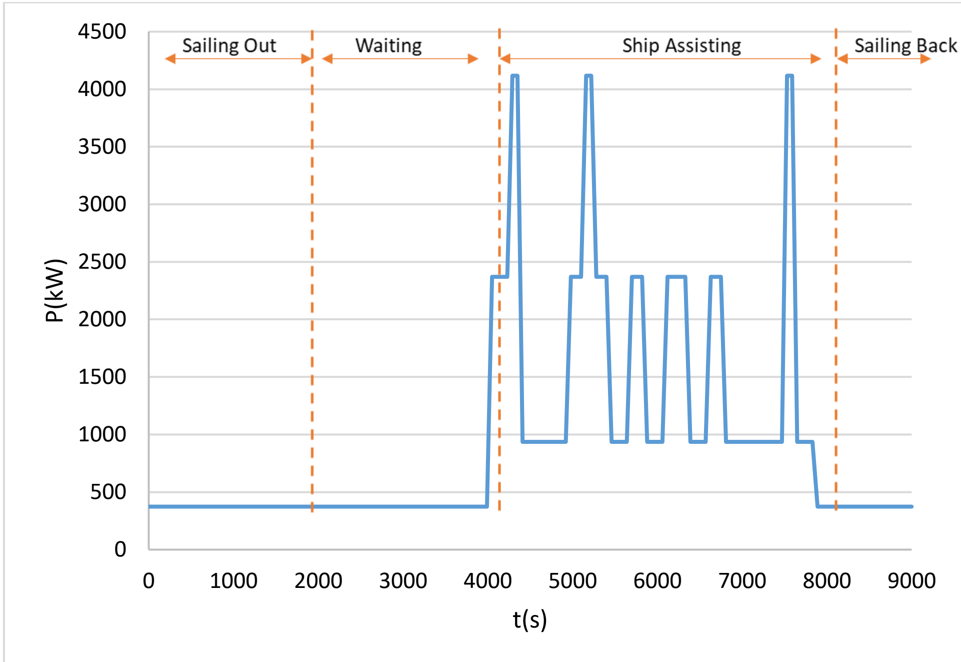

Figure 29: Generated Tugboat Dynamic Operation Profile with Timescale

With this created power requirement profile, the original diesel mechanical and the newly proposed hybrid electric propulsion system can be modelled using previously developed hybrid electric marine propulsion system modeling tools implemented in MATLAB/Simulink.

4.2.2 Design of Hybrid Tugboat Propulsion System

The design of hybrid propulsion for this harbour tugboat involves three aspects, regarding the architecture, different component types, and control strategy. Firstly, it has to decide the hybrid architecture. Pure electric propulsion is not realistic for this tugboat due to the high energy requirement. According to the discussion in Chapter 3, a series architecture is better for tugboat. Since the engine seldom work in high MCR, the advantage of using parallel propulsion cannot be reflected in this case. Series propulsion, on the other hand, can be more efficient when the vessel operates at low power demand. Therefore, an integrated series hybrid electric propulsion architecture is chosen for this case study, with a DC power bus. To keep the redundancy, two engines are adopted but probably only one is needed during operation. The propulsion is presented in Figure 30, the arrows indicate energy flow directions in the hybrid system.

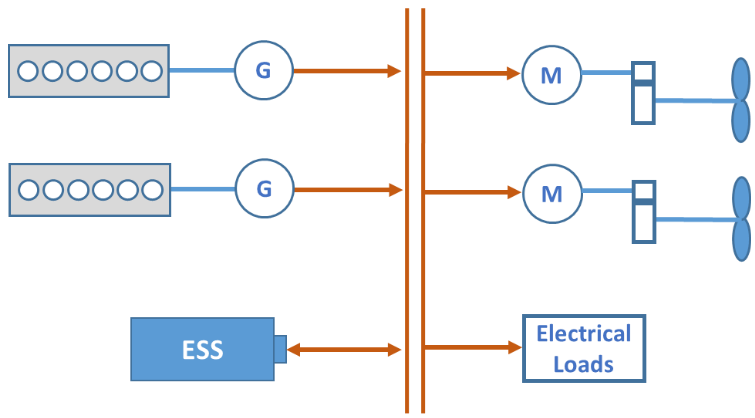

Figure 30: Integrated Hybrid Electric Propulsion System

Secondly, the component type (mainly the engine) must be determined. Diesel engines has mature technology and lower investment cost, but LNG engine has cheaper fuel price and produce lower emissions. It obviously has to be optimized to decide which one is better for the tugboat. Therefore, the two choices are both considered in the propulsion system design.

Last, depending on if the battery ESS can be charged from onshore power grid or not, this system can be hybrid electric system (HES) or plug-in hybrid electric system (PHES). In HES, all energy must come from fuels burned in main engines. Plug-in hybrid needs additional charging facilities, but can save operational cost by using cheap electricity from power grid. In general, four different hybrid propulsions are designed for this harbour tugboat.

- HES with diesel engine
- HES with LNG engine

- PHES with diesel engine
- PHES with LNG engine

The previously proposed nested optimal component sizing and optimal control will be applied to each of these four hybrid propulsions in the following content. Eventually, the best solution can be obtained after the comparison.

4.3 Integrated Design and Control Optimization of Hybrid Marine Propulsions

The ultimate goal of optimal design of hybrid marine propulsion, in this research, is to maintain the lowest total life cycle cost and achieve the highest environmental benefit in the meantime. For proposed hybrid propulsions, the bi-level nested optimization problem must be properly formulated first to address the component sizing in the upper level and the control algorithm in the lower level. In general, it has been assumed that the life cycle of designed propulsion systems must sustain for 20 years operation, with appropriate maintenance and replacement.

4.3.1 Optimal Sizing of Key Components –Upper Level

The sizing of key powertrain components in a hybrid system is critical to the system performance and cost. As discussed in previous chapter, the total life cycle cost (LCC) of hybrid propulsion system can reflect the economic influences caused by key powertrain components, which are the engine size and battery ESS size. Other components, such as electrical machines and power converters are mainly related to these two. Therefore, the upper level design variables are chosen as the maximum continuous rating (MCR) power of engine ($x_1 = P_{eng}$) and the total energy capacity of battery ESS ($x_2 = E_{ess}$).

Moreover, the variation of Li-ion battery depth-of-discharge (DOD) in one driving cycle can heavily affect the battery performance and degradation rate. Generally, the HES tends to keep battery DOD in a short window to avoid the harsh usage, while the PHES prefers to almost100% battery DOD to fully take advantage of the cheap electricity and avoid using fossil fuels. Consequently, the battery lifetime and required total capacity in HES and PHES are different. The specific DOD in hybrid marine propulsions is another variable and needs to be optimized ($x_3 = DOD$). The variables in upper level optimization problem can be summed as

$$x_{up} = [x_1 \quad x_2 \quad x_3]' \tag{46}$$

The main objective for the upper-level optimization is to minimize the total LCC of hybrid propulsion systems over 20-year ship operation. This is a non-convex problem subject to a number of inequality constraints which can be formed as

$$\min_{x_{up} \in X_{up}} F_{up} = LCC(x_{up}, c^*)$$

subject to:

$$\begin{gathered} P_{eng,min} \le x_1 \le P_{eng,max} \\ E_{ess,min} \le x_2 \le E_{ess,max} \\ DOD_{min} \le x_3 \le DOD_{max} \\ c^* = \underset{c \in C, s \in S}{\operatorname{argmin}} f_{low}(s, c, t) \end{gathered} \tag{47}$$

where F_{up} and f_{low} are the upper- and lower-level objective functions; x_{up} and c are the upper-level design variable and lower-level control variable; the design space and control space are referred as X_{up} and C, respectively. The system state variables are $s \in$ S. Each cycle the upper-level optimization needs a complete optimization process of the lower-level problem, imposing high computational cost. c^* indicated the global optimal control policy at each time step t in a driving cycle.

Operating temperature is a critical factor. However, with advanced thermal management techniques, batteries can be kept within the appropriate temperature range. Therefore, the effect from temperature can be ignored in normal usage conditions. The battery cycling current rate (C_{rate}) and variation of DOD are more important in the hybrid system design and energy management strategy development. Therefore, this study will build a semi-empirical model for battery life prediction that can quantify both the influence of C_{rate} and DOD. Since the battery capacity decay in storage is trivial compare to cycling, the storage performance deterioration has been ignored.

4.3.2 Optimal Control of Hybrid Energy Management – Lower Level

The lower-level optimization problem aims at developing the global optimal control policy for hybrid energy management system under a given load profile and pre-determined component sizes. The global optimal control strategy should achieve multiple objectives during system operation, specifically:

- minimize the total energy consumption, including the mass of fossil fuel consumption (m_f) and electricity charged from grid (d_{ele});
- reduce the battery performance degradation (Q_d) in each mission cycle;

The multi-objective character has been reformulated and scaled to fit into one single objective formulation.

$$J = aK \tag{48}$$

where,

$K = [k_{mf} \quad k_{ele} \quad k_{bat}]$ contains scaled value for the total fuel mass flow, electricity consumption and battery degradation, each of them are within range [0,1].

$a = [a_1 \quad a_2 \quad a_3]'$ is the weighted factor to adjust the importance of three sub-objectives, $a_1 + a_2 + a_3 = 1$.

The goal of low-level optimization problem is to find the control laws to achieve the global optimum value of objective function. This can be formulated as:

$$\min_{c(t)\in C, s(t)\in S} f_{low} = \Phi\big(s(t_f), t_f\big) + \int_{t_0}^{t_f} J(s(t), c(t), t)dt$$

subject to:

$$\dot{s(t)} = f(s(t), c(t), t) \tag{49}$$

$$s(t_0) = s_0$$

$$s(t_f) = s_f$$

$$\eta(c(t), t) \leq 0$$

where $s \in S$ is the state variable and $c \in C$ is the control variable, the state variable is subject to certain constraints at the initial and end of time, η is the inequality constraints for control variable, Φ and J are objective functions for final state variable and the total cycle from t_0 to t_f.

Specifically, the control logic determines the power distribution between engine and battery ESS, i.e., $c = [P_{eng} \quad P_{bat}]$. The state variation in this series hybrid propulsion system in only reflected by the battery state of charge, i.e., $s = SOC$. For HES propulsion, the SOC at the end of trip should be the same as initial SOC at the beginning. For PHES, the initial SOC always 100% and the end of SOC can be decided by user. Local constraints, also known as instantaneous constraints, are imposed on the state and control variables at each simulation step. Battery SOC must remain between a maximum and minimum value to ensure prolonged lifetime. Moreover, the charging/discharging current rate (C_{rate}) must be controlled within a certain range according to the battery specification. The torque and speed from the engine and electric motor must also meet certain constraints.

Dynamic programming is a recursive method for solving sequential decision problems by backward induction. It can find the optimal trajectory over a fixed horizon. To solve the overall optimization problem, it has to solve all the sub-problems, hence computationally expensive [37]. It is an off-line method as it requires a priori knowledge about the entire optimization horizon to give the optimal trajectory. To implement DP in the hybrid system control algorithm, the state variable is discretized with time step δt. The length of the control vector is T, where $T = \frac{t_f}{\delta t}$. The state and control variables are quantized into finite grids, as showed in Figure 31.

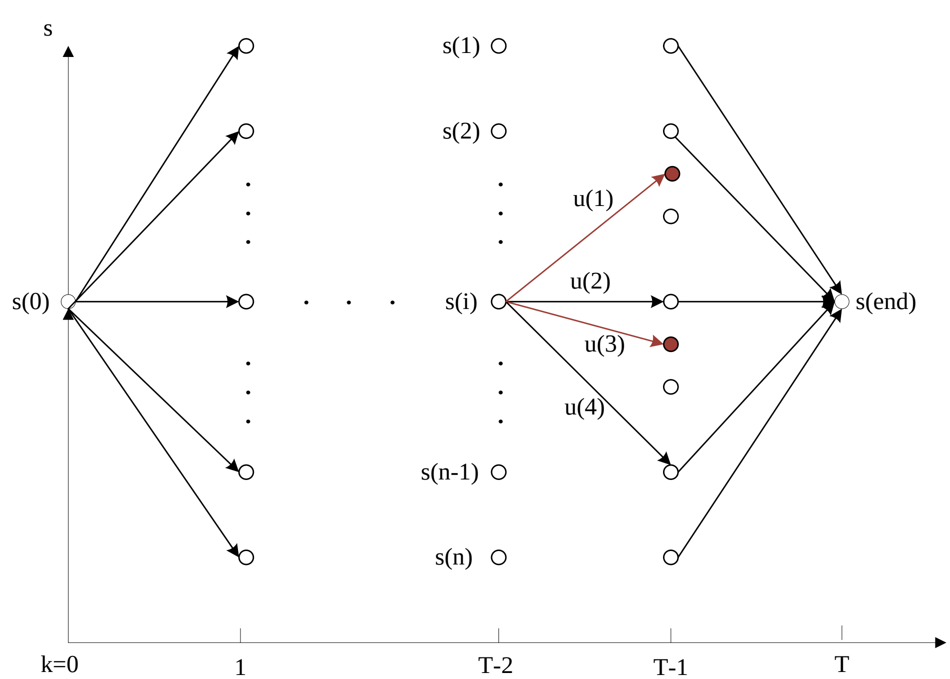

Figure 31: Implementation of DP in Hybrid Marine Propulsion Control

The purpose of DP is to find the optimal control policy $c^* = [c_1\ c_2\ \dots\ c_T]'$ in the discretized time zone which can lead to the minimum value of cost function. To achieve that, the cost-to-go function at each step must be modelled. Starting from the final time step when $k = T$, the final cost function is $J_T(s_T, c_T)$ as

$$f = J_T(s_T, c_T) = a_T K_T \tag{50}$$

When it progresses backward, the cost-to-go function at $t = k$ captures all possible pathways from k to T for all feasible states at each computational node ($k = 1,2, \dots, T - 1$).

$$f(s_k, k) = \min_{u_k}(J_k(s_k, c_k) + f^*(s_{k+1}, k + 1)) \tag{51}$$

One thing that must be noticed is that the updated state variable at time step $k + 1$ sometimes will not land on the discretized state grid, as showed by the red circles in Figure 31. Under such conditions, interpolation is needed to find the optimal value of $f^*(s_{k+1}, k + 1)$.

The DP algorithm is based on Bellman's principle of optimality. It states that no matter what the initial state and initial decision are, "the remaining decision must constitute an optimal policy with regard to the state resulting from the first decision". So at any step k, the optimized control vector can be obtained as:

$$c^*(s_k, k) = \arg\min(f(s_k, k)) \tag{52}$$

The optimization equation is solved backwards in time series until reaches to the initial step $k = 1$. The optimal control policy is determined by solving cost-to-go function at every node in the discretized state-time space.

4.3.3 Combined Nested Optimization Problem

Given the circumstances of coupled optimal sizing and optimal control problem as discussed in former sections, this research introduced a model-based design and optimization method to find the global optimal solution for the hybrid electric propulsion system through a bi-level, nested approach. With the top level optimizing key component sizes and bottom level searching for the optimal control logics, this method can solve the problem in an integrated framework. The overall objective function of nested problem is to minimize the total life cycle cost of hybrid propulsion systems in 20 years operational time. The bi-level, nested optimization problem for the hybrid electric marine propulsion system is formulated as:

$$\min_{x_{up} \in X_{up}} F_{up} = LCC(x_{up}, c^*)$$

subject to:

$$c^* = \underset{c \in C, s \in S}{\operatorname{argmin}} f_{low}(s, c, t)$$

$$\begin{cases} P_{eng,min} \le x_1 \le P_{eng,max} \\ E_{ess,min} \le x_2 \le E_{ess,max} \\ DOD_{min} \le x_3 \le DOD_{max} \\ s(t_0) = SOC_0 \\ s(t_f) = SOC_f \\ s_k = f(s_{k-1}, c_{k-1}) + s_{k-1} \\ SOC_{min} \le s_k \le SOC_{max} \\ C_{rate,min} \le C_{rate,k} \le C_{rate,max} \\ P_{bat,min} \le P_{bat,k} \le P_{bat,max} \\ T_{eng,min} \le T_{eng,k} \le T_{eng,max} \\ \omega_{eng,min} \le \omega_{eng,k} \le \omega_{eng,max} \\ T_{mtr,min} \le T_{mtr,k} \le T_{mtr,max} \\ \omega_{mtr,min} \le \omega_{mtr,k} \le \omega_{mrt,max} \end{cases} \tag{53}$$

As discussed before, the initial and end of SOC in the hybrid propulsions are both 0.5. For the consideration of best utilizing the electrical energy and also prolonging battery lifetime, the initial SOC of battery in the plug-in systems is 1 and the end of SOC is defined as 0.1. Therefore, the DOD in the PHES is no longer a design variable. The specific lower and upper bound for the other two design variables are: $x_1 \in [1800,4000]$ and $x_2 \in [400,1500]$. For HES designs, the design range of battery DOD is defined as $x_3 \in [0.4,0.8]$.

This problem can be solved using a global optimizer (such as GA, PSO, GWO, etc.), or through aforementioned surrogate model-based approach. The two methods have different searching algorithms and may result in different results under the same iterations, thus, are discussed and compared in here through the optimal design of hybrid tugboat.

The GWO algorithm showed superior performance compared to other well-known global optimizer [128], therefore, has been chosen to use in this research to solve the nested co-design problem. Inspired by the leadership hierarchy and hunting mechanism of grey wolves in nature, this global optimization algorithm has demonstrated extraordinary ability in solving engineering design problems compared to other meta-heuristic algorithms such as GA and PSO [128]. Usually a group of grey wolves has a very strict social dominant hierarchy and can be ranked as alpha, beta, delta, and omega with decreased dominances. The best solution in the GWO will be considered as the alpha, the second and third best solutions go to the beta and delta, while the rest of the candidates are the omega. The grey wolf hunting technique includes searching for prey, encircling prey, and attacking prey. Through mathematically modelling the grey wolf hunting mechanism, the positions of alpha, beta and delta are updated iteratively till reach the prey (i.e., the best solution). Though there are possibilities to integrate mutation and other evolutionary operators in the GWO algorithm, most of the researchers have kept it simple and efficient enough with fewer parameters to be adjusted. The source codes of GWO are acquired through [128].

If assuming the grey wolf population is $X_i(i - 1,2, \ldots, n)$, the searching algorithm of GWO is demonstrated in Figure 32.

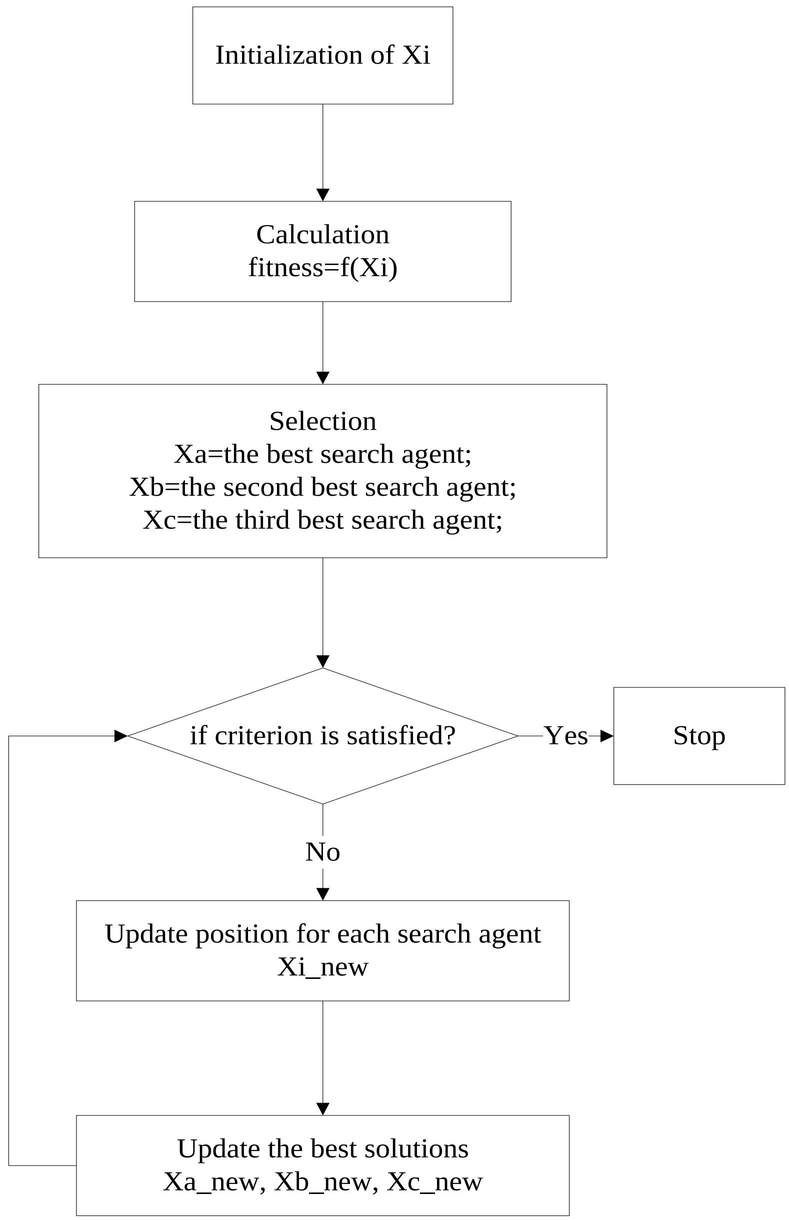

Figure 32: Flowchart of the GWO Algorithm

A surrogate model-based method is more attractive in solving computational intensive problems. Given that the hierarchical structure of developed nested optimization problem may introduce non-convexity and disconnectedness, a surrogate model is constructed through the DOE and supervised sampling. To ensure the lower level search can acquire the global optimal control sequence, DP has been employed. Although DP can provide optimal control over the entire trip, it also leads to longer computational time. For the upper level, data-driven global optimization techniques are then essential to reduce the computation cost in completing the entire integrated optimization process. Figure 33 summarizes the proposed optimization framework and the required techniques, including unsupervised sampling, supervised learning, global optimization, approximate modelling, DP, and optimization integration. In the upper level, OLHS [153], Kriging and the widely used expected improvement (EI) [144] online sampling criterion are used to carry out a “small data”-driven global optimization.

In the supervised learning process, the sampling path is determined by solving another optimization problem. The EI function appeals to lead the searching algorithm to sample points where the uncertainty in the model is highest. In this optimization process, the EI criterion is used to select the new sampling data.

Before getting the LCC value, the whole lower-level DP process needs to be finished to find the optimal pathway, which can be regarded as an expensive black-box model. Kriging is a robust approximation method that is good at predicting nonlinear model, and the EI sampling criterion can guide the surrogate-assisted global optimization. Therefore, Kriging is used to predict LCC, and “maximizing EI” is used to update the Kriging model, and to perform the data-driven global optimization. In addition, in each search cycle, the grey wolf optimization (GWO) algorithm [128] is used to capture the maximum EI value whose corresponding sample point will be supplemented to the database for the subsequent update of Kriging.

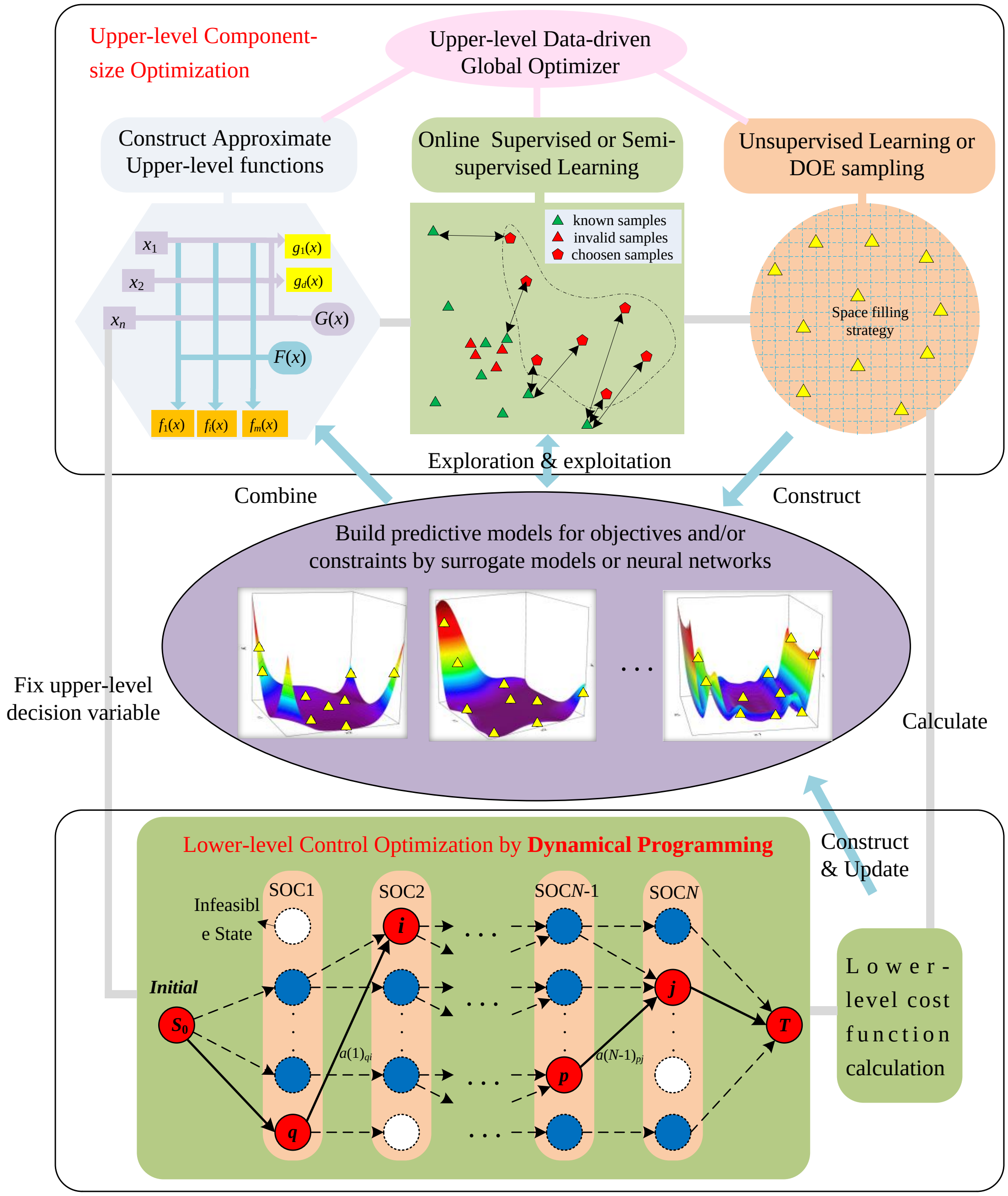

Figure 33: Integrated Metamodeling-based Global Optimization Framework

Specifically, EI is summarized as below,

$$EI(\boldsymbol{x}) = \begin{cases} I \cdot \Phi\left(\frac{I}{s}\right) + s \cdot \Phi\left(\frac{I}{s}\right) & \text{if } s > 0 \\ 0 & \text{if } s = 0 \end{cases} \tag{54}$$

$$I(\boldsymbol{x}) = y_{\min} - \hat{y}(\boldsymbol{x})$$

where s refers to the estimated mean square error at a to-be-tested point $\boldsymbol{x}$, $y_{\min}$ denotes the present best LCC value, $\hat{y}$ is the predictive LCC value from Kriging, and $I(\boldsymbol{x})$ is the estimated improvement. Figure 34 shows the demonstration of EI. The blue area denotes the "Probability Improvement" (PI) that reflects the size of EI values.

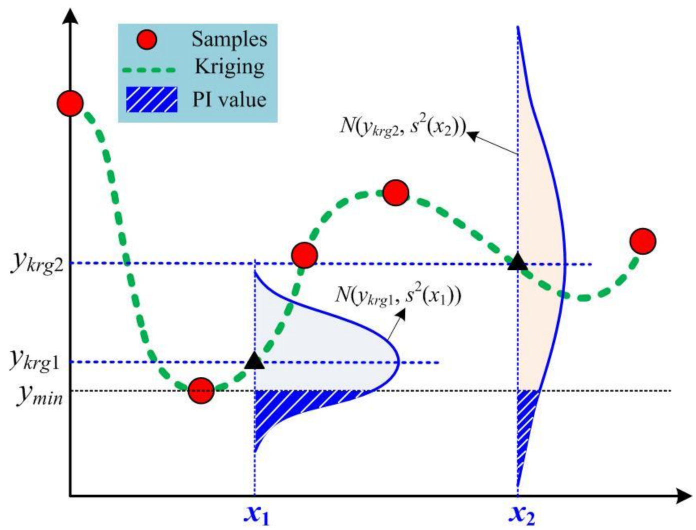

Figure 34: Demonstration of EI

Since the simulation model is computationally expensive, only a relatively small number of sample points are affordable. Initially, the unsupervised sampling takes some random variables from design space, runs a deterministic simulation model, and analyzes the stochastic properties of the solution. The adaptive metamodeling-based design optimization approach is generated in solving the nested optimization problem. It involves the validation and/or optimization in the loop in deciding the resampling and remodeling strategy [142]. The MATLAB-based software package DACE (Design and Analysis of Computer Experiments) is obtained from the internet website of Technical University of Denmark [154]. It provides a well-written modelling code for applying kriging approximations to computer models. Figure 35 presents the flowchart of proposed metamodelling-based global optimization method.

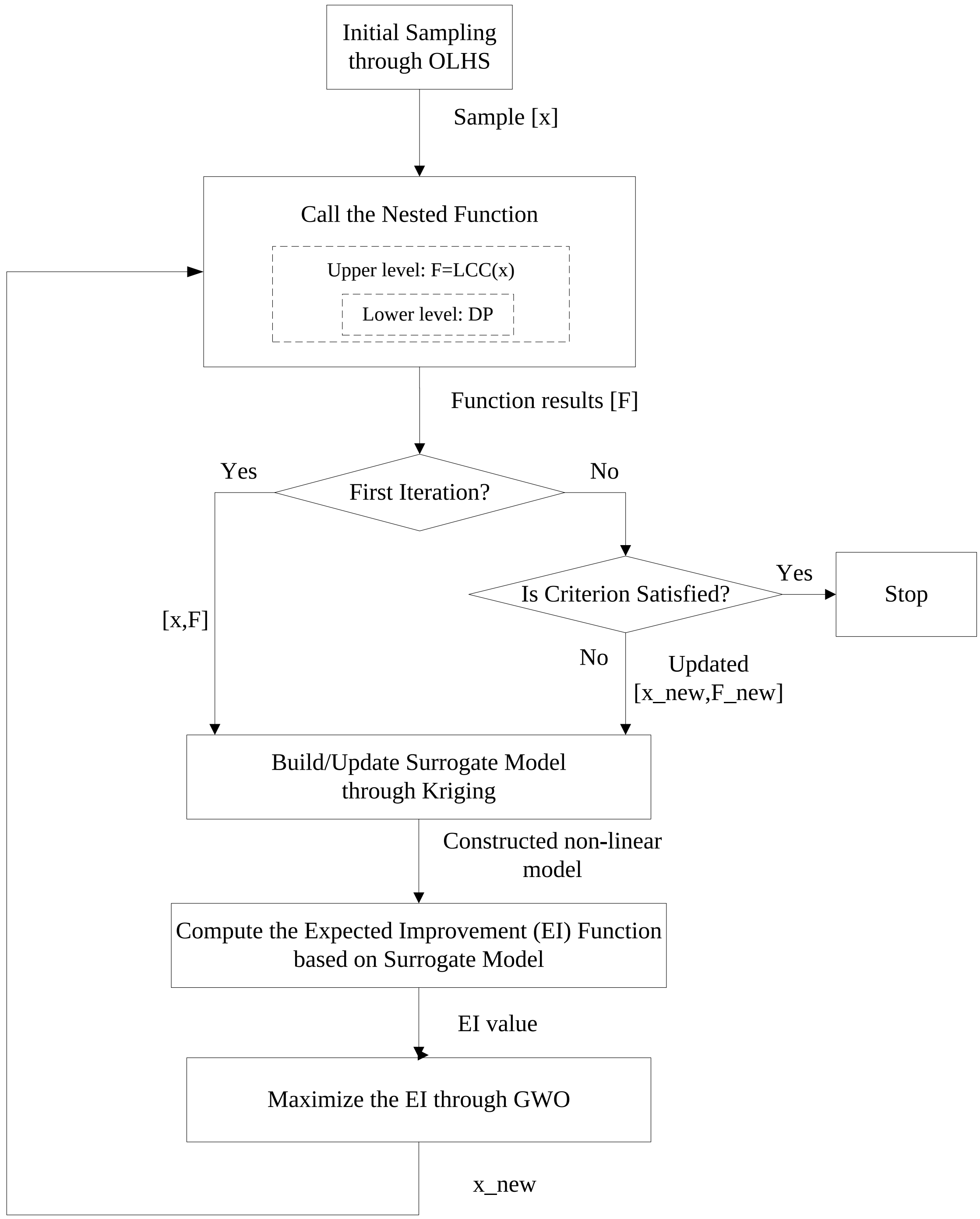

Figure 35: Flowchart of Surrogate Model-based Global Optimization Method

The optimized results using surrogate model-based method will be showed in the next section, as well as the comparisons between directly using GWO and adopting proposed metamodelling approach. The computational time for running one DP for each candidate plant sizes takes 1530.02 seconds and 3553.96 seconds for the HES and PHES configuration, respectively (on a 4-core computer with Intel i7 processor). The computational burden would be unbearable if the DP is executed in a population-based global optimization algorithm. The surrogate model-based approach can solve this problem more efficiently to find the global optimal value under the same iterations of DP.

4.4 Results

The optimal solution of proposed hybrid tugboat propulsion design is achieved after running optimization algorithms each of the cases: HES with diesel engine, HES with NG-fueled engine, PHES with diesel engine, and PHES with NG-fueled engine. At last, the HES configuration with a 1945 kW LNG engine and a 866 kWh Li-ion battery ESS presents the lowest life cycle cost in 20 years' operation. The optimal results and final LCC are showed in Table 11.

Table 11: Optimized Component Sizes and LCC Results

Hybrid Propulsions		Optimal Results				LCC (C$M)
Architecture	Engine	P_{eng}(kW)	E_{ess}(kWh)	DOD	L_{bat} (yr)	
HES	Diesel	2374.88	727.55	0.41	10.78	9.95
	LNG	1944.98	866.33	0.43	10.41	5.63
PHES	Diesel	1903.89	1609.09	0.9*	5.26	8.60
	LNG	2026.32	1178.95	0.9*	5.09	6.94

*: the DOD of PHES systems is pre-defined as 0.9.

Generally, plug-in hybrid configurations tend to have a larger battery ESS compared to hybrid propulsions due to their aspiration of using cheap electricity than fossil fuels. Since the battery can be fully charged to 100% SOC at the beginning of operation, the battery

DOD of PHES has been pre-defined as 90% to take full advantages of energy from battery ESS. Accordingly, the lifetime of battery in PHES is shorter due to the extensive cycling. The searching results of HES with a LNG engine and a battery ESS using proposed surrogate model-based optimization algorithm has been showed in Figure 36.

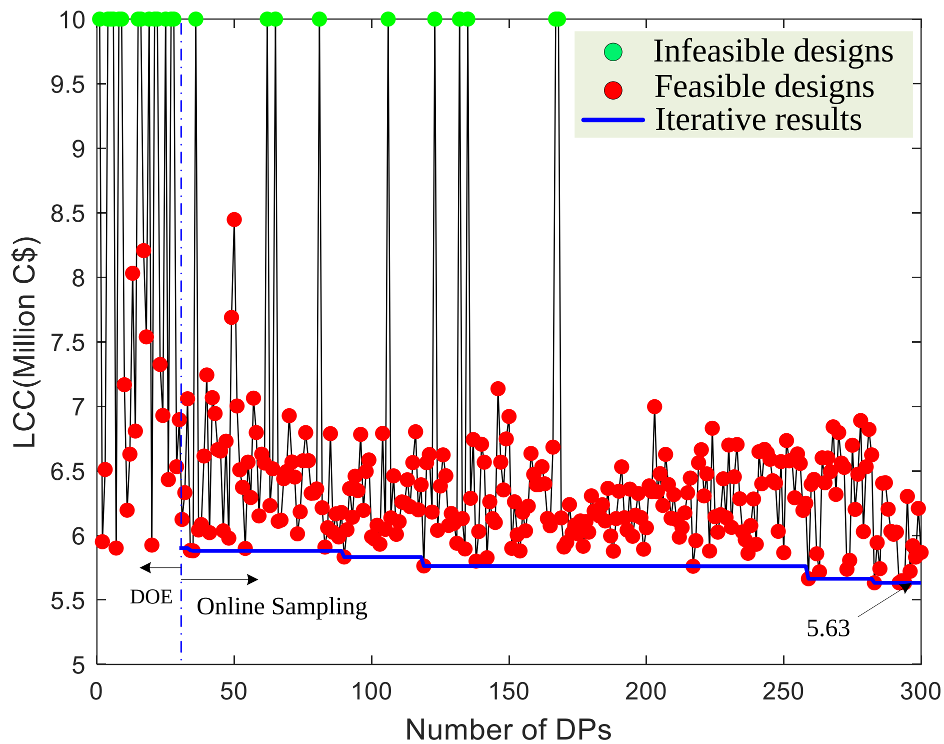

Figure 36: Iteration Results of Proposed Optimization Algorithm

The advantages of using surrogate model-based optimization approach have been demonstrated through comparing the optimized objective result with other conventional optimization methods, such as GWO. Under the same evaluations of DP, the developed surrogate model can find a better global result than GWO, as showed in Figure 37.

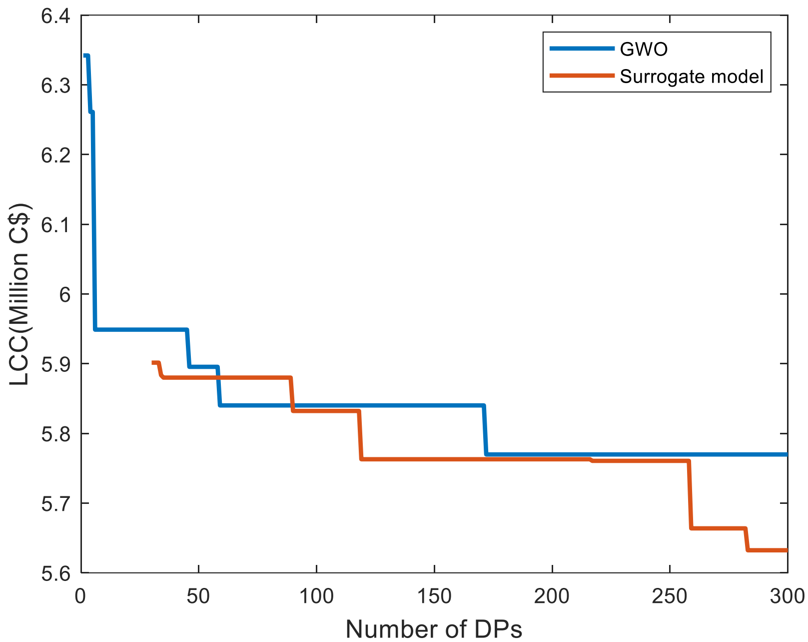

Figure 37: Comparison of Optimized Results between Two Different Approaches

4.4.1 LCC Comparison

The total life cycle costs are obtained as a summation of the capital cost, operational cost, and residual cost based on optimized component sizes and energy management strategy. As counterparts of newly proposed hybrid propulsions, the LCC of traditional mechanical propulsions with diesel engines and LNG engines are also calculated. The LCC comparison of six different tugboat propulsions has been showed in Figure 38. Based on previously developed LCC model, the capital cost includes costs from engines (C_eng), LNG bunkering system (C_bunkering), hybridization (C_hyb), battery ESS (C_ess), charging facility (C_chag), and reinvestment cost (C_rin). C_rin, presented as NPV, is highly affected by the optimized battery total lifetime (L_{bat}).

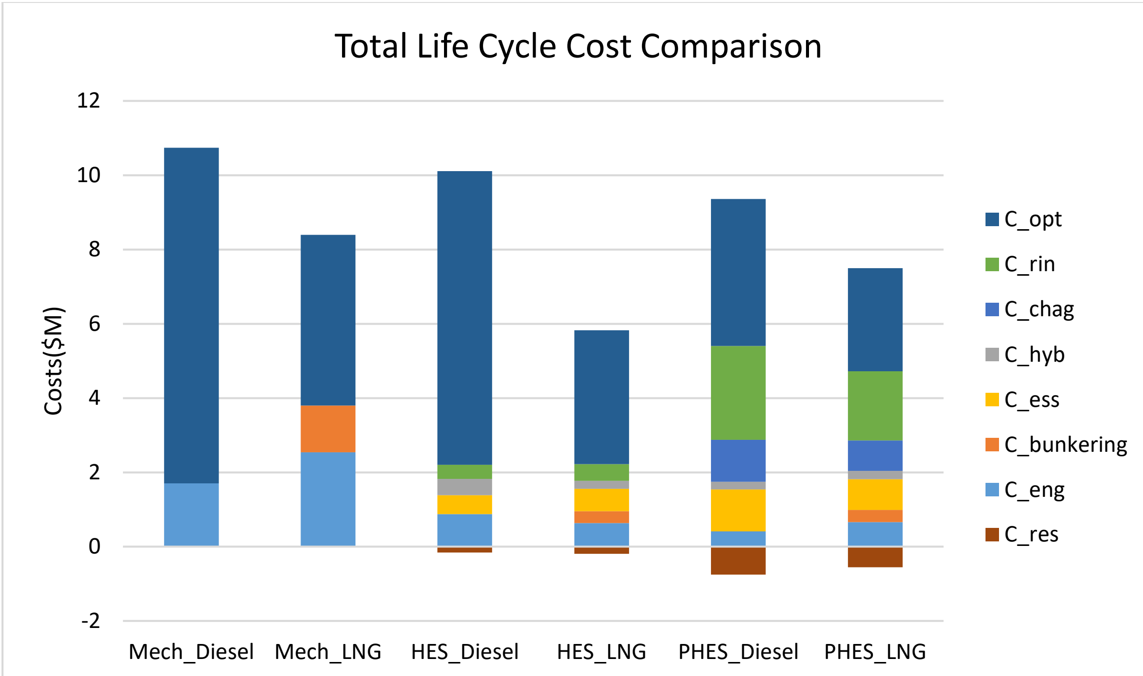

Figure 38: Total Life Cycle Cost Comparison of Six Tugboat Propulsions

One important feature has been noticed that the ship operational cost is way much higher than capital cost in its lifetime operation. Therefore, saving operational cost can significantly reduce total LCC. A general trend of reduced operational cost can be observed when clean energy is used in marine propulsions. In each propulsion architecture (mechanical, hybrid, and plug-in hybrid), LNG-fueled systems have showed lower LCC compared to their diesel counterparts. Although the capital cost of LNG-fueled systems is higher due to the increased engine and bunkering system cost, the operational cost shows an exactly contradictory trend. LNG-fueled systems have about 50% total operation costs savings, compared to their diesel-fueled counterparts. Moreover, the reduced operation cost has overweighed the increased capital cost and achieved relatively lower total life cycle cost. The total LCC savings by changing fuel into LNG range from 35% to 47%, depending on the architectures.

Similarly, hybrid propulsion configurations present 7% to 48% total LCC reductions compared to the original mechanical propulsion. Even though the hybridization and electrification increase capital cost from 1.4 to 2.9 times of original mechanical propulsion, the increased capital cost has been offset by saving operational cost using less expensive fuels such as LNG and electricity to reduce engine operational times and downsize the engine. The comparison is showed in Figure 39.

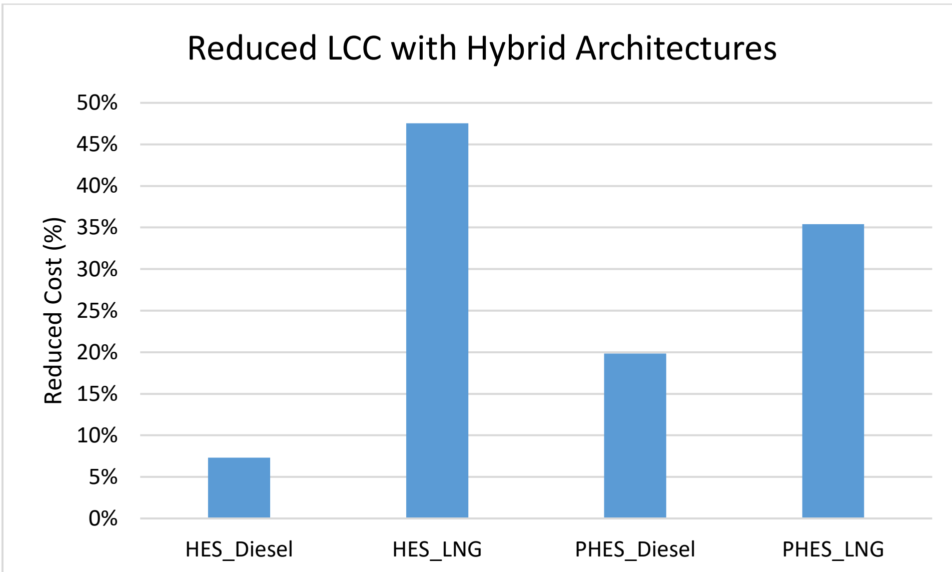

Figure 39: Reduced LCC by Using Hybrid and Plug-in Hybrid Electric System

The payback period of proposed hybrid electric marine propulsions has been evaluated. Compared to the original mechanical propulsion with two diesel engines, the payback period in this research refers to the amount of time the new propulsion takes to recover the increased investment cost. The length of time to reach a breakeven point is determined by the saved operational cost versus the increased cost. As showed in Figure 40, although both HES and PHES propulsion with NG-fueled engine have pretty close 20-year-LCC, the payback time shows that HES system can recover the increased investment cost sooner than PHES propulsion. The final payback period is very case-dependent and shows deep insight in the system design. The comparison of LCC and payback period also confirms the importance of using LCC model for system design and optimization.

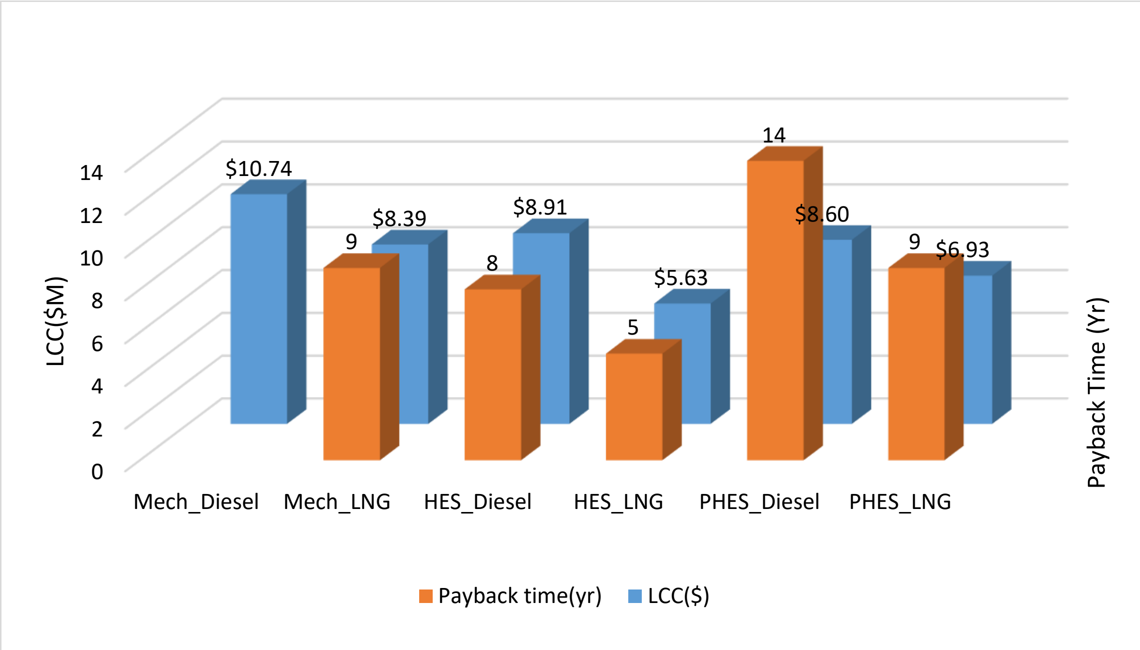

Figure 40: LCC and Payback Times

4.4.2 Powertrain Performance

The optimized energy management strategy in hybrid propulsions and plug-in hybrid propulsions are different. Due to the global constraints of HES propulsions, the initial and end of SOC must keep the same level. The plug-in hybrid systems tend to take full advantage of all stored energy in the battery, therefore the SOC is varied from 100% to a very low value (in this case 10%). The optimized SOC variation for both HES and PHES are showed in Figure 41.

The power distribution between the engine and Li-ion battery ESS in each driving cycle is determined by DP in the lower level optimization program. The total requested power (P_{req}) is satisfied by the battery ESS (P_{bat}) and engine (P_{eng}), as showed in Figure 42. When the power demand is low, battery ESS is adopted to provide energy and the engine is shut off to avoid inefficient operation. While in high demand, the engine is started to work collaboratively with the battery. The surplus energy from engine is used to charge the battery, and allowed it to maintain a certain level of SOC.

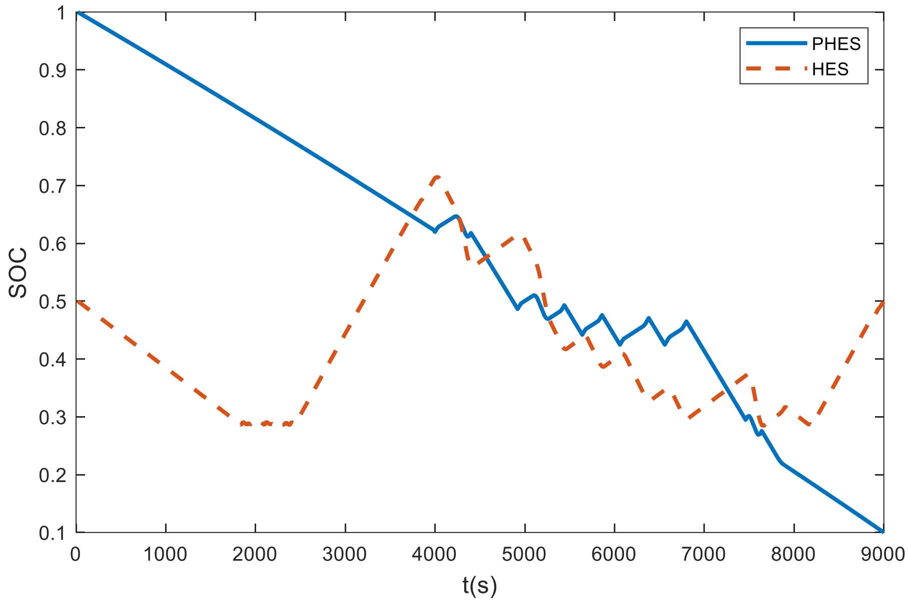

Figure 41: Comparison of Battery SOC Variation for PHES and HES

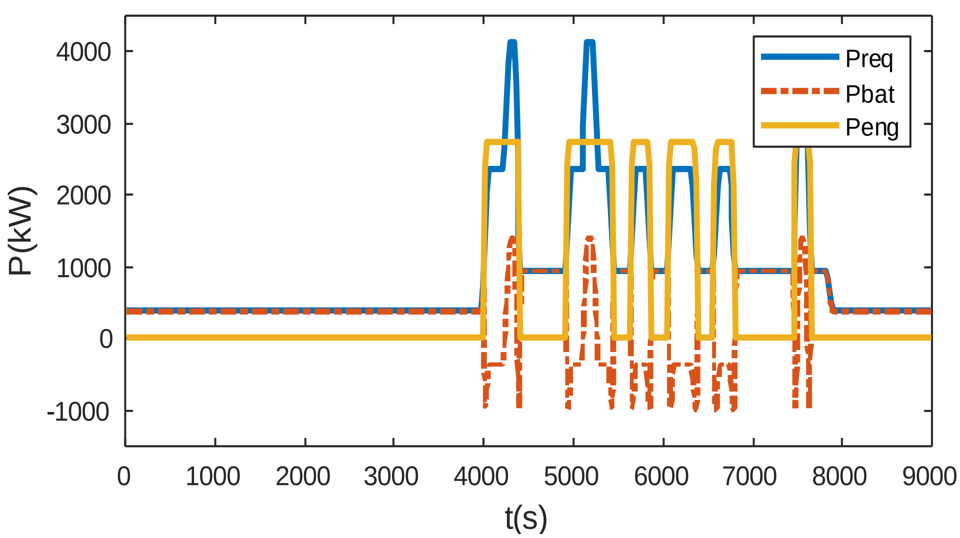

Figure 42: Power Distribution between Battery ESS and Engine

4.4.3 Environmental Assessments

Emission reduction is always one of the primary goals to adopt hybrid electric propulsion systems. The greenhouse gases emissions, mainly CO_2, CH_4, and N_2O from six different propulsion systems are plotted in Figure 43. CH_4 and N_2O emissions from LNG were much lower in comparison; therefore, they are scaled to be included in one illustration.

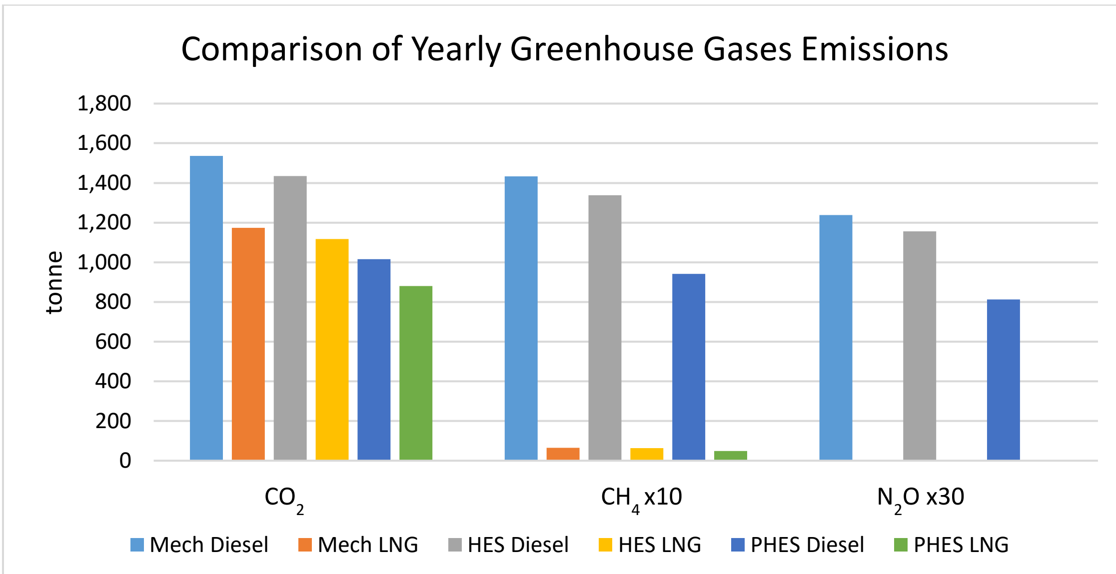

Figure 43: Yearly Greenhouse Gases Emissions of Different Propulsion Systems

The CO_2e of different propulsion systems have shown a clear decreasing trend with hybrid and LNG-fueled propulsions. LNG engines can greatly reduce GHG emissions compared to diesel ones (as shown in Figure 44). Moreover, the plug-in hybrid system can also cut the CO_2e. Hybrid diesel system can reduce 6.67% CO_2e, while plug-in hybrid can reduce 34.30%. For conventional diesel-fueled mechanical propulsion systems, switching to LNG-fueled system can reduce more GHG emissions than using hybrid or plug-in hybrid technologies.

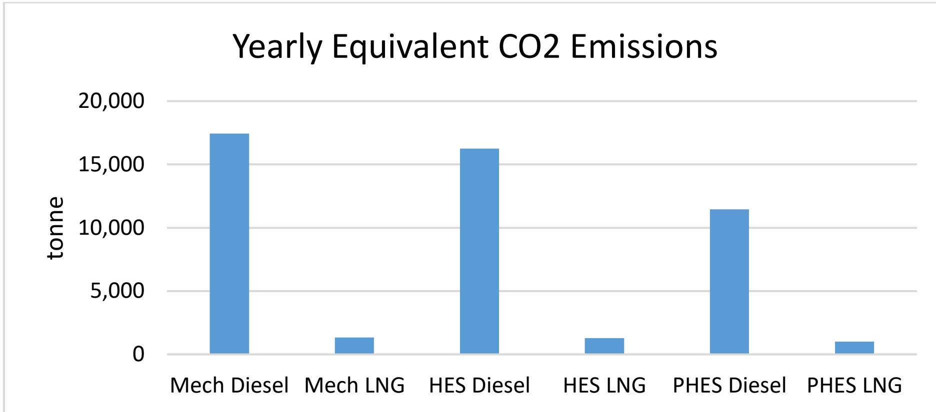

Figure 44: CO_2e of Different Propulsion Systems

Air pollutants, including SO_x, NO_x, and PM, also show the same trend as CO_2e (in Figure 45). LNG fueled systems have negligible SO_x emissions and much less NO_x and PM emissions. The deeper the hybridization, the less is the emissions.

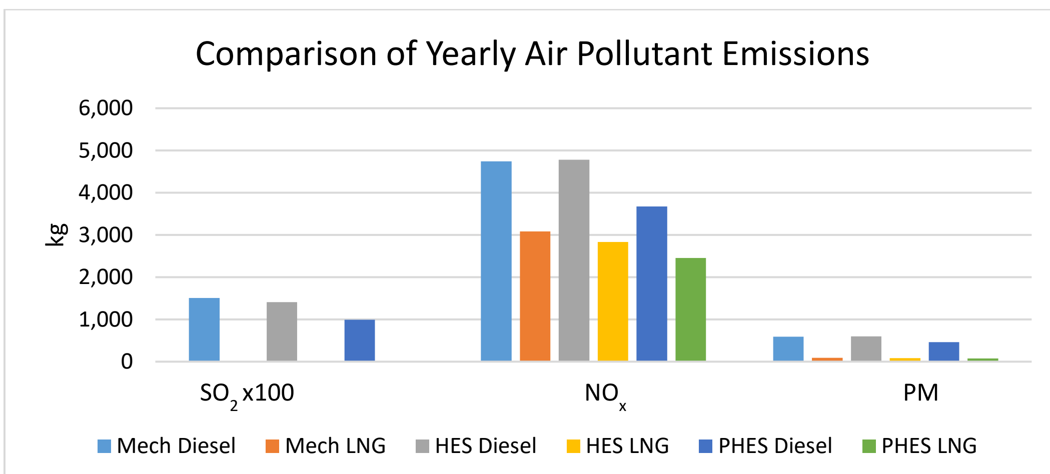

Figure 45: Air Pollutants Emissions of Different Propulsion Systems

Chapter 5 Conclusions

5.1 Summary

This research presents a new and an effective method to solve the interrelated optimal powertrain component sizing and optimal control problem for the hybrid marine propulsion system. The combined plant design and system control problems have been jointly formulated as a bi-level, nested global optimization problem. The upper-level of the optimization searches for optimal powertrain component sizes to minimize the total life cycle cost, while the lower-level optimization ensures the optimal powertrain control/energy management solution of each feasible powertrain system design under given power load patterns. The complex and computationally intensive optimization problem is solved using a surrogate model-based global optimization method.

The integrated hybrid electric ship modelling tool platform is developed in this dissertation to support the design and modelling of different propulsion configurations. One key powertrain system component, Li-ion battery ESS, has been closely investigated considering materials, aging phenomena, and other affecting factors. Based on extensive experimental data, the performance degradation and life prediction model of lithium iron phosphate ($LiFePO_4$ or LFP) battery has been developed and validated. The economic and environmental benefits of using NG-fueled engine in marine propulsions are examined and compared with its diesel-fueled counterpart. In general, six different propulsion systems are proposed and applied on a harbour tugboat, including mechanical propulsion with diesel and NG-fueled engines; hybrid electric systems with diesel and NG-fueled engines; plug-in hybrid electric systems with diesel and NG-fueled engines. The global optimal energy management strategy is developed for hybrid propulsions through dynamic programming (DP). The best solution is acquired through optimization using proposed surrogate model-based method to solve the nested system design and control problem. The optimized hybrid electric propulsion system offers improved fuel efficiency, reduced emissions and less life cycle cost compared to the original mechanical propulsion.

5.2 Major Research Contributions

This research further improved the methodology of model-based design and optimization of hybrid electric marine propulsion systems, and demonstrated the feasibility and benefits associated new methods through their applications to tugboat propulsion system design and control developments.

Specifically, major contributions of this research include:

a) introduced a new integrated model-based design and control optimization method for hybrid electric marine propulsion system;

b) established a high fidelity Li-ion battery performance degradation model and incorporated the modeling to the size optimization and optimal energy management of battery ESS;

c) presented a systematic model-based design and optimization technique considering LCC of diesel and LNG engine in hybrid electric powertrain systems;

d) developed an effective method for the computationally intensive powertrain system component size and control optimization problem; and

e) demonstrated a new approach for designing the clean marine propulsion system of typical harbour tugboats.

5.3 Future Work

The proposed model-based design and optimization framework can be applied to solve any hybrid powertrain systems, not only in the automotive or marine industry, but also in smart power grid and hybrid ESS. Although it has been implemented in this dissertation for a hybrid marine vessel propulsion design, it would be of interest to many other applications. Moreover, the proposed series-parallel hybrid powertrain can support more flexible vessel operations therefore can be applied to other types of marine vessels in the future.

While the DP-based optimal control investigated in this dissertation can serve for an ideal benchmark for powertrain system operation, it is not suitable for direct real-time applications. Further studies on various real-time optimal control strategies based upon results obtained in this study can be developed.

The sensitivity analysis of the LCC model is a good way to measure the importance of different parameters in the model, including the price variation of different fuels, the engine and battery sizes, as well as the control variable changes. This will be studied and analyzed in the future.

Bibliography

[1] "Review of Maritime Transport 2017," *United Nations Conference on Trade and Development (UNCTAD)*.

[2] "The Paris Agreement," *2018 United Nations Framework Convention on Climate Change*.

[3] "World Nations Agree to At Least Halve Shipping Emissions by 2050.," *https://unfccc.int/news*.

[4] IMO. Available: www.imo.org

[5] IMO, "Energy Efficiency Measures," 2011.

[6] "2015 Port of Vancouver Emissions Inventory Report," *Port of Vancouver*.

[7] "1990-2015 Canada's Air Pollutant Emission Inventory," *Environment and Climate Change Canada*, 2016.

[8] EPA. Available: www.epa.gov/ghgemissions

[9] E. DeColar, T. Reberton, M. Fisher, and L. Blair, "Phasing out heavy fuel oil in the Canadian arctic," 2018.

[10] S. Wang and T. Notteboom, "The adoption of liquefied natural gas as a ship fuel: A systematic review of perspectives and challenges," *Transport Reviews*, vol. 34, pp. 749-774, 2014.

[11] E. Molitor, A. Bakosch, and B. Forsman, "Feasibility Study on LNG Fuelled Short Sea and Coastal Shipping in the Wider Caribbean Region," 2012.

[12] "RAstar 4000-DF LNG-fueled Tugboat," *www.ral.ca*.

[13] "ABS Advisory on Hybrid Electric Power Systems," *American Bureau of Shipping*.

[14] G. Sulligoi, A. Vicenzutti, and R. Menis, "All-Electric Ship Design: From Electrical Propulsion to Integrated Electrical and Electronic Power Systems," *IEEE Transactions on Transportation Electrification*, vol. 2, pp. 507-521, 2016.

[15] G. Faber and J. Aspin, "The foss hybrid tug: From innovation to implementation," in *Proc. of The 20th International Tug & Salvage convention and exhibition*, 2008, pp. 149-156.

[16] "Case Study: E-Kotug, RT Adriaan," *Corvus Energy*, 2015.

[17] T. Nishio and H. Kifune, "A Study on Fuel Saving Effect in Hybrid Propulsion System for Tugboat," *Proceedings of 7th PAAMES and AMEC2016*, vol. 13, p. 14, 2016.

[18] K. Koprubasi, "Modeling and control of a hybrid-electric vehicle for drivability and fuel economy improvements," Doctor of Philosophy, Mechanical Engineering, The Ohio State University, 2008.

[19] R. Geertsma, R. Negenborn, K. Visser, and J. Hopman, "Design and control of hybrid power and propulsion systems for smart ships: A review of developments," *Applied Energy*, vol. 194, pp. 30-54, 2017.

[20] J. Dong, "Modeling and real-time optimal energy management for hybrid and plug-in hybrid electric vehicles," 2017.

[21] A. Haseltalab, R. R. Negenborn, and G. Lodewijks, "Multi-level predictive control for energy management of hybrid ships in the presence of uncertainty and environmental disturbances," *IFAC-PapersOnLine*, vol. 49, pp. 90-95, 2016.

[22] J. F. Hansen and F. Wendt, "History and state of the art in commercial electric ship propulsion, integrated power systems, and future trends," *Proceedings of the IEEE,* vol. 103, pp. 2229-2242, 2015.

[23] S. Bengtsson, K. Andersson, and E. Fridell, "A comparative life cycle assessment of marine fuels: liquefied natural gas and three other fossil fuels," *Proceedings of the Institution of Mechanical Engineers, Part M: Journal of Engineering for the Maritime Environment,* vol. 225, pp. 97-110, 2011.

[24] "DNV GL: LNG as Ship Fuel," *www.dnvgl.com*.

[25] R. T. Madsen, "144-Car Ferry LNG Fuel Conversion Feasibility Study: Life Cycle Cost Analysis," *The Glosten Associates,* 2011.

[26] M. Baumgart and J. H. B. Olsen, "LNG-fueled vessels in the Norwegian short-sea market: a cost-effective response to environmental regulation," 2010.

[27] P. A. Nelson, K. G. Gallagher, I. D. Bloom, and D. W. Dees, "Modeling the performance and cost of lithium-ion batteries for electric-drive vehicles," Argonne National Laboratory (ANL)2012.

[28] Y. Zhang, C.-Y. Wang, and X. Tang, "Cycling degradation of an automotive LiFePO4 lithium-ion battery," *Journal of Power Sources,* vol. 196, pp. 1513-1520, 2011.

[29] E. Sarasketa-Zabala, I. Gandiaga, E. Martinez-Laserna, L. Rodriguez-Martinez, and I. Villarreal, "Cycle ageing analysis of a LiFePO 4/graphite cell with dynamic model validations: Towards realistic lifetime predictions," *Journal of Power Sources,* vol. 275, pp. 573-587, 2015.

[30] S. Santhanagopalan, Q. Guo, P. Ramadass, and R. E. White, "Review of models for predicting the cycling performance of lithium ion batteries," *Journal of Power Sources,* vol. 156, pp. 620-628, 2006.

[31] P. Ramadass, B. Haran, R. White, and B. N. Popov, "Mathematical modeling of the capacity fade of Li-ion cells," *Journal of Power Sources,* vol. 123, pp. 230-240, 2003.

[32] M. Doyle, T. F. Fuller, and J. Newman, "Modeling of galvanostatic charge and discharge of the lithium/polymer/insertion cell," *Journal of the Electrochemical Society,* vol. 140, pp. 1526-1533, 1993.

[33] A. A. Alexander, "Modeling power distribution system of an electric ship for design and control," 2015.

[34] T. L. Vu, J. S. Dhupia, A. A. Ayu, L. Kennedy, and A. K. Adnanes, "Optimal power management for electric tugboats with unknown load demand," in *American Control Conference (ACC), 2014*, 2014, pp. 1578-1583.

[35] L. C. W. Yuan, T. Tjahjowidodo, G. S. G. Lee, R. Chan, and A. K. Ådnanes, "Equivalent consumption minimization strategy for hybrid all-electric tugboats to optimize fuel savings," in *American Control Conference (ACC), 2016*, 2016, pp. 6803-6808.

[36] J. Shen, S. Dusmez, and A. Khaligh, "Optimization of sizing and battery cycle life in battery/ultracapacitor hybrid energy storage systems for electric vehicle applications," *IEEE Transactions on industrial informatics,* vol. 10, pp. 2112-2121, 2014.

[37] O. Sundström, D. Ambühl, and L. Guzzella, "On implementation of dynamic programming for optimal control problems with final state constraints," *Oil &*

Gas Science and Technology–Revue de l'Institut Français du Pétrole, vol. 65, pp. 91-102, 2010.

[38] H. K. Fathy, J. A. Reyer, P. Y. Papalambros, and A. Ulsov, "On the coupling between the plant and controller optimization problems," in *Proceedings of the 2001 American Control Conference.(Cat. No. 01CH37148)*, 2001, pp. 1864-1869.

[39] R. M. Patil, "Combined Design and Control Optimization: Application to Optimal PHEV Design and Control for Multiple Objectives," 2012.

[40] Y. Zou, F. Sun, X. Hu, L. Guzzella, and H. Peng, "Combined optimal sizing and control for a hybrid tracked vehicle," *Energies*, vol. 5, pp. 4697-4710, 2012.

[41] O. Hegazy and J. Van Mierlo, "Particle swarm optimization for optimal powertrain component sizing and design of fuel cell hybrid electric vehicle," in *2010 12th International Conference on Optimization of Electrical and Electronic Equipment*, 2010, pp. 601-609.

[42] X. Liu, Y. Wu, and J. Duan, "Optimal sizing of a series hybrid electric vehicle using a hybrid genetic algorithm," in *2007 IEEE international conference on automation and logistics*, 2007, pp. 1125-1129.

[43] B. Scrosati and J. Garche, "Lithium batteries: Status, prospects and future," *Journal of Power Sources,* vol. 195, pp. 2419-2430, 2010.

[44] A. Y. Shenouda and K. Murali, "Electrochemical properties of doped lithium titanate compounds and their performance in lithium rechargeable batteries," *Journal of Power Sources,* vol. 176, pp. 332-339, 2008.

[45] J. Qian, W. A. Henderson, W. Xu, P. Bhattacharya, M. Engelhard, O. Borodin*, et al.*, "High rate and stable cycling of lithium metal anode," *Nature communications,* vol. 6, 2015.

[46] P. Poizot, S. Laruelle, S. Grugeon, L. Dupont, and J. Tarascon, "Nano-sized transition-metal oxides as negative-electrode materials for lithium-ion batteries," *Nature,* vol. 407, pp. 496-499, 2000.

[47] G. Zhou, D.-W. Wang, F. Li, L. Zhang, N. Li, Z.-S. Wu*, et al.*, "Graphene-wrapped Fe3O4 anode material with improved reversible capacity and cyclic stability for lithium ion batteries," *Chemistry of Materials,* vol. 22, pp. 5306-5313, 2010.

[48] N. Nitta, F. Wu, J. T. Lee, and G. Yushin, "Li-ion battery materials: present and future," *Materials today,* vol. 18, pp. 252-264, 2015.

[49] H. Wu and Y. Cui, "Designing nanostructured Si anodes for high energy lithium ion batteries," *Nano Today,* vol. 7, pp. 414-429, 2012.

[50] G. Berckmans, M. Messagie, J. Smekens, N. Omar, L. Vanhaverbeke, and J. Van Mierlo, "Cost Projection of State of the Art Lithium-Ion Batteries for Electric Vehicles Up to 2030," *Energies,* vol. 10, p. 1314, 2017.

[51] X. Dai, A. Zhou, J. Xu, Y. Lu, L. Wang, C. Fan*, et al.*, "Extending the High-Voltage Capacity of LiCoO2 Cathode by Direct Coating of the Composite Electrode with Li2CO3 via Magnetron Sputtering," *The Journal of Physical Chemistry C,* 2015.

[52] B. Wang, J. Bates, F. Hart, B. Sales, R. Zuhr, and J. Robertson, "Characterization of Thin-Film Rechargeable Lithium Batteries with Lithium Cobalt Oxide Cathodes," *Journal of The Electrochemical Society,* vol. 143, pp. 3203-3213, 1996.

[53] G. Amatucci, J. Tarascon, and L. Klein, "Cobalt dissolution in LiCoO 2-based non-aqueous rechargeable batteries," *Solid State Ionics*, vol. 83, pp. 167-173, 1996.

[54] H. Xia, S. Y. Meng, L. Lu, and G. Ceder, "Electrochemical Behavior and Li Diffusion Study of $LiCoO_2$ Thin Film Electrodes Prepared by PLD," 2007.

[55] P. Arora, R. E. White, and M. Doyle, "Capacity fade mechanisms and side reactions in lithium-ion batteries," *Journal of the Electrochemical Society,* vol. 145, pp. 3647-3667, 1998.

[56] S. Bourlot, P. Blanchard, and S. Robert, "Investigation of aging mechanisms of high power Li-ion cells used for hybrid electric vehicles," *Journal of Power Sources,* vol. 196, pp. 6841-6846, 2011.

[57] T. Ashwin, Y. M. Chung, and J. Wang, "Capacity fade modelling of lithium-ion battery under cyclic loading conditions," *Journal of Power Sources,* vol. 328, pp. 586-598, 2016.

[58] Y. Itou and Y. Ukyo, "Performance of LiNiCoO 2 materials for advanced lithium-ion batteries," *Journal of Power Sources,* vol. 146, pp. 39-44, 2005.

[59] D. Linden, "Handbook of batteries," in *Fuel and Energy Abstracts*, 1995, p. 265.

[60] I. Bloom, B. Cole, J. Sohn, S. Jones, E. Polzin, V. Battaglia*, et al.*, "An accelerated calendar and cycle life study of Li-ion cells," *Journal of Power Sources,* vol. 101, pp. 238-247, 2001.

[61] M. Broussely, S. Herreyre, P. Biensan, P. Kasztejna, K. Nechev, and R. Staniewicz, "Aging mechanism in Li ion cells and calendar life predictions," *Journal of Power Sources,* vol. 97, pp. 13-21, 2001.

[62] B. Y. Liaw, G. Nagasubramanian, R. G. Jungst, and D. H. Doughty, "Modeling of lithium ion cells—A simple equivalent-circuit model approach," *Solid state ionics,* vol. 175, pp. 835-839, 2004.

[63] M. Doyle and J. Newman, "The use of mathematical modeling in the design of lithium/polymer battery systems," *Electrochimica Acta,* vol. 40, pp. 2191-2196, 1995.

[64] J. C. Forman, S. J. Moura, J. L. Stein, and H. K. Fathy, "Genetic identification and fisher identifiability analysis of the Doyle–Fuller–Newman model from experimental cycling of a LiFePO 4 cell," *Journal of Power Sources,* vol. 210, pp. 263-275, 2012.

[65] R. Ahmed, M. El Sayed, I. Arasaratnam, J. Tjong, and S. Habibi, "Reduced-order electrochemical model parameters identification and SOC estimation for healthy and aged Li-ion batteries Part I: parameterization model development for healthy batteries," *IEEE journal of emerging and selected topics in power electronics,* vol. 2, pp. 659-677, 2014.

[66] K. A. Severson, P. M. Attia, N. Jin, N. Perkins, B. Jiang, Z. Yang*, et al.*, "Data-driven prediction of battery cycle life before capacity degradation," *Nature Energy,* p. 1, 2019.

[67] R. Hassan, B. Cohanim, O. De Weck, and G. Venter, "A comparison of particle swarm optimization and the genetic algorithm," in *46th AIAA/ASME/ASCE/AHS/ASC Structures, Structural Dynamics and Materials Conference*, 2005, p. 1897.

[68] D. Andre, M. Meiler, K. Steiner, C. Wimmer, T. Soczka-Guth, and D. Sauer, "Characterization of high-power lithium-ion batteries by electrochemical impedance spectroscopy. I. Experimental investigation," *Journal of Power Sources*, vol. 196, pp. 5334-5341, 2011.

[69] L. Wang, J. Zhao, X. He, J. Gao, J. Li, C. Wan, *et al.*, "Electrochemical impedance spectroscopy (EIS) study of LiNi1/3Co1/3Mn1/3O2 for Li-ion batteries," *Int. J. Electrochem. Sci*, vol. 7, pp. 345-353, 2012.

[70] K. A. Smith, C. D. Rahn, and C.-Y. Wang, "Model-Based Electrochemical Estimation and Constraint Management for Pulse Operation of Lithium Ion Batteries," *IEEE Transactions on Control Systems Technology*, vol. 16, pp. 654-663, 2010.

[71] A. M. Bizeray, S. Zhao, S. R. Duncan, and D. A. Howey, "Lithium-ion battery thermal-electrochemical model-based state estimation using orthogonal collocation and a modified extended Kalman filter," *Journal of Power Sources*, vol. 296, pp. 400-412, 2015.

[72] K. Uddin, S. Perera, W. D. Widanage, L. Somerville, and J. Marco, "Characterising lithium-ion battery degradation through the identification and tracking of electrochemical battery model parameters," *Batteries*, vol. 2, p. 13, 2016.

[73] D. Di Domenico, A. Stefanopoulou, and G. Fiengo, "Lithium-Ion Battery State of Charge and Critical Surface Charge Estimation Using an Electrochemical Model-Based Extended Kalman Filter," *Journal of Dynamic Systems, Measurement, and Control*, vol. 132, p. 061302, 2010.

[74] S. Santhanagopalan, Q. Guo, and R. E. White, "Parameter estimation and model discrimination for a lithium-ion cell," *Journal of the Electrochemical Society*, vol. 154, pp. A198-A206, 2007.

[75] G. Ning and B. N. Popov, "Cycle life modeling of lithium-ion batteries," *Journal of The Electrochemical Society*, vol. 151, pp. A1584-A1591, 2004.

[76] M. Ecker, J. B. Gerschler, J. Vogel, S. Käbitz, F. Hust, P. Dechent, *et al.*, "Development of a lifetime prediction model for lithium-ion batteries based on extended accelerated aging test data," *Journal of Power Sources*, vol. 215, pp. 248-257, 2012.

[77] K. Smith, A. Saxon, M. Keyser, B. Lundstrom, Z. Cao, and A. Roc, "Life prediction model for grid-connected Li-ion battery energy storage system," in *American Control Conference (ACC), 2017*, 2017, pp. 4062-4068.

[78] J. Li, A. M. Gee, M. Zhang, and W. Yuan, "Analysis of battery lifetime extension in a SMES-battery hybrid energy storage system using a novel battery lifetime model," *Energy*, vol. 86, pp. 175-185, 2015.

[79] J. Wang, P. Liu, J. Hicks-Garner, E. Sherman, S. Soukiazian, M. Verbrugge, *et al.*, "Cycle-life model for graphite-LiFePO4 cells," *Journal of Power Sources*, vol. 196, pp. 3942-3948, 2011.

[80] Z. Song, J. Li, X. Han, L. Xu, L. Lu, M. Ouyang, *et al.*, "Multi-objective optimization of a semi-active battery/supercapacitor energy storage system for electric vehicles," *Applied Energy*, vol. 135, pp. 212-224, 2014.

[81] P. Liu, J. Wang, J. Hicks-Garner, E. Sherman, S. Soukiazian, M. Verbrugge, *et al.*, "Aging mechanisms of LiFePO4 batteries deduced by electrochemical and

structural analyses," *Journal of the Electrochemical Society*, vol. 157, pp. A499-A507, 2010.

[82] L. Guzzella and A. Sciarretta, *Vehicle propulsion systems* vol. 1: Springer, 2007.

[83] T. I. Bø, T. A. Johansen, A. R. Dahl, M. R. Miyazaki, E. Pedersen, B. Rokseth, *et al.*, "Real-time marine vessel and power plant simulation," in *ASME 2015 34th International Conference on Ocean, Offshore and Arctic Engineering*, 2015, pp. V001T01A007-V001T01A007.

[84] T. Perez and T. I. Fossen, "A matlab toolbox for parametric identification of radiation-force models of ships and offshore structures," 2009.

[85] T. I. Fossen and Ø. N. Smogeli, "Nonlinear time-domain strip theory formulation for low-speed manoeuvering and station-keeping," *Modeling, identification and control*, vol. 25, p. 201, 2004.

[86] J. F. Hansen, A. K. ådnanes, and T. I. Fossen, "Mathematical modelling of diesel-electric propulsion systems for marine vessels," *Mathematical and Computer Modelling of Dynamical Systems*, vol. 7, pp. 323-355, 2001.

[87] W. A. L. Truelove, "A general methodology for generating representative load cycles for monohull surface vessels," 2018.

[88] J. Thongam, M. Tarbouchi, A. Okou, D. Bouchard, and R. Beguenane, "All-electric ships—A review of the present state of the art," in *Ecological Vehicles and Renewable Energies (EVER), 2013 8th International Conference and Exhibition on*, 2013, pp. 1-8.

[89] S. Onori, L. Serrao, and G. Rizzoni, *Hybrid electric vehicles: Energy management strategies*: Springer, 2016.

[90] E. A. Sciberras, "Shipboard electrification: emission reduction and energy control," 2016.

[91] MAN, "Hybrid Propulsion. Flexibility and maximum efficiency optimally combined.."

[92] MAN, "Diesel-electric Propulsion Plants: a brief guideline how to engineer a diesel-electric propulsion system."

[93] A. K. Ådnanes, *Maritime electrical installations and diesel electric propulsion*: ABB, 2003.

[94] K. Ç. Bayindir, M. A. Gözüküçük, and A. Teke, "A comprehensive overview of hybrid electric vehicle: Powertrain configurations, powertrain control techniques and electronic control units," *Energy conversion and Management*, vol. 52, pp. 1305-1313, 2011.

[95] C. Rossi, P. Corbelli, L. Zarri, and D. Casadei, "Power split e-CVT ship propulsion system," in *2009 IEEE Electric Ship Technologies Symposium*, 2009, pp. 505-514.

[96] EPA, "Criteria Air Pollutants."

[97] L. Browning and K. Bailey, "Current methodologies and best practices for preparing port emission inventories," *ICF Consulting report to Environmental Protection Agency*, 2006.

[98] "National Inventory Report 1990–2016: Greenhouse Gas Sources and Sinks in Canada," *CANADA'S SUBMISSION TO THE UNITED NATIONS FRAMEWORK CONVENTION ON CLIMATE CHANGE*, 2018.

[99] www.bchydro.com.

[100] PoLB, "Port of Long Beach 2016 Air Emissions Inventory," *Starcrest Consulting Group LLC report to Port of Long Beach*, 2017.

[101] A. Banawan, M. M. El Gohary, and I. Sadek, "Environmental and economical benefits of changing from marine diesel oil to natural-gas fuel for short-voyage high-power passenger ships," *Proceedings of the Institution of Mechanical Engineers, Part M: Journal of Engineering for the Maritime Environment,* vol. 224, pp. 103-113, 2010.

[102] "Liquefied Natural Gas: A Marine fuel for Canada's West Coast.," *Canadian Natural Gas Vehicle Alliance*, 2014.

[103] B. A. Bassham, "An evaluation of electric motors for ship propulsion," Monterey, California. Naval Postgraduate School, 2003.

[104] T. Völker, "Hybrid propulsion concepts on ships," 2015.

[105] L. Busoniu, R. Babuska, B. De Schutter, and D. Ernst, *Reinforcement learning and dynamic programming using function approximators*: CRC press, 2010.

[106] N. Kim, S. Cha, and H. Peng, "Optimal control of hybrid electric vehicles based on Pontryagin's minimum principle," *IEEE Transactions on Control Systems Technology,* vol. 19, pp. 1279-1287, 2011.

[107] K. J. Hunt, D. Sbarbaro, R. Żbikowski, and P. J. Gawthrop, "Neural networks for control systems—a survey," *Automatica,* vol. 28, pp. 1083-1112, 1992.

[108] A. Vahidi, A. G. Stefanopoulou, and H. Peng, "Current management in a hybrid fuel cell power system: A model-predictive control approach," *IEEE Transactions on Control Systems Technology,* vol. 14, pp. 1047-1057, 2006.

[109] H.-D. Lee and S.-K. Sul, "Fuzzy-logic-based torque control strategy for parallel-type hybrid electric vehicle," *IEEE Transactions on Industrial Electronics,* vol. 45, pp. 625-632, 1998.

[110] C. Hou, M. Ouyang, L. Xu, and H. Wang, "Approximate Pontryagin's minimum principle applied to the energy management of plug-in hybrid electric vehicles," *Applied Energy,* vol. 115, pp. 174-189, 2014.

[111] W. Li, G. Xu, Z. Wang, and Y. Xu, "Dynamic energy management for hybrid electric vehicle based on adaptive dynamic programming," in *2008 IEEE International Conference on Industrial Technology*, 2008, pp. 1-6.

[112] "Life Cycle Cost for Systems and Equipment," *NORSOK Standard,* April, 1996.

[113] "Natural Resources Canada," *www.nrcan.gc.ca*.

[114] "Natural Gas Price," *www.eia.gov*.

[115] "ICE NGX Albert Market Price," *http://www.ngx.com*.

[116] "British Columbia Ferry Services Inc. Fuel Strategies-Update Report," 2016.

[117] "www.bchydro.com."

[118] "2015 Indicative Industrial Electricity Prices " 2015.

[119] "British Columbia Hydro & Power Authority (BC Hydro) Fiscal 2017-Fiscal 2019 Revenue Requirements Application – AMPC Evidence " Feb 27, 2017.

[120] S. R. Nikolaisen, "Life Cycle Cost Comparison Study-An analysis of a LNG ferry's performance and potential for improvement," NTNU, 2014.

[121] C. Heymans, S. B. Walker, S. B. Young, and M. Fowler, "Economic analysis of second use electric vehicle batteries for residential energy storage and load-levelling," *Energy Policy,* vol. 71, pp. 22-30, 2014.

[122] C.-S. Ernst, A. Hackbarth, R. Madlener, B. Lunz, D. U. Sauer, and L. Eckstein, "Battery sizing for serial plug-in hybrid vehicles: A model-based economic analysis for Germany," 2011.

[123] S. J. Moura, H. K. Fathy, D. S. Callaway, and J. L. Stein, "A stochastic optimal control approach for power management in plug-in hybrid electric vehicles," *IEEE Transactions on control systems technology,* vol. 19, pp. 545-555, 2011.

[124] D. Sinoquet, G. Rousseau, and Y. Milhau, "Design optimization and optimal control for hybrid vehicles," *Optimization and Engineering,* vol. 12, pp. 199-213, 2011.

[125] Y. Zou, D.-g. Li, and X.-s. Hu, "Optimal sizing and control strategy design for heavy hybrid electric truck," *Mathematical Problems in Engineering,* vol. 2012, 2012.

[126] E. Silvas, E. Bergshoeff, T. Hofman, and M. Steinbuch, "Comparison of bi-level optimization frameworks for sizing and control of a hybrid electric vehicle," in *2014 IEEE Vehicle Power and Propulsion Conference (VPPC)*, 2014, pp. 1-6.

[127] A. Antoniou and W.-S. Lu, *Practical optimization: algorithms and engineering applications*: Springer Science & Business Media, 2007.

[128] S. Mirjalili, S. M. Mirjalili, and A. Lewis, "Grey wolf optimizer," *Advances in engineering software,* vol. 69, pp. 46-61, 2014.

[129] S. Sivanandam and S. Deepa, *Introduction to genetic algorithms*: Springer Science & Business Media, 2007.

[130] E. Rashedi, H. Nezamabadi-Pour, and S. Saryazdi, "GSA: a gravitational search algorithm," *Information sciences,* vol. 179, pp. 2232-2248, 2009.

[131] Y. Shi, "Particle swarm optimization: developments, applications and resources," in *Proceedings of the 2001 congress on evolutionary computation (IEEE Cat. No. 01TH8546)*, 2001, pp. 81-86.

[132] M. Dorigo and G. Di Caro, "Ant colony optimization: a new meta-heuristic," in *Proceedings of the 1999 congress on evolutionary computation-CEC99 (Cat. No. 99TH8406)*, 1999, pp. 1470-1477.

[133] M. Yazdani and F. Jolai, "Lion optimization algorithm (LOA): a nature-inspired metaheuristic algorithm," *Journal of computational design and engineering,* vol. 3, pp. 24-36, 2016.

[134] D. H. Wolpert and W. G. Macready, "No free lunch theorems for optimization," *IEEE transactions on evolutionary computation,* vol. 1, pp. 67-82, 1997.

[135] R. T. Marler and J. S. Arora, "Survey of multi-objective optimization methods for engineering," *Structural and multidisciplinary optimization,* vol. 26, pp. 369-395, 2004.

[136] J. A. Reyer, H. K. Fathy, P. Y. Papalambros, and A. G. Ulsoy, "Comparison of combined embodiment design and control optimization strategies using optimality conditions," in *Proceedings of the 2001 ASME Design Engineering Technical Conferences*, 2001.

[137] D. R. Herber and J. T. Allison, "Nested and simultaneous solution strategies for general combined plant and control design problems," *Journal of Mechanical Design,* vol. 141, p. 011402, 2019.

[138] D. L. Peters, "Coupling and Controllability in Optimal Design and Control," 2010.

[139] E. Silvas, T. Hofman, N. Murgovski, L. P. Etman, and M. Steinbuch, "Review of optimization strategies for system-level design in hybrid electric vehicles," *IEEE Transactions on Vehicular Technology,* vol. 66, pp. 57-70, 2016.

[140] A. Sinha, P. Malo, and K. Deb, "A review on bilevel optimization: from classical to evolutionary approaches and applications," *IEEE Transactions on Evolutionary Computation,* vol. 22, pp. 276-295, 2018.

[141] B. G. Husslage, G. Rennen, E. R. Van Dam, and D. Den Hertog, "Space-filling Latin hypercube designs for computer experiments," *Optimization and Engineering,* vol. 12, pp. 611-630, 2011.

[142] G. G. Wang and S. Shan, "Review of metamodeling techniques in support of engineering design optimization," *Journal of Mechanical design,* vol. 129, pp. 370-380, 2007.

[143] M. Liefvendahl and R. Stocki, "A study on algorithms for optimization of Latin hypercubes," *Journal of statistical planning and inference,* vol. 136, pp. 3231-3247, 2006.

[144] R. Jin, W. Chen, and A. Sudjianto, "An efficient algorithm for constructing optimal design of computer experiments," in *ASME 2003 International Design Engineering Technical Conferences and Computers and Information in Engineering Conference,* 2003, pp. 545-554.

[145] J.-F. Barthelemy and R. T. Haftka, "Approximation concepts for optimum structural design—a review," *Structural optimization,* vol. 5, pp. 129-144, 1993.

[146] J. P. Kleijnen, "Kriging metamodeling in simulation: A review," *European journal of operational research,* vol. 192, pp. 707-716, 2009.

[147] M. Schonlau, "Computer experiments and global optimization," 1997.

[148] M. J. Sasena, "Flexibility and efficiency enhancements for constrained global design optimization with kriging approximations," University of Michigan Ann Arbor, 2002.

[149] J. Gu, G. Li, and Z. Dong, "Hybrid and adaptive metamodel based global optimization," in *ASME 2009 International Design Engineering Technical Conferences and Computers and Information in Engineering Conference,* 2009, pp. 751-765.

[150] H. E. Lindstad and I. Sandaas, "Emission and fuel reduction for offshore support vessels through hybrid technology," *Journal of Ship Production and Design,* vol. 32, pp. 195-205, 2016.

[151] T. L. Vu, A. A. Ayu, J. S. Dhupia, L. Kennedy, and A. K. Adnanes, "Power management for electric tugboats through operating load estimation," *IEEE Transactions on Control Systems Technology,* vol. 23, pp. 2375-2382, 2015.

[152] H. Kifune and T. Nishio, "Fuel Saving Effect of Hybrid Propulsion System-Case: Tugboat is not in Service," *Marine Engineering,* vol. 52, pp. 811-817, 2017.

[153] D. R. Jones, M. Schonlau, and W. J. Welch, "Efficient global optimization of expensive black-box functions," *Journal of Global optimization,* vol. 13, pp. 455-492, 1998.

[154] S. N. Lophaven, H. B. Nielsen, and J. Søndergaard, "DACE-A Matlab Kriging toolbox, version 2.0," 2002.

[155] P. Ramadass, B. Haran, P. M. Gomadam, R. White, and B. N. Popov, "Development of first principles capacity fade model for Li-ion cells," *Journal of the Electrochemical Society*, vol. 151, pp. A196-A203, 2004.

Appendix A- Single Particle Model

The single particle model (SPM) simplifies the complex PDEs in the Doyler-Fuller-Newman model to improve the computational ability. It is assumed that compound particles on each electrode have the same size, therefore, only one spherical particle is needed on each side. Also, the electrolyte concentration is assumed uniform inside battery. The concentration variation and ions movement in discharging process was demonstrated in Figure 46.

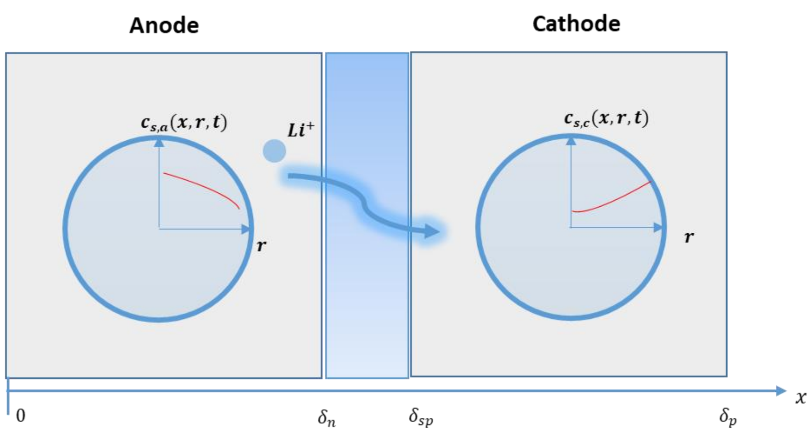

Figure 46: Demonstration of Single Particle Model.

All the governing equations of SPM model are concluded in Table 12. Detailed discussions and explanations regarding these equations can also be found in the literature [32, 73, 74, 155]. It is hard to find the closed-form analytical solution for this set of PDEs. A more realistic method is using MATLAB to find numerical solutions. This paper adopted the finite-difference method (FDM).

Table 12: Governing Equations and Boundary Conditions

	Governing Equations	Boundary Conditions
Anode	$\frac{\partial c_s}{\partial t} = \nabla_r(D_s \nabla_r c_s)$	$\left.\frac{\partial c_s}{\partial r}\right\rvert_{r=0} = 0$ $\left.\frac{\partial c_s}{\partial r}\right\rvert_{r=R} = -\frac{j^{Li}}{D_s a_{s,n} F}$
	$\frac{\partial \varepsilon_e c_e}{\partial t} = \frac{1-t^0}{F} j^{Li}$	$c_e(x,t) = c_e(t)$
	$\frac{\partial^2 \phi_s}{\partial \mathrm{x}^2} = \frac{j^{Li}}{\sigma^{\mathrm{eff}}}$	$i_s = \left.\frac{\partial \phi_s}{\partial x}\right\rvert_{x=0} = \frac{I}{A}$ $i_s = \left.\frac{\partial \phi_s}{\partial x}\right\rvert_{x=\delta_n} = 0$
	$\frac{\partial^2 \phi_e}{\partial \mathrm{x}^2} = -\frac{j^{Li}}{\mathrm{k}^{\mathrm{eff}}}$	$i_e = \left.\frac{\partial \phi_e}{\partial x}\right\rvert_{x=0} = 0$ $i_e = \left.\frac{\partial \phi_e}{\partial x}\right\rvert_{x=\delta_n} = \frac{I}{A}$
Separator	$\frac{\partial \varepsilon_e c_e}{\partial t} = \frac{1-t^0}{F} j^{Li}$	$c_e(x,t) = c_e(t)$
	$\frac{\partial^2 \phi_e}{\partial \mathrm{x}^2} = -\frac{j^{Li}}{\mathrm{k}^{\mathrm{eff}}}$	$i_e = \frac{\partial \phi_e}{\partial x} = \frac{I}{A}$
Cathode	$\frac{\partial c_s}{\partial t} = \nabla_r(D_s \nabla_r c_s)$	$\left.\frac{\partial c_s}{\partial r}\right\rvert_{r=0} = 0$ $\left.\frac{\partial c_s}{\partial r}\right\rvert_{r=R} = -\frac{j^{Li}}{D_s a_{s,p} F}$
	$\frac{\partial \varepsilon_e c_e}{\partial t} = \frac{1-t^0}{F} j^{Li}$	$c_e(x,t) = c_e(t)$
	$\frac{\partial^2 \phi_s}{\partial \mathrm{x}^2} = -\frac{j^{Li}}{\sigma^{\mathrm{eff}}}$	$i_s = \left.\frac{\partial \phi_s}{\partial x}\right\rvert_{x=L} = \frac{I}{A}$ $i_s = \left.\frac{\partial \phi_s}{\partial x}\right\rvert_{x=\delta_{sp}} = 0$
	$\frac{\partial^2 \phi_e}{\partial \mathrm{x}^2} = \frac{j^{Li}}{\mathrm{k}^{\mathrm{eff}}}$	$i_e = \left.\frac{\partial \phi_e}{\partial x}\right\rvert_{x=L} = 0$ $i_e = \left.\frac{\partial \phi_e}{\partial x}\right\rvert_{x=\delta_{sp}} = \frac{I}{A}$

By discretizing the solid particle along its radius direction, the solid phase diffusion can be measured as volume concentration changing in the equally discretized m layers. Each layer has the thickness of $\delta r = \frac{R}{m}$. For the i^{th} layer, the concentration change with time can be described as the net molar flux in and out of this layer, according to the conservation of mass.

$$\frac{\delta c_i}{\delta t} = \frac{M_1 - M_2}{A_i \delta r} \tag{A-1}$$

where $A_i = 4\pi r_i^2$ is the surface area of the i^{th} layer . M_1, M_2 are the molar flux in and out of the i^{th} layer. By substituting and rearranging these equations, a generalized form can be deduced as:

$$\frac{\partial c_i}{\partial t} = \frac{D}{\delta r^2}\left[\left(\frac{i-1}{i}\right) c_{i-1} - 2c_i + \left(\frac{i+1}{i}\right) c_{i+1}\right] \tag{A-2}$$

Combing with its boundary conditions, a state space equation can be formed to demonstrate the cathode and anode ion fluxes, where $\dot{c_i} (i = 1, \dots m-1)$ is the concentration changing of each layer with time.

$$\begin{bmatrix} \dot{c_1} \\ \dot{c_2} \\ \dot{c_3} \\ \vdots \\ \dot{c_{m-2}} \\ \dot{c_{m-1}} \end{bmatrix} = \frac{D}{\delta r^2} \begin{bmatrix} -2 & -2 & 0 & 0 & \dots & 0 \\ \frac{1}{2} & -2 & \frac{3}{2} & 0 & \dots & 0 \\ 0 & \frac{2}{3} & -2 & 0 & \dots & 0 \\ \vdots & \vdots & \vdots & \ddots & \vdots & \vdots \\ 0 & 0 & 0 & \dots & -2 & \frac{m-1}{m-2} \\ 0 & 0 & 0 & \dots & \frac{m-2}{m-1} & -\frac{m-2}{m-1} \end{bmatrix} \begin{bmatrix} c_1 \\ c_2 \\ c_3 \\ \vdots \\ c_{m-2} \\ c_{m-1} \end{bmatrix} + \begin{bmatrix} 0 \\ 0 \\ 0 \\ \vdots \\ 0 \\ \frac{m}{m-1} \end{bmatrix} \frac{j^{Li}}{\delta r F a_s} \tag{A-3}$$

It was showed clearly in Figure 47 that if one particle was discretized into 20 layers, the 20th layer responded quickly on the outermost shell while the 1st layer next to the core changed slowly.

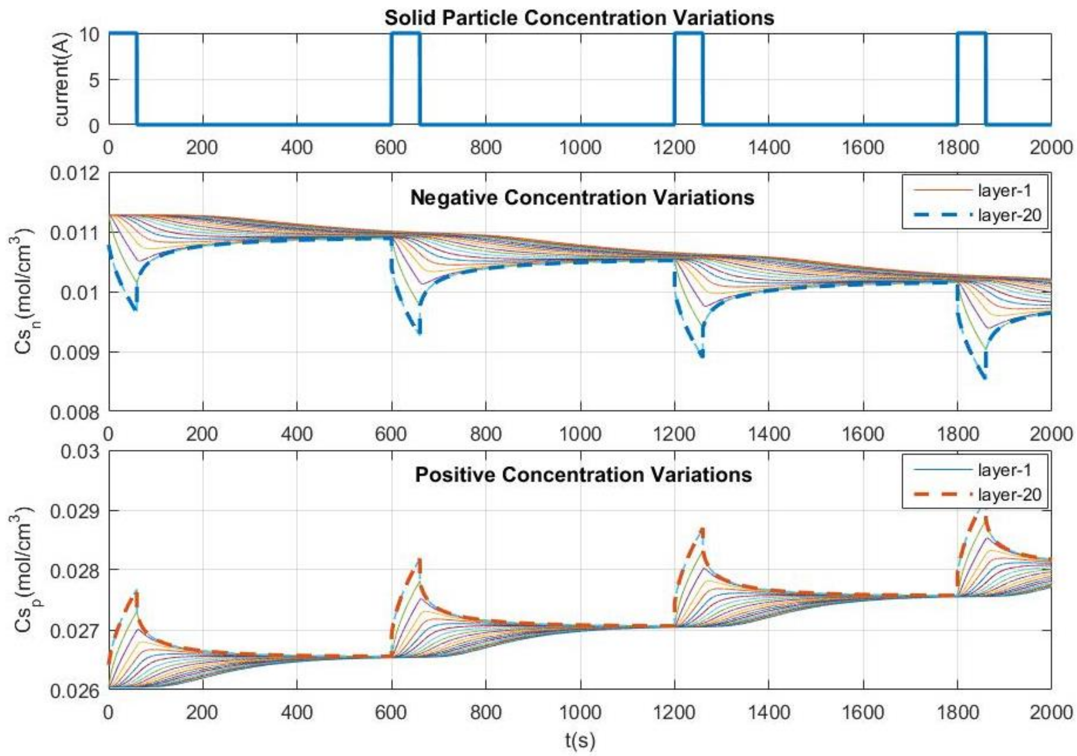

Figure 47: Solid Particle Concentration Variation with Pulse Current

In conclusion, totally 20 parameters are needs to be identified through GA in the optimization problem as showed in Table 13.

Table 13: Summation of Parameters in the SPM Model

Parameters		Symbol	Unit	Lower Bound	Upper Bound
1	Maximum Li-ion concentration in negative particle	$c_{s,n,max}$	mol/cm^3	1E-04	1E-01
2	Maximum Li-ion concentration in positive particle	$c_{s,p,max}$	mol/cm^3	1E-04	1E-01
3	Minimum stoichiometric number in negative material	$\theta_{n,0}$	/	1E-02	5E-01
4	Maximum stoichiometric number in negative material	$\theta_{n,100}$	/	5E-01	9.9E-01
5	Minimum stoichiometric number in positive material	$\theta_{p,0}$	/	1E-02	5E-01
6	Maximum stoichiometric number in positive material	$\theta_{p,100}$	/	5E-01	9.9E-01
7	Average electrolyte concentration	c_e	mol/cm^3	1E-05	1E-01
8	Negative particle radius	$R_{s,n}$	cm	1E-06	1E-02
9	Positive particle radius	$R_{s,p}$	cm	1.E-06	1E-2
10	Electrode area	A	cm^2	1E+02	1E+06
11	Thickness of negative electrode	δ_n	cm	1E-05	1E-03
12	Thickness of positive electrode	δ_p	cm	1E-05	1E-03
13	Electrolyte phase ionic conductivity	k_e	1/(Ω.cm)	1E-01	13+03
14	Active surface area per negative electrode unit volume	$a_{s,n}$	1/cm	1E+04	1E+06
15	Active surface area per positive electrode unit volume	$a_{s,p}$	1/cm	1E+04	1E+06
16	Solid phase diffusion coefficient in negative active material	$D_{s,n}$	cm^2/s	1E-14	1E-05
17	Solid phase diffusion coefficient in positive active material	$D_{s,p}$	cm^2/s	1E-14	1E-05
18	Film Ohmic resistance	R_f	Ω	0.0001	0.1
19	Anode reaction rate	k_a	/	1E-10	1E+05
20	Cathode reaction rate	k_c	/	1E-10	1E+05